IMPROVEMENT OF ELECTROMAGNETIC RAILGUN BARREL PERFORMANCE AND LIFETIME BY METHOD OF INTERFACES AND AUGMENTED PROJECTILES

A Thesis

Presented to

the Faculty of California Polytechnic State University

San Luis Obispo

In Partial Fulfillment

of the Requirements for the Degree

Master of Science in Aerospace Engineering

by

Aleksey Pavlov

June 2013

COMMITTEE MEMBERSHIP

TITLE:	Improvement of Electromagnetic Railgun Barrel Performance and Lifetime by Method of Interfaces and Augmented Projectiles
AUTHOR:	Aleksey Pavlov
DATE SUBMITTED:	June 2013
COMMITTEE CHAIR:	Kira Abercromby, Ph.D., Associate Professor, Aerospace Engineering
COMMITTEE MEMBER:	Eric Mehiel, Ph.D., Associate Professor, Aerospace Engineering
COMMITTEE MEMBER:	Vladimir Prodanov, Ph.D., Assistant Professor, Electrical Engineering
COMMITTEE MEMBER:	Thomas Guttierez, Ph.D., Associate Professor, Physics

Abstract

Improvement of Electromagnetic Railgun Barrel Performance and Lifetime by Method of Interfaces and Augmented Projectiles

Aleksey Pavlov

Several methods of increasing railgun barrel performance and lifetime are investigated. These include two different barrel-projectile interface coatings: a solid graphite coating and a liquid eutectic indium-gallium alloy coating. These coatings are characterized and their usability in a railgun application is evaluated. A new type of projectile, in which the electrical conductivity varies as a function of position in order to condition current flow, is proposed and simulated with FEA software.

The graphite coating was found to measurably reduce the forces of friction inside the bore but was so thin that it did not improve contact. The added contact resistance of the graphite was measured and gauged to not be problematic on larger scale railguns. The liquid metal was found to greatly improve contact and not introduce extra resistance but its hazardous nature and tremendous cost detracted from its usability.

The simulated resistivity augmented projectiles were able to mitigate harmful current build-up on the back of a projectile using different conductivity gradients. Within the range of conductivity of aluminum alloys no simulated gradient was able to fully level the current density, however, once the range was expanded to include the lower conductivity of titanium, nearly uniform current density was achieved.

Acknowledgements

First of all, I would like to dedicate this work to my grandfather, Alexander Zavorine, whose life of hard work in science and mathematics provided my family the opportunity to move to the United States and allowed for me to follow down a similar path of physics and engineering.

I would like to thank Dr. Abercromby, Jeff Maniglia, Guy Zohar, Jordan Smiroldo and Alex Westfall for creating this project and allowing me to be a part of it. Thank you Dr. Abercromby for her help, guidance and uncanny ability to deal with my humor. I am especially grateful for her helping me back off the edge after the unfortunate loss of my computer and thesis data. Thanks to Jeff Maniglia for working alongside me the entire time and radiating railgun information and knowledge.

Large amounts of data in this work was taken using other Cal Poly departments' equipment. I would like to thank the MATE department, specifically Dr. Chen and Nash Anderson for allowing me to use their XRD, scanning electron microscope and profilometer, numerous times. I would like to thank the EE department for giving me access anytime to their labs so I could use their electrical test equipment. Thank you to Dr. Maier and the NPS in Monterey for donating all of their hardware which made a lot of this work feasible. Thank you to the Aerospace department for letting this project live inside the propulsion lab for an entire year.

Thank you to Jeff Puschell and Raytheon for providing most of this project's funding. Finally, I am grateful to Albert Tamashausky and Asbury Carbons for donating the graphite used for this work.

Contents

List of Tables

List of Figures

Chapter 1

Introduction and Motivation

Modern methods of accelerating persons, projectiles or payloads typically use exothermic reactions fueled by propellants or pressurized non-combustible gases. For example, firearms use fast burning powders which create tremendous pressures due to expanding gases. Missiles, launch vehicles, jet engines, rocket sleds and things alike use solid or liquid fuels to generate thrust. On aircraft carriers pressurized steam is used to quickly accelerate aircraft so they can take off in short distances. These methods all have their limitations. An increase in desired velocity means carrying more fuel which causes problems of requiring more weight and having to deal with more dangerous materials. For practically all applications the maximum achievable velocity is bounded. For example, in the case of launch vehicles adding more stages does not increase the final velocity proportionally; instead the maximum velocity achieved by adding more stages quickly reaches a limit. In firearms the maximum velocity is bounded by the efficiency of the powders, the amount of powder used, the geometry of the barrel, and the aerodynamics and integrity of the projectile. More generally, velocities are bounded by the speed of sound of the expanding or propelling gas; the pro-

jectile rides the pressure differential caused by pressure wave of the expanding gas which is moving at its speed of sound.

There is a need for accelerating matter quicker and to greater velocities which these conventional methods cannot achieve. Electromagnetic railguns which propel projectiles with large currents seem to fit the bill. Since there is no expanding gas propelling the projectile, but rather current, the velocity is no longer bounded by a certain speed of sound of a gas[1]. There are already a few methods, some of which are briefly described in section 2, of achieving these tremendous velocities in short time spans but their size, cost, and complexity limit their widespread use. Properly made railguns can take much less space to operate and the operational costs consist of essentially only electricity.

Railgun technology, as promising as it seems, has not been perfected and is faced with many problems which need to be overcome before railguns can be used in potential applications. In this paper, after discussing applications of railgun technology and current railgun problems, three different methods are explored for lessening the amount of damage railguns sustain when they fire. Two different coatings which go between the railgun barrel and projectile are investigated and characterized. Their use in a railgun application is evaluated. Lastly, a more theoretical approach is taken; the current flow through a theoretical type of projectile which would decrease the amount of melting at the projectile-rail interface is simulated.

[1]Some specific type of railguns, plasma railguns, fire tiny amounts of plasma at velocities up to 200km/s. In this case the plasma "gas" is the projectile itself and is able to accelerate to such large velocities because the very high density of the plasma makes its speed of sound very high [27].

1 Military Applications of Railguns

The Navy has been researching railguns as a possible next-generation weapon system for fleet ships for several decades. The advantages of railguns in a weaponized application is that a railgun of sufficient size could hit and destroy a target hundreds of miles inland while the ship is a safe distance off the coast. There is no need for warheads as the projectile's kinetic energy is what does the damage on impact. This is because the kinetic energy of the projectile is larger than the chemical energy of a conventional explosive round of similar mass. A naval fleet railgun with desired specifications, some of which are listed in Table 1 would be able to hit a target on the horizon within seconds and targets hundreds of miles inland within minutes [7]. A 2MJ railgun made by General Atomics, called "The Blitzer," is the first weaponized railgun that has the possibility of going into production in the future.

Table 1: Desired Weaponized Railgun Specifications

Property	Value
Projectile Mass	15kg
Launch Velocity	2.5km/s
Muzzle Energy	∼60MJ
Breech Energy	∼150MJ
Barrel Length	10m

Railgun type technology is also a contender to replace the current steam-powered aircraft catapults on aircraft carriers. In this case instead of launching a projectile the system accelerates an attachment connected to a 100,000lb aircraft to 240mph in about 300ft. The Electromagnetic Aircraft Launch System (EMALS) technology greatly outperforms the steam catapults; it takes less space, is more efficient, requires less maintenance and is more powerful. An important difference between EMALS and a railgun is that the moving armature in EMALS

does not carry any current itself and performs like a linear induction motor. At the time of the writing of the this paper the Navy has successfully tested EMALS with aircraft on land and is planning to install them on the Ford-class aircraft carriers [11].

While the Navy is interested in large railguns, smaller railguns with higher rates of fire, which can be carried by personnel or mounted on vehicles, are of interest to the Army. No railgun so far is able to fire rapidly and continuously, one of the reasons being the required power draw for continuous fire would be unrealistically high. Also, no railgun power supply is small enough yet to be carried by personnel or mounted on a small vehicle.

2 Orbital Debris Impact Testing Applications

While railguns show promise of being efficient and devastating weapons, the technology also has non-military applications. In aerospace, railgun technology can be useful for orbital debris impact testing. Since orbital debris impacts occur at velocities on the order of several km/s they cannot be simulated with conventional methods. Given that the energies that orbital debris impacts occur at are so high even the smallest piece of debris can cause devastating, if not critical, damage to spacecraft. This provides the motivation to simulate orbital debris impacts with spacecraft components to characterize their reaction and durability.

Orbital debris impacts are currently simulated with light gas guns and shaped charge launchers. Light gas guns are very complex and large apparatuses that compress hydrogen gas with a precursor explosion until it bursts through a small wall allowing the built up pressure be released onto a projectile. Shaped charge

launchers make a projectile ride the wave of a hyper-velocity shaped charge explosion and are very dangerous. A railgun designed for orbital debris impact testing would be small and safe enough to be implemented at a university laboratory rather than requiring a government or military facility. The NASA Orbital Debris Program Office estimates that there are 500,000 pieces of debris between 1cm and 10cm in size and over 100 million which are smaller than 1cm [21]. This makes small bore railguns which fire metal projectiles at high velocities great tools for simulating impacts. The railguns discussed in this work are designed to eventually achieve orbital velocities and be applicable for orbital debris impact testing. As of now the railguns at Cal Poly have not been able to achieve orbit velocities and do not have the robustness to be used repeatedly and reliably.

Chapter 2

Railgun Basics

1 Railgun Mechanics

Railguns accelerate conducting projectiles by the Lorentz force. The Lorentz force, given by Equation 1, describes the force on a particle with charge q moving with velocity $\vec{v}$ in the presence of electric and magnetic fields $\vec{E}$ and $\vec{B}$, respectively. In the case of a railgun the interacting field is the magnetic field so the quation reduces to Equation 2.

$$\vec{F} = q[\vec{E} + (\vec{v} \times \vec{B})] \tag{1}$$

$$\vec{F} = q(\vec{v} \times \vec{B}) \tag{2}$$

A conventional railgun design consists of two parallel conducting rails which act as the barrel. The projectile which also conducts electricity completes a circuit by contacting both rails. Current flowing along the length of the rails and through the projectile creates a magnetic field, $\vec{B}$. The current that is flowing through the projectile interacts with the magnetic field and the result is the Lorentz force

on the charge flowing through projectile. The resultant force is perpendicular to the current flow through the projectile which is the direction down the bore. Figure 1 illustrates the current flow and the generated magnetic field along with the force cause by the interaction with the field.

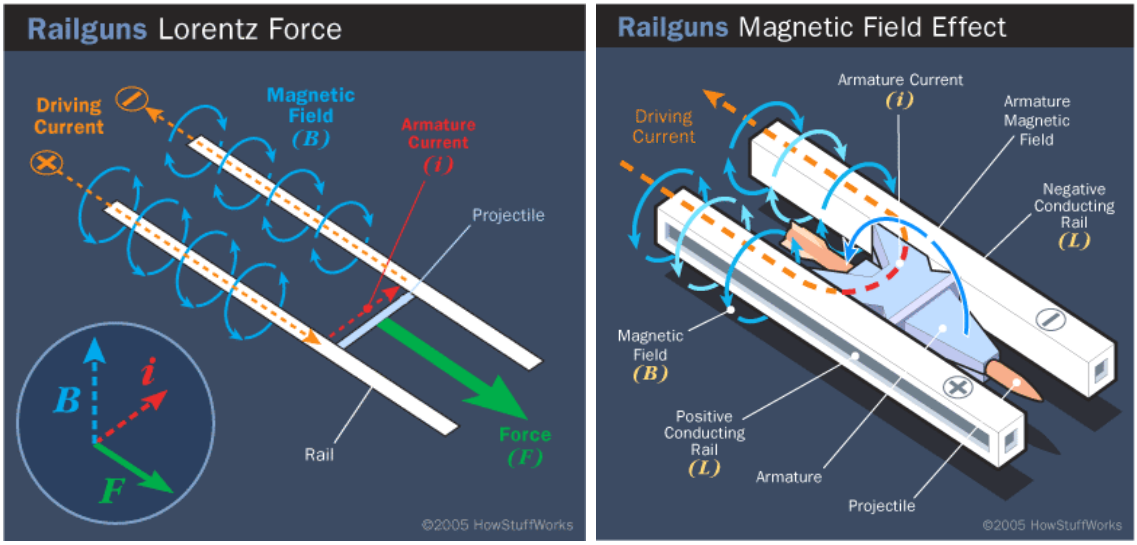

Figure 1: The basics of railguns. The interactions of current and magnetic fields in a railgun are shown. The left diagram generalizes the current flow paths while the right shows an example barrel, projectile and armature geometry. Since the rails are fixed the projectile accelerates down the bore due to the force upon it [16].

The Lorentz force equation can be manipulated to be a function of current rather than individual charge and charge velocity, a much more useful form for working with railguns. In this form, Equation 3 gives the magnitude of the force on the projectile and is a function of the current I and the inductance gradient L' which is fixed and determined by the geometry of the rails. Typically, thousands to millions of amps are passed through the rails and the projectile in a span of milliseconds to generate strong magnetic fields inside the bore. For a derivation of Equation 3 from Equation 2 along with the calculation for L' from rail geometry

see reference [19].

$$F = \frac{L' I^2}{2} \tag{3}$$

The objects that railguns shoot are called projectiles or armatures. When the object that is intended to impact a target is the entire package in the bore it is called a projectile. In other cases when only a part of what is in the bore interacts with the rails it is called the armature. The non-interacting object is the projectile. For example, in weaponized railguns the projectile is encased in a conducting sabot, the armature, which carries all the current. When the armature and projectile leave the barrel the armature is separated from the projectile by springs or aerodynamic forces and the projectile carries on downrange. Sometimes a solid armature may be placed behind a non-conducting projectile in order to accelerate it by pushing on it.

2 Types of Railguns

Conventional railguns are ones where there are only two parallel rails which make up the barrel, as seen in Figure 2. Conventional railguns have the simplest design; the current simply flows into one of the rails, through the projectile and out the other rail.

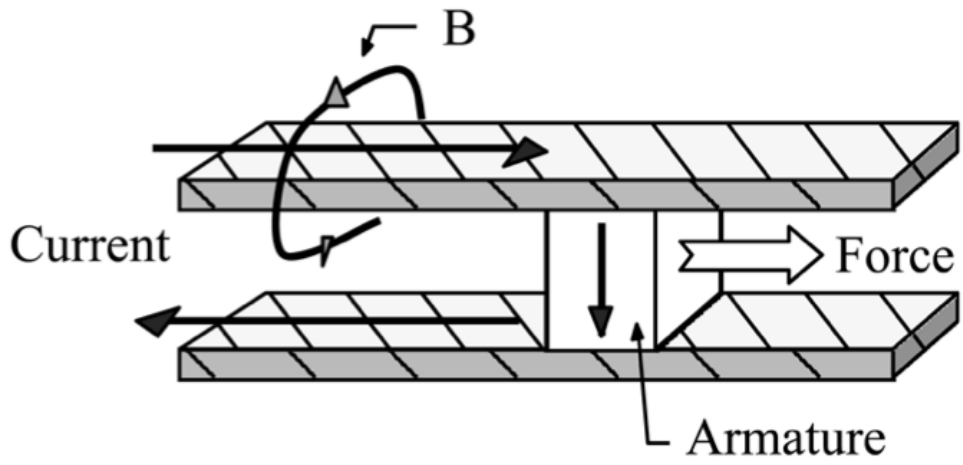

Figure 2: A conventional railgun setup. The rail and projectile with current flow of a conventional railgun [12].

Augmented railguns use many rails in parallel. Only the inner two rails contact the projectile and the result of the current flowing through and around the system is much stronger magnetic fields in bore. This creates stronger forces to push on the projectile. Augmented railguns have much higher inductance gradients than conventional railguns. See Figure 3 for the current flow in an augmented railgun. Augmented railguns present challenges due to the increased complexity of the mechanical structure required to accommodate for multiple rails in parallel.

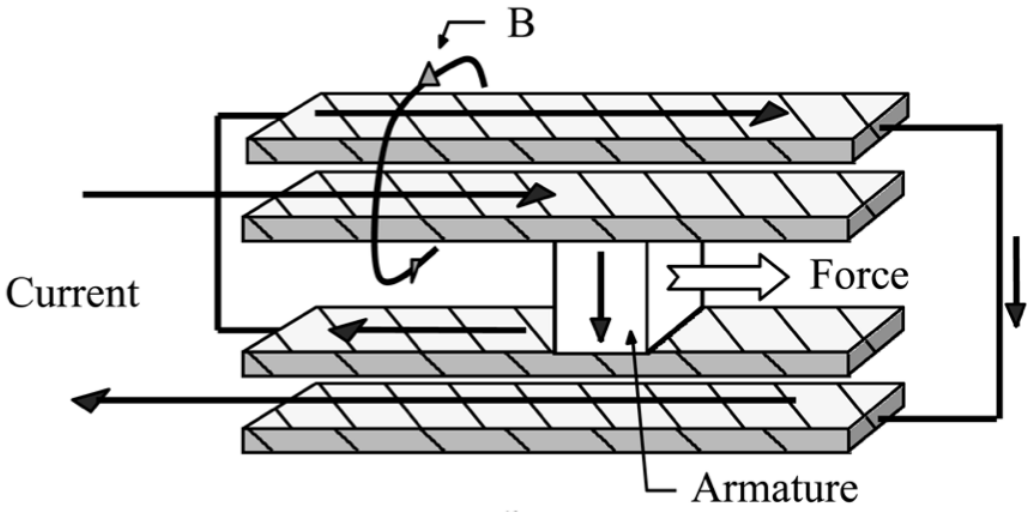

Figure 3: An augmented railgun setup. The rail and projectile with current flow of an augmented railgun. The current flows through several pairs of rails creating a stronger magnetic field in the bore. Only the inner two rails interact with the projectile. The parallel rails are separated by strong insulating material to prevent shorting and structural failure. [12].

Coaxial Railguns have a barrel configuration that is circular rather than flat parallel rails. The current flows throughout the entire barrel, into the cylindrical projectile, and out through the back of the projectile through either a plasma channel or a long metal rod. Coaxial railguns are advantageous over parallel railguns because the current distribution is much more uniform and the inductance gradient L' is easily increased by changing the radius of the projectile. Coaxial railguns are not practical for weaponized applications because of the limitation of the projectile design. However, they seem applicable as possible orbiting launchers for interplanetary mission probes [25].

3 Railgun Power Supplies

Railguns require tremendous amounts of current delivered within milliseconds to generate the necessary magnetic fields. High energy pulsed power supplies are used to store energy and then discharge it into the railgun. Most of the time, large banks of capacitors are used to store electrical energy. A switching mechanism which can handle the large current is used to release the energy into the railgun. Common components are solid state switches such as thyristors or spark gap switches. Inductors are used to condition the current into an optimum pulse for the railgun at hand. Table 2 compares some different pulsed power supply configurations [3, 20, 13, 5]. If the operating voltage of the capacitors is known is it included next to the number of capacitors.

Table 2: Comparisons of Railgun Power Supplies

Railgun	Number of Capacitors	Stored Energy	Switching
Powerlabs 2.0	32 (450V)	20kJ	none (injection)
Cal Poly Mk 1.0	16 (450V)	16kJ	none (injection)
Cal Poly Mk 1.1	16 (450V)	16kJ	Ignitron Switches
Cal Poly Mk 2.0	2 (9kV)	67kJ	Spark Gap Switch
GA Blitzer	unknown	2MJ	Solid State Switches
GA/Navy	>200 (11kV)	9MJ	Solid State Switches
BAE/Navy	29 banks (11kV)	>32MJ	unknown

Chapter 3

Current Problems with Railguns

Currently railguns are not deployed by the Navy[1] and they are not used for orbital debris testing. Several unresolved problems are holding the technology from being reliable and practical. So far, researchers have not been able to fully mitigate the damage and deterioration railgun barrels suffer with each firing. Railguns cannot be practical systems with operational longevity until the damage which occurs in the barrel is greatly reduced.

1 Types of Damage

The extreme conditions inside of the bore during firing cause deterioration of the rails and the projectile. In their ongoing research the Navy has classified three main types of railgun damage inside the barrel of the gun: gouging, arcing and deposition.

[1] General Atomics has recently delivered a prototype of a weaponized railgun to the Navy, so ship-borne railguns are progressing towards operational status.

1.1 Gouging

Gouging is removal of barrel material by the projectile. It is caused when the projectile digs into the rails with a strong enough force to deform and embed into the rail material. Gouging occurs when contact between the bore and projectile is not evenly flat or when the size of the bore varies down the length of the rails. If the bore has a pinch point somewhere down the barrel where it gets smaller by a few thousandths of an inch, the leading edge of a moving projectile will dig in and try to remove those few thousandths of an inch of barrel material.

It is worth noting that gouging is also caused by the rail material being softer than the projectile material. In conventional firearms it is the opposite; the barrel material is much harder than the projectile material. Rifle barrels are often made with Chrome-Molybdenum lined steel while bullets are made of lead or have a soft copper jacket. The bullet is made to be slightly larger than the bore to ensure that there is a seal between the bullet and bore. The projectile has to compress to fit the bore and there is essentially no damage to the barrel. In railguns, electrical conductivity of the materials used is most important and rail materials are chosen accordingly. Copper and its alloys are the most common rail materials because of their high electrical conductivity. Also, the densities of the projectiles is sought to be as low as possible so that they are easier to accelerate. Hence, aluminum is a common choice for projectile materials. Aluminum is harder than copper so therefore the rails sustain gouging damage. If one were to make the rails out of aluminum and the projectile out of copper, gouging damage would be mitigated, however the lower conductivity of the rails and the heavier mass of the projectile would cause serious if not mission critical efficiency losses. Often alloys like copper-chromium are used for rail material due to their increased hardness,

but there is always a loss in conductivity when straying from the most copper-pure alloys. With regards to the orbital debris impact testing application, since a majority of the space debris environment is made of aluminum or has the average density similar to aluminum, it makes sense to use it as the projectile material.

Gouging was not seen in the Cal Poly Mk 1 firings because after the projectile was injected into the rails it instantly began to melt and soften due to poor contact. In preparation for static testing on the Mk 1.1, as described in section 3, gouging was seen from simply pushing the projectile down the bore with push rod. Inconsistencies of <0.003in in the bore and <0.001in on projectiles were enough to cause serious gouging in several points in the bore. When a projectile gouges into the rails there is a tremendous force against it. This force slows the projectile down, limiting the railgun's efficiency.

1.2 Arcing

Arcing damage is the damage done to the rails when electrical arching occurs between the rails and projectile. When contact is poor and there is a small gap between a projectile and rail the electromagnetic field may be strong enough to jump the gap and make an arc. When an arc jumps from the rails it causes small pitting at each point where the arc formed. Often, arcing occurs in great quantities when large plasma plumes form inside the barrel from poor contact and huge currents. Arcing damage was seen in the Mk 1 close to the muzzle end of the gun. Since the projectile lost around half of its mass from melting, as described in the next section, and therefore had a smaller cross sectional area, the current jumped the gaps between the projectile and the rails. The Mk 1 firing also saw large plasma plumes confirming that there was arcing between the rails.

Figure 4 shows the resultant pitting from arching on the muzzle end of a Mk 1 rail after a firing.

Figure 4: An example of transition damage. Arcing damage seen on the muzzle end of one of the half inch wide Mk 1 rails.

Since only the center quarter inch wide section of the rail interacts with the projectile and the rest is covered by insulating material, pitting is only found in the center of the rails.

1.3 Deposition

Deposition damage is the most harmful damage to the rails, projectile, and overall performance. It is when projectile material is deposited onto the rails due to melting or peeling. When aluminum melts onto the copper rails it can penetrate and ruin the smooth finish of the copper. While liquid, the aluminum can act as a conducting lubricant. However, once it solidifies it leaves a thick,

flaky, porous and uneven coating on the rails [8, 10]. As mentioned earlier, the precision required for decent performance on the rails and projectiles is very high and the deposition of aluminum coating can make a railgun unfirable.

Better contact can help mitigate deposition damage, but only to a certain degree. If a projectile has perfect contact over its entire surface area the current will still only flow through the back end of the projectile, as discussed later, and cause ohmic heating and melting. However, having poor contact and smaller contact area only increases and quickens the melting.

The Mk 1 saw tremendous amounts of deposition damage. This is because the projectile never had good contact to begin with. Since there was no trigger system on the Mk 1 the projectile was injected from a nonconducting housing into the rails, which were at 450 volts. Since the projectile completed the circuit, the instant one of its corners touched the rails and completed the circuit, melting began. The projectiles also did not have the precision that was necessary and never had good contact upon entering the bore. After firing the Mk 1 rails had aluminum heavily deposited on more than a third of their length on the breech side. Since the current pulses which ran though the gun rose quickly and decayed exponentially, most deposition is seen in the regions where the current was around its peak value, which is near the breech. On the muzzle end where the current was near zero and projectile had already lost approximately 50% of its mass arcing damage is seen instead of deposition. Figure 5 shows the deposition damage on one of the Mk 1 rails and a comparison of a fired projectile and a new one.

Figure 5: An example of deposition damage. Deposition damage on the breech end of a rail and the resultant mass loss of a projectile.

The fired projectile in Figure 5 seems to have maintained a flat surface on one of its sides and seems to have melted mostly on its other side. The curved bit at the front is from the impact of the projectile with the target backstop.

2 Velocity Skin Effect

The contact velocity skin effect (VSEC) is the phenomenon of concentrated current flow though projectiles. It is the major cause of most railgun problems and is one of the main factors limiting a railgun's efficiency. When the current flowing though the rails encounters a projectile it attempts to flow through the back of the projectile. With enough time, and given proper magnetic properties of the rails and projectile, the current and magnetic fields will eventually diffuse and the current will spread out over the entire contact surface area. When current flow is idealized in a railgun it said to flow through the entire area of the projectile as seen in Figure 6. In reality, most of it flows through the back of the projectile. When

current flows through a smaller area than the projectile has to offer the resistance seen by the rails and the heating and melting of the projectile is increased.

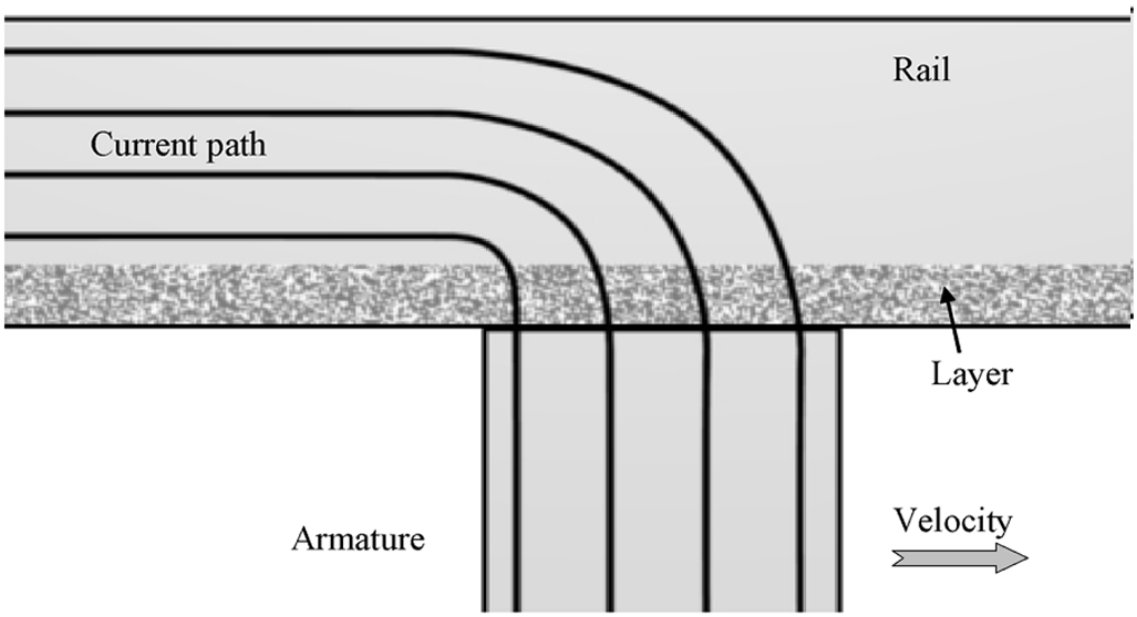

Figure 6: A display of idealized current flow. Idealized or steady state current flow which diffuses through the entire contact interface between the projectile and rails is shown. The layer in this figure refers to the very thin contact interface between the projectile and rail and its thickness is greatly exaggerated [12].

At higher velocities the current gets pinched in the back even more and it does not have time to diffuse. Comparing Figures 7 and 6 shows the difference in ideal steady state flow and actual flow in a moving projectile. At high velocities VSEC can cause 80% of the current to flow through the back of the projectile. The quick heating of the projectile can almost instantly pass the melting temperature of aluminum causing projectile to melt at the interface.

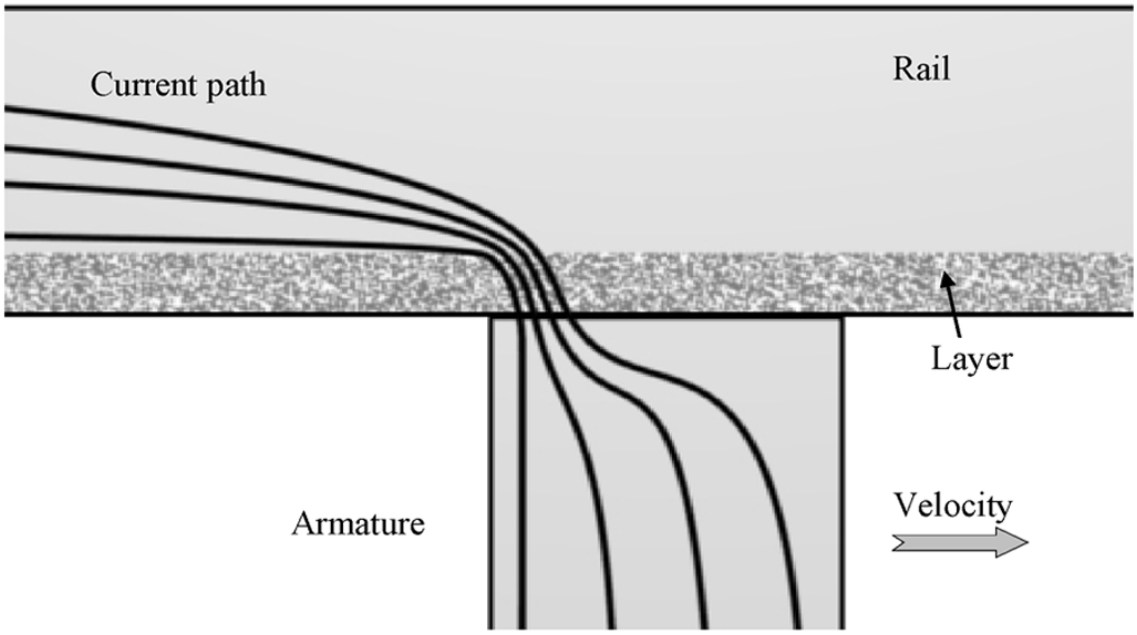

Figure 7: A display of velocity skin effect current flow. Pinched current flow caused by VSEC and high projectile velocity is shown. This effect is increased at higher velocities. [12].

Since this effect increases with velocity, higher performance railguns have to deal with more current build-up and melting. The simulations discussed in chapter 5 aimed at minimizing the harmful effects of the velocity skin effect.

Chapter 4

Interface Coatings

Interface coatings are layers of material between the rail and projectile. Interface coatings can be used to protect the rails from melting aluminum, reduce the amount of friction, and control the amount of current build up at the back of projectiles. Interface coatings need to be conductive in order to let the current pass from the rails through the projectile. This chapter explores two different interface coatings: solid lubricating graphite and a liquid metal alloy. After going over important measurements of each coating static test firings done with the coatings are discussed.

1 Graphite Interface Coating

Graphite was chosen as a coating to study because of its lubricating properties along with the fact that it conducts electricity. If applied on the rails, graphite can reduce the coefficient of friction from 0.28 (aluminum-copper contact) to 0.16 (aluminum-graphite contact)[15]. If graphite is also applied on the projectile then the graphite-graphite contact coefficient of friction can reach as low as 0.10. But

since the graphite on the projectile would be removed quickly, the aluminum-graphite contact would occur for most of the time in the bore. Also, since adding a resistive layer between railgun rails and projectiles is known to help mitigate the velocity skin effect and the amount of current build up[1] and heating a graphite coating was worth exploring [26]. An aerosol graphite lubricant made by Asbury Carbons was chosen to be evaluated. See Appendix C for material data of the graphite product used.

In order to characterize its application in a railgun system, properties of the coating needed to be examined. These include the thickness of the coating and amount of resistance added. When discussing resistive layers between rails and projectiles they are often called "high resistance layers." It is important to note than when the word "high" is used in this context it still means within the high range of conductivity of conducting metals. A common material used as a resistive layer is titanium which has a resistivity of $42\mu\Omega\cdot$cm compared to $1.7\mu\Omega\cdot$cm of copper. In the larger scheme of things this is still very conductive. However, something that is truly very resistive compared the resistances of the materials in railguns could seriously limit the amount of current flowing through the system. Also, the more resistive a material the hotter it will get and possibly a lesser amount of current is needed before the material breaks down. For this reason it is important to see exactly how much resistance the coating adds. In the following sections the measured contact resistance of regular projectiles of different quality and ones coated with graphite is discussed. Also, the thickness and surface of the graphite coating was examined using scanning electron microscopy and profilometry.

[1]The mitigating of current build up using a resistive coating is simulated in chapter 5.

1.1 Projectile Contact Resistance

Contact resistance, the resistance between two contacting materials, is an important quantity to keep track of in a railgun system. It is caused by non-ideal contact of materials which restricts current flow to specific paths rather than allowing it to run through entire surface areas. Contact resistance is added on top of the intrinsic resistance of system materials. In all railguns there is contact resistance between the barrel and the projectile. In this case the projectile contacts two rails on two of its faces. Since the efficiency of a railgun system is heavily dependent on the lack of resistance throughout its components it is important to limit contact resistance. It is this reason why highly conducting pastes or lubricants are used in static electrical connections.

The contact resistances of the Mk 1 projectiles were measured to better understand the system and to later compare to the effects of a graphite film application on the projectile and rails. Since the resistances dealt with are very low ($\ll 1\Omega$), a four wire resistance measurement is needed. A four wire measurement uses two more wires than a regular two wire measurement to carry a separate force current. The two other wires measure the voltage drop across the object being measured which has the force current running through it. Since the current is decoupled from the measurement wires the inherent resistance of the test leads is not included in the measurement.

Figure 8 shows the system used to measure the contact resistance. In order for the current to diffuse two pieces, 3.875in and 2.91in long, with a cross sectional area of 1in^2 were used. The pieces were faced off on a mill and then carefully wet-sanded with 1500 grit sandpaper to ensure a smooth contact surface.

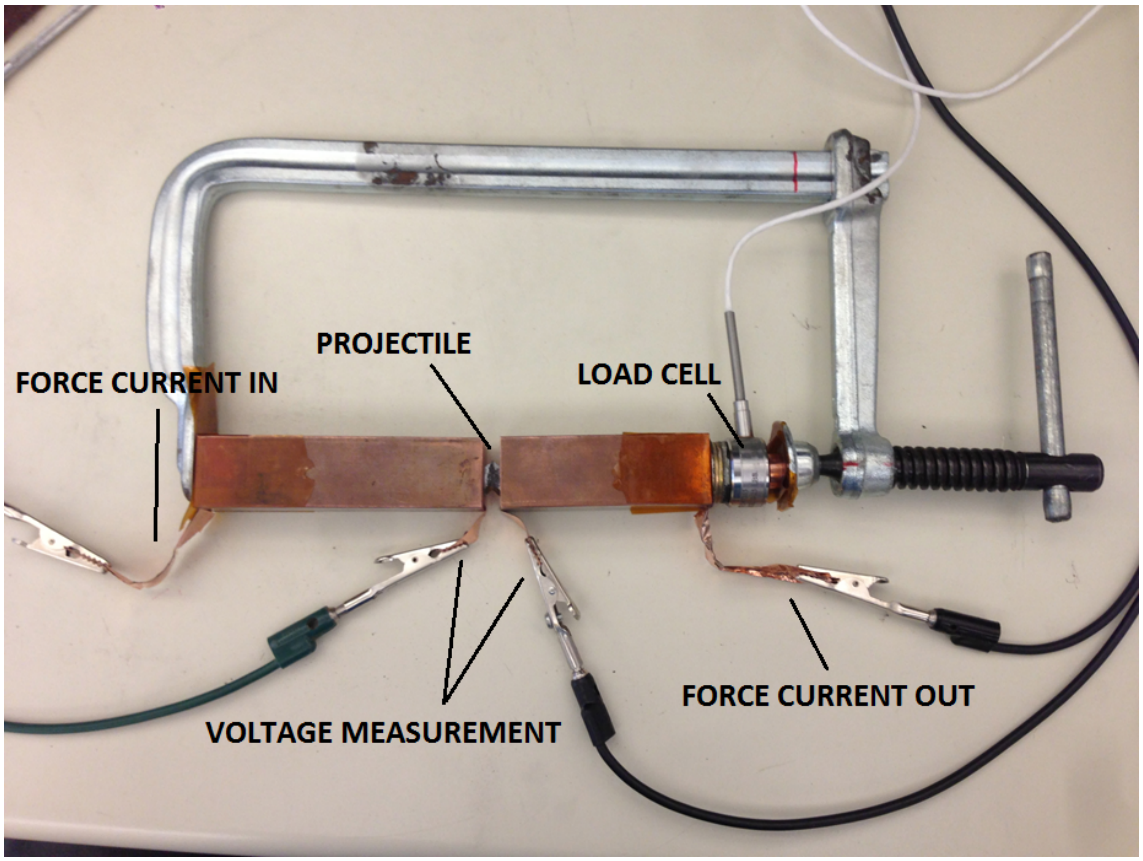

Figure 8: The setup for measuring projectile contact resistance. The clamp holds the copper blocks, projectile and load cell together. The two outside wires run the known constant current through the system. The two inside cables measure the voltage on the contact face. The load cell on the right measures the force on the copper blocks which can be translated to pressure on the projectile.

The copper pieces needed to be longer than wide so that the current would diffuse throughout their entire cross sectional area along the length and then pinch down through the entire cross sectional area of the projectile. To ensure this was happening the current flow of the setup was modeled in COMSOL Multiphysics and confirmed to be as desired, as seen in Figure 9.

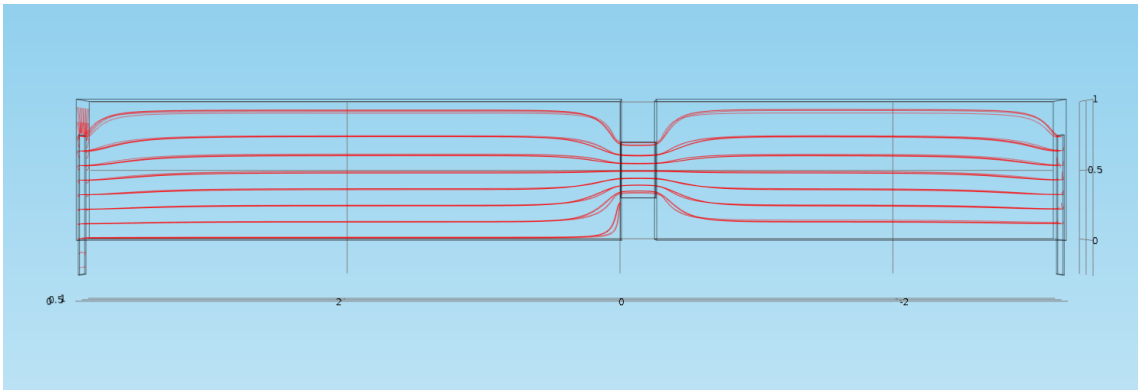

Figure 9: Current flow simulated in COMSOL. This shows that the copper pieces are long enough to diffuse the current so that it flows though the entire cross sectional area of the projectile.

As a check the four wire measurement was used to measure the resistance of the long copper block. Knowing the dimension of the copper and the resistivity of the 110 alloy (1.72$\mu\Omega$·cm) the resistance of the piece can be calculated to 2.6$\mu\Omega$. When measured by the four wire measurement the reading was oscillating between 0.002mΩ and 0.003mΩ with the value being at the last digit of accuracy of the Agilent U3606A meter. This confirms the measurement is accurate to 1$\mu\Omega$.

When measuring a projectile, both pieces of copper were used and a projectile was sandwiched between them. The copper pieces were put into C-clamp and the pressure was monitored by a load cell. It is important to note that contact resistance is dependent on pressure. As pressure increased the contact resistance decreased.

Two different aluminum alloy projectiles were used. Three projectiles were made out of 6061 aluminum with a resistivity of 4.06$\mu\Omega$·cm and three out of 2024 alloy with a resistivity of 5.7$\mu\Omega$·cm. The Al 2024 was used because it was the alloy with the best tolerances available from the supplier. The Al 6061 projectiles were previously made for the Mk 1 railgun. Table 3 summarizes their dimensions

and expected volumetric resistances. Projectile 1-3 had ideal flat faces while 5-6 were either poorly sanded or machined. The width dimension is the one between the rail contact faces of the projectile.

Table 3: Properties of the Projectiles Measured

Projectile	Summary	Material	l × w × h (in)	Resistance ($\mu\Omega$)
1	Super Flat	Al 2024	.419 × .249 × .250	5.33
2	Super Flat	Al 2024	.411 × .249 × .250	5.44
3	Super Flat	Al 2024	.381 × .249 × .250	5.87
4	Unsanded Mk 1	Al 6061	.352 × .248 × .251	4.49
5	Unsanded Mk 1	Al 6061	.360 × .248 × .250	4.40
6	Sanded Mk 1	Al 6061	.350 × .245 × .250	4.48

Since the resistance of the projectiles were so low the contact resistance was expected to be the major contributing factor in the resistance at the projectile rail interface. Between each measurement the projectiles were taken out and put back in between the copper pieces in a slightly different orientation. There was variation between each measurement, especially with the 6061 projectiles. This is because the 6061 projectiles had different degrees of smoothness on their contact faces. Projectile six had been sanded with fine grit sandpaper and inconsistently applied sanding pressure caused there to be a variance of about $\pm$0.0005in on its faces. Upon close inspection two different planes could be seen on the contact face. Projectiles four and five were made using the old cutting process used to make the Mk 1 projectiles. In the process the contact faces required two cuts and the projectiles had to be removed and placed on its other side in the jig causing inconsistencies of several thousandths on their faces. In comparison to projectile six the different planes were parallel. Figure 10 shows projectile four in between the two copper blocks with a good amount of pressure. However, a gap is easily seen between the right face of the projectile and the right copper block.

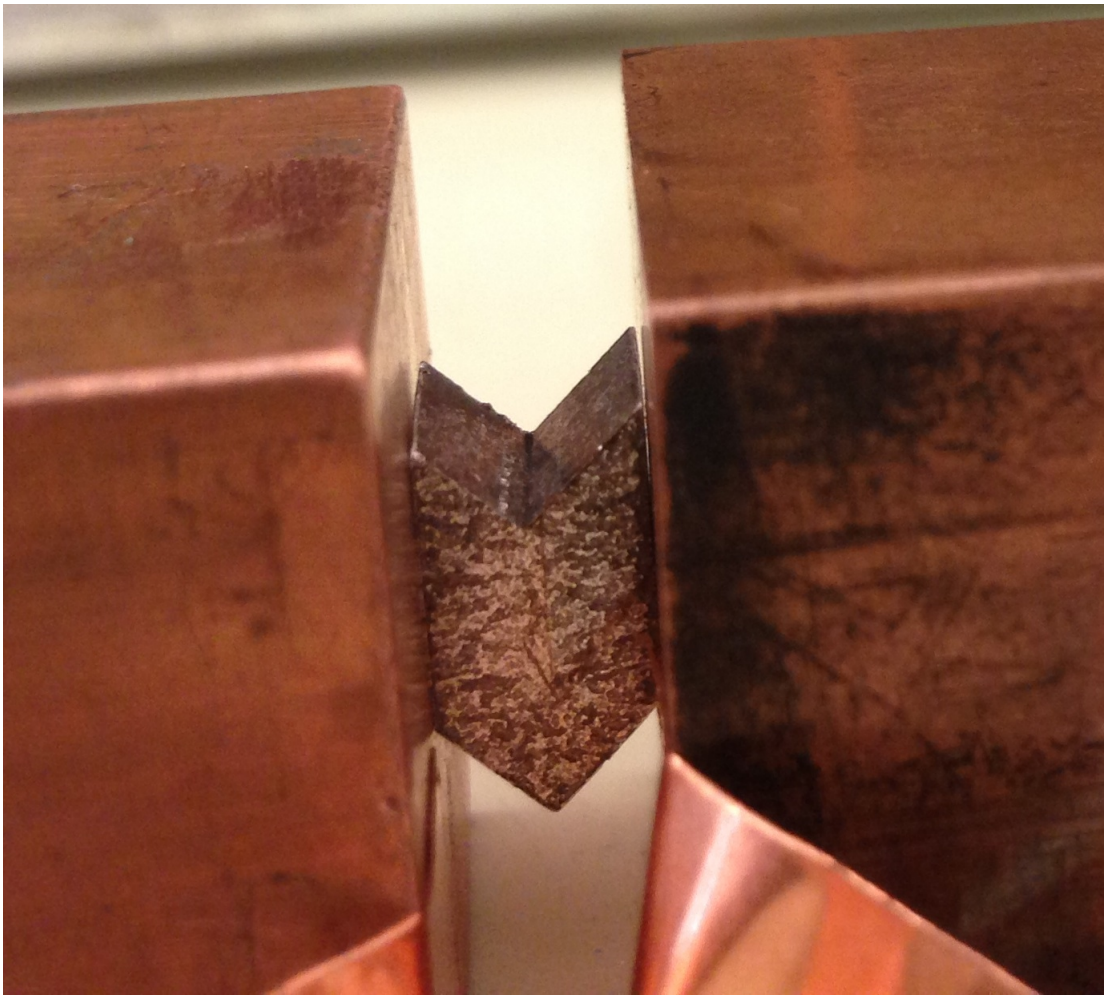

Figure 10: A gap between the right face of the projectile and copper block used for four wire measurement. The dark spotting on the projectile is from a previous application of graphite.

The projectiles made out of Al 2024 were the smoothest. Even though Al 2024 is a little more resistive, it was chosen because it had a tolerance of .002in along a 6ft long piece. When the stock was cut up into smaller $\frac{3}{8}$in projectiles the surfaces were essentially an "exact" 0.249 or 0.250, depending on which two of the four square faces were chosen as contact faces. Figure 11 shows the contact resistance of projectile one as a function of pressure in four different pressings. Since the load cell provided the force on it in pounds the contact area of the

projectile was used to convert the force to psi.

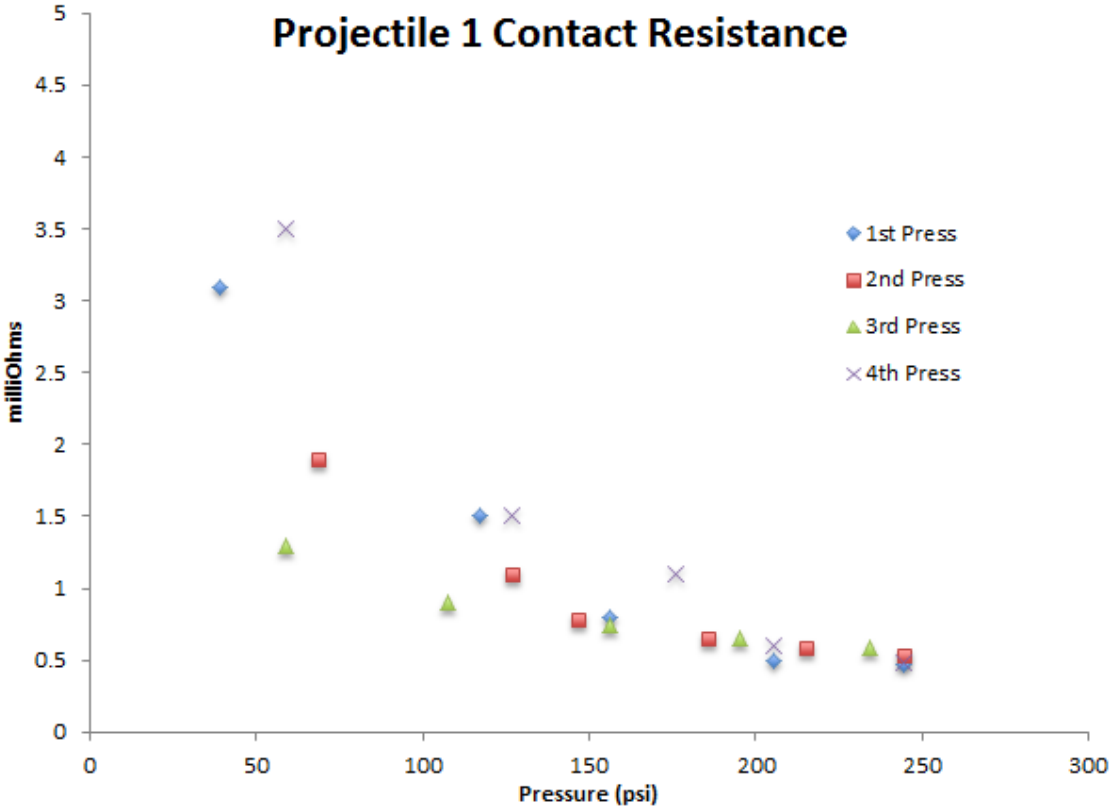

Figure 11: Contact resistance of a flat projectile as a function of pressure. Each data series is a different pressing of the projectile between the two copper blocks. The resistance converges at higher pressures between each press because of the super flat surface.

The data for the other Al 2024 projectiles looked the same. The great smoothness of this projectile (along with projectiles two and three) is the reason there is so little variation at higher pressures. The contact resistance of projectile five, a projectile with an uneven surface, is shown in Figure 12. This time there is much more variation between each pressing.

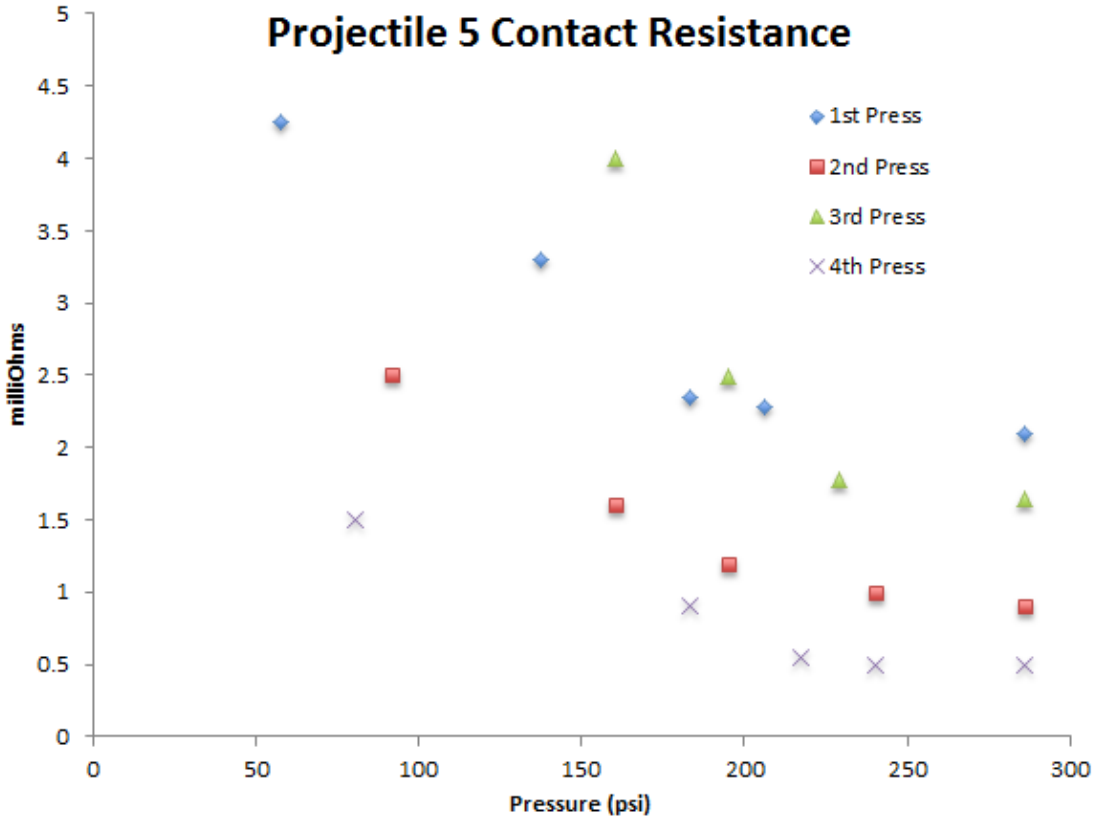

Figure 12: Contact resistance of an uneven projectile as a function of pressure. Each data series is a different pressing of the projectile between the two copper blocks. The resistance varies so much due to the imperfect contact surface.

The variations make it clear that contact resistance is not constant and is greatly dependent on the quality of the contact faces. Projectile six, which had a variation of one thousands on non parallel planes had the worst range of contact resistance, reaching up to $100m\Omega$ at low pressures..

It is worth noting that greatly increasing the pressure on the clamp did show a significant decrease of contact resistance of all the projectiles. The range of pressures in the previous plots was limited to the amount of force the load cell could handle without being damaged. In the case of the load cell used the maximum was 25 pounds. To see how low the contact resistance could go, for each projectile

the load cell was removed and the clamp was tightened as much as possible, until the system buckled from the pressure. Table 4 lists the lowest contact resistances measured for each projectile. Since there is no force measurement there is no way to know what the respective pressures were for these low resistances. The error on all the values in Table 4 is on the order of 0.01mΩ.

Table 4: Lowest Measured Contact Resistances for Plain Projectiles

Projectile	Resistance (mΩ)
1	0.13
2	0.11
3	0.10
4	0.17
5	0.19
6	0.21

As expected, the flatter projectiles had the lowest contact resistances. These contact resistance are still several orders of magnitude higher than the volumetric resistance of the projectiles. These low contact resistances are great but trying to have as much pressure as possible may not be a useful measurement. In the railgun the normal force and pressure on the projectile from the rail cannot be too high, otherwise the Lorentz force would not be strong enough to overcome it and move the projectile.

1.2 Conductivity of Graphite

Graphite in its solid and basic form is anisotropically conductive: it conducts electricity differently depending in which axis the current is trying to flow. The conductivity can be three orders of magnitude less in the plane perpendicular to the layer plane because the distance between the planes is larger than the distance between the individual atoms in the planes. While graphite does have

a published conductivity it is not a value one finds in all instances, rather it is the best conductivity one can get out of graphite. Even in the best case graphite conductivity is several times lower than that of copper or aluminum. Table 5 compares the conductivity of some of the materials used in the railgun [2, 9, 14, 23, 24]. The values listed for graphite are in a range because they vary with the specific molecular structure of the graphite.

Table 5: Conductivity and Resistivity of Materials Used

Material	Conductivity ($10^6 S/m$)	Resistivity ($\mu\Omega \cdot cm$)
Copper	60	1.72
Aluminum	36	2.8
Eutectic Indium Gallium	3.4	29.4
Graphite	2.5-11	9-40
316 Stainless Steel	1.3	74.9

While it might conduct well in the sheet plane it can, as mentioned before, conduct poorly in the other plane. This feature can be a benefit and a detractor in using graphite as the interface between the barrel and projectile. If graphite is applied in such a way that it conducts well in the plane perpendicular to the rails then current is more likely to flow straight down through it rather than horizontally. Since current flowing in the y direction is the component which contributes to the force vector down the bore this straightening of the current is beneficial. However, if the direction of conductivity cannot be controlled in the application then the coating, as thin as it may be, may be too resistive and limit the current flowing through the system. In order to maintain favorable efficiencies of the system, the resistances in the system must remain low. The $\sim$10mΩ resistance in the Mk 1.1 system ignitron switches was enough to limit the current so much that the lorentz force could not overcome even the most conservative frictional forces, resulting in a projectile which did not move.

One of the hopes of using the synthetic graphite dry conductive lubricant provided by Asbury Carbons was that the particles, being smaller than a micron, would deposit themselves in such a manner that there would be a uniform conductivity on the rails.

In the measurements done for this work the volumetric resistivity of graphite was not measured. Like in the case of the projectiles where the contact resistance greatly overshadowed the volumetric resistance, the contact resistance of the graphite was measured instead. Volumetric resistivity is in units of $\Omega \cdot m$ and is multiplied by the length and divided by the cross sectional area of an object to get its resistance. An increase in length causes an increase in resistance while a larger cross sectional area causes a smaller resistance. Contact resistance is in units of $\Omega \cdot m^2$ and is divided by the cross sectional area to get resistance; the thickness is not included.

The contact resistance was measured in the same way as in section 1.1 but with 2 ± 1 coatings of graphite applied to each contact face of the projectiles or copper blocks. The data behaved in the same way: the contact resistance decreased as pressure was increased. Figure 13 shows the same behavior of the contact resistance on the flat projectile as in section 1.1 however the scale of resistance went up to tens of $m\Omega$ rather than fractions of $m\Omega$.

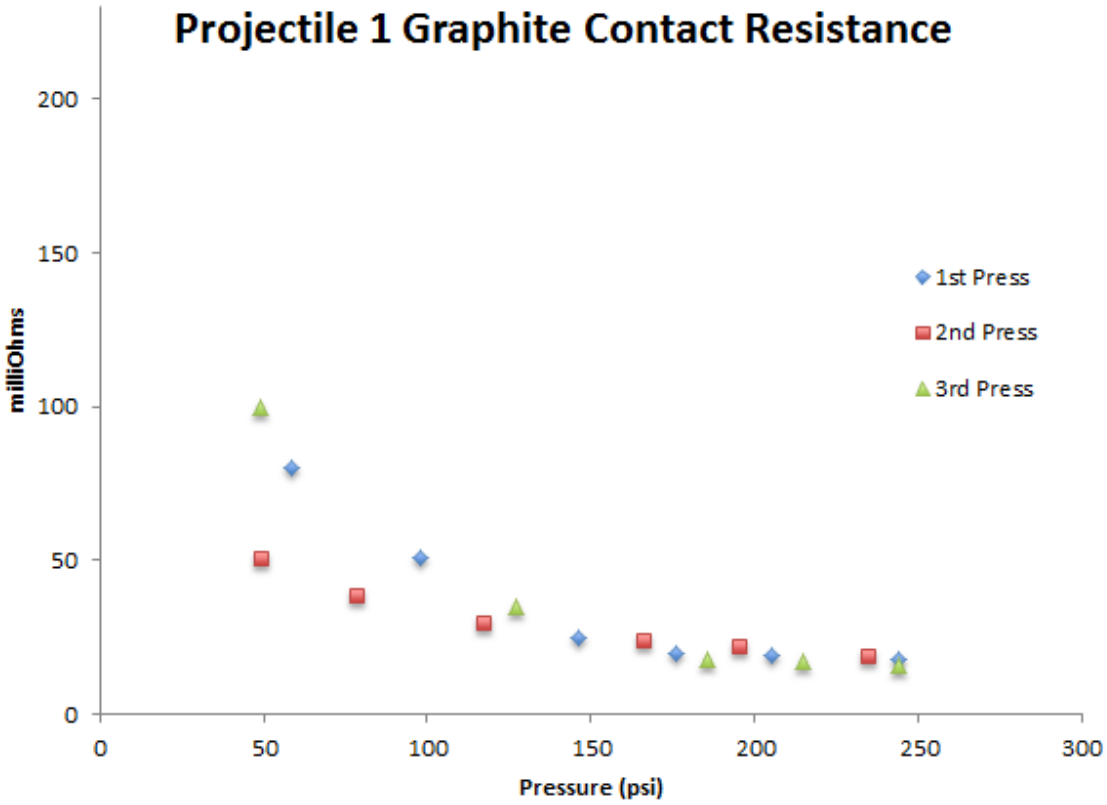

Figure 13: Contact resistance of a flat projectile with a coating of graphite as a function of pressure. Each data series is a different pressing of the projectile between the two copper blocks. The resistance converges at higher pressures between each pressing because of the super flat surface, but is an order of magnitude higher than when measured without graphite.

Once again, projectiles with very flat faces showed the same contact resistances at higher pressures during different pressings. The contact resistance of projectile five, a projectile with uneven contact faces coated with graphite, is shown in Figure 14.

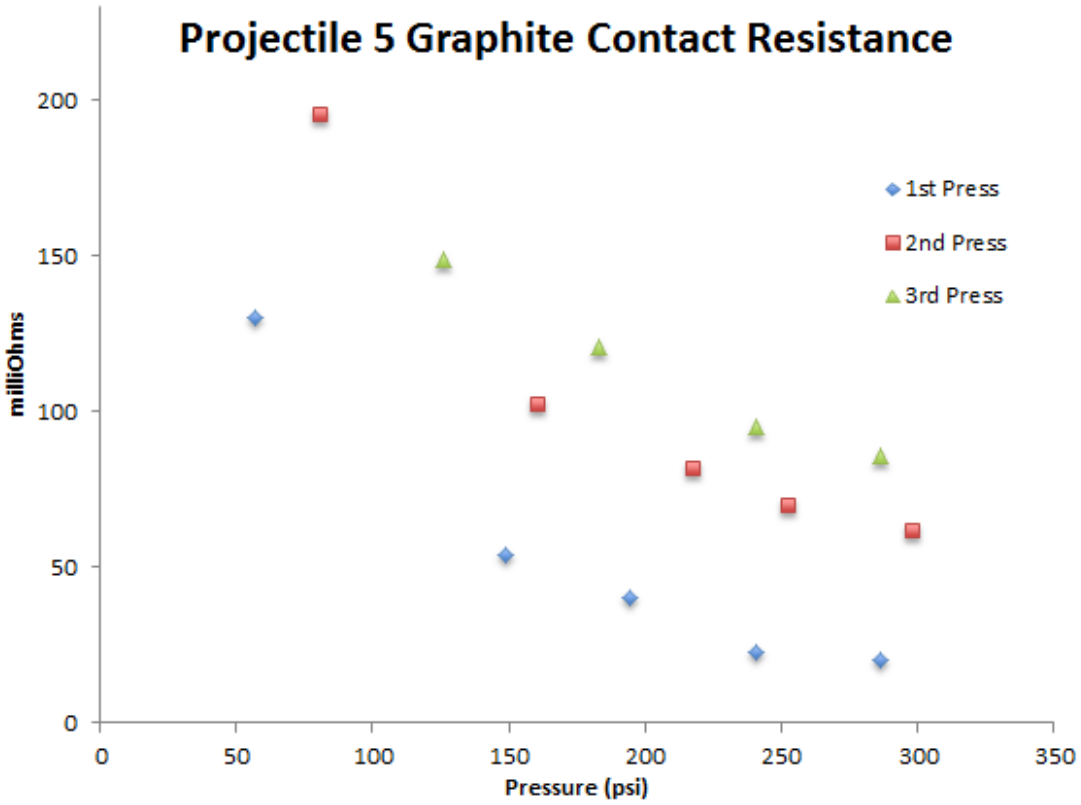

Figure 14: Contact resistance of an uneven projectile with graphite as a function of pressure. Each data series is a different pressing of the projectile between the two copper blocks. The resistance varies each time the projectile is put in due to the imperfect contact surface.

It is clear that within the range of pressures tested the contact resistance was higher than the amount of resistance in the ignitron switches which caused the failure of the Mk 1.1 system. However, this does not mean graphite is unusable. The larger a railgun system and the currents that run through the larger the allowable resistances. Even though in the small Mk 1.1 system 10mΩ was enough to cripple the system, in larger systems the amount of resistance added by the graphite might be well within acceptable limits. Also, the larger the bore and the projectile the bigger the contact surface area. Since contact resistance decreases with contact area larger bore railguns could very easily use a graphite coating with seriously affecting the system efficiency.

As before, the lowest contact resistance with graphite was measured by taking out the load cell and tightening the clamp as much as possible. See Table 6 for the results.

Table 6: Lowest Measured Contact Resistances with Graphite

Projectile	Resistance (mΩ)
1	1.6±.1
2	1.3±.1
3	2.9±.1
4	6.6±.1
5	8.3±.1
6	16±2

The values are only about ten times higher than when the projectiles were not coated, but once again these resistances were achieved with great pressures on the clamp that might not be representative of the pressures inside of a bore.

1.3 Graphite Film Thickness

The thickness of the graphite coating needed to be measured to know how it compared to the variances in bore thickness. The materials data for the graphite, which can be found in Appendix C, indicated that the graphite particles were smaller than a micron in size. Initial attempts at applying a coating to a piece of copper and measuring the thickness with a micrometer failed, indicating that the coating was thinner than a fraction of a thousandths of an inch. In order to measure the thickness of the very thin coating equipment from the Cal Poly Materials Engineering Department were used. First, a scanning electron microscope was used to look at the border of the graphite film and the copper. Then a profilometer was used to measure the roughness and thickness of the coating accurately.

1.3.1 Electron Microscopy of Graphite Coating

A Quanta 200 series scanning electron microscope was used to look at the graphite coating on copper. See Appendix C for its specifications. The first measurements were done on a piece of copper with one coating of graphite. The graphite was discretized into coatings of quick passes with the aerosol can until the surface was covered entirely. Figure 15 shows one of the two prepared samples with graphite on one half of the sample. Masking tape was used to mask off half the sample.

Figure 15: SEM sample one with a graphite coating. The sides of the copper are .5in wide.

Upon looking at the sample with the SEM it was discovered that the film was so thin that it adhered in the surface features of the copper without filling in the valleys and grooves. Figure 16 shows the surface topography of the copper with one coating of graphite. As shown later this coating is less than a micron thick.

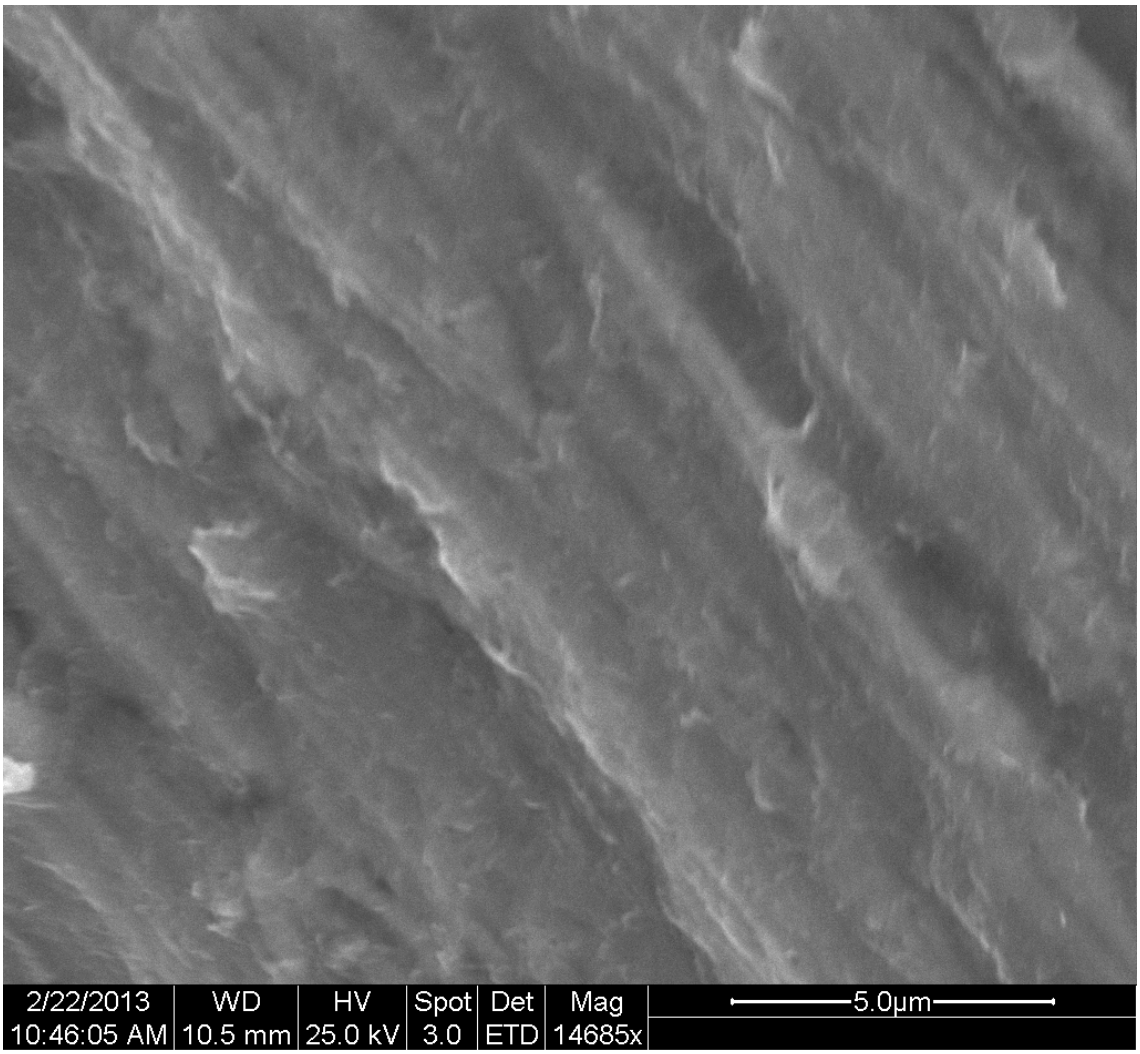

Figure 16: The surface topography of one coating of graphite. This is seen with approximately 15000x zoom. The surface features of the copper are clearly visible indicating a very thin coating.

It was not possible to see a discrete thickness of the graphite with this ultra thin application since the surface variations of the copper were on the same order as the apparent thickness of the coating. The thinness of the coating is evident in Figure 17 where the samples are viewed with less magnification and in back-scatter mode. The back-scatter mode of the SEM colors different parts of the sample by its elemental make-up. The back-scatter mode showed a very slight difference in color between the graphite and copper. This indicated that the film

is so thin that the SEM was also seeing the copper under the coating.

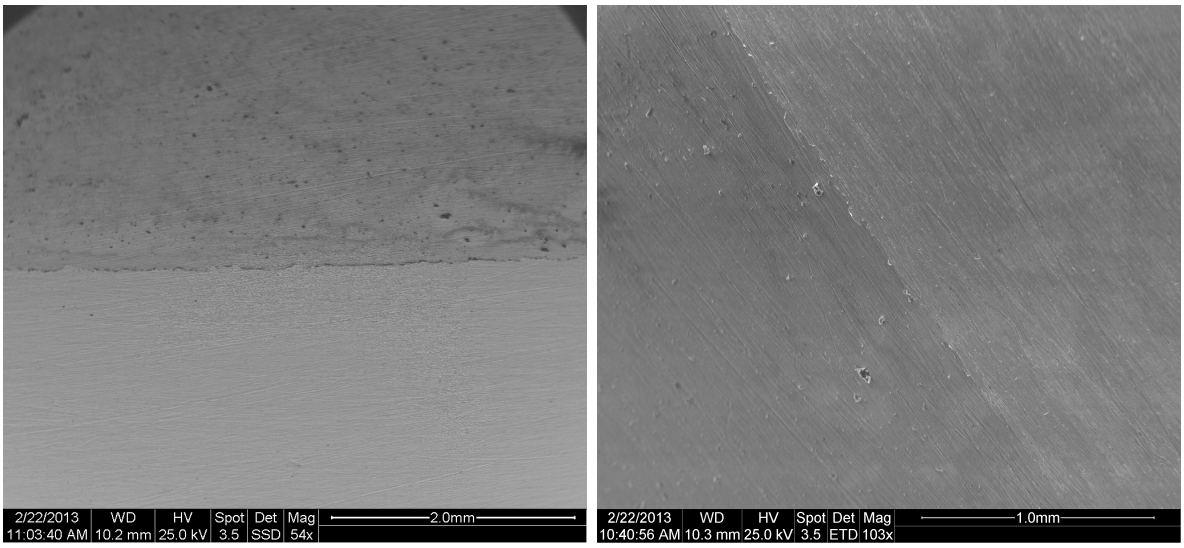

Figure 17: One coating application of graphite on copper. This is magnified 54 times (left) and 103 times (right). In the left image the copper can be seen as an even color in the bottom half and the thin graphite as the darker shade on the top half. The graphite can again be seen on the left diagonal in the right image. The very slight difference in color indicates a very thin ($<\mu$m) coating.

After not being able to measure the thickness of one coating with an SEM a sample was prepared with ten coatings of graphite. Once again half of the copper was masked off. This time the results were a lot better. In Figure 18 the border between the copper and ten coatings is much more clear.

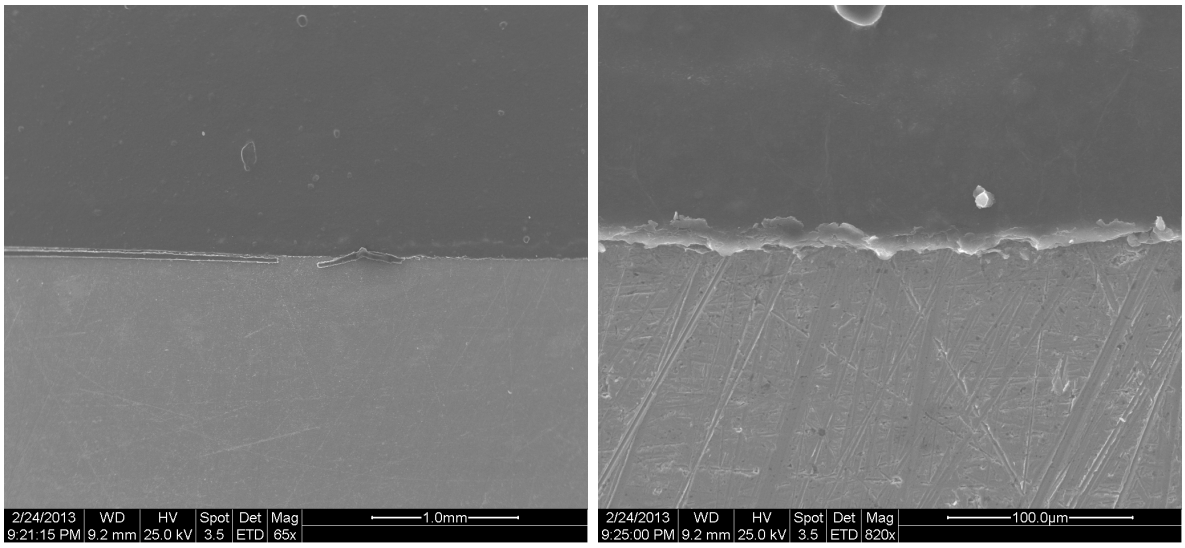

(a) 64x Magnification **(b) 820x Magnification**

Figure 18: Ten coating application of graphite on copper. This time the border is much more pronounced. The parallel line of graphite in 18a is a result of imperfect masking. 18b shows the border with more zoom. The surface features of the copper are seen. The whiter color on the edge of the graphite indicated it is higher than the darker area behind it.

When the masking tape was removed it was discovered with the SEM that it lifted and curled up some of the graphite at the border and created tall waves and lips. Since these had thicknesses and height much higher than the actual thickness it was important to find parts along the border without these lips. The samples were then looked at parallel to their surface in an attempt to see the profile of the coating. Figure 19 shows how much taller the masking lips are compared to the actual thickness of graphite behind them. The brief area without the lip reveals the approximate size of actual thickness.

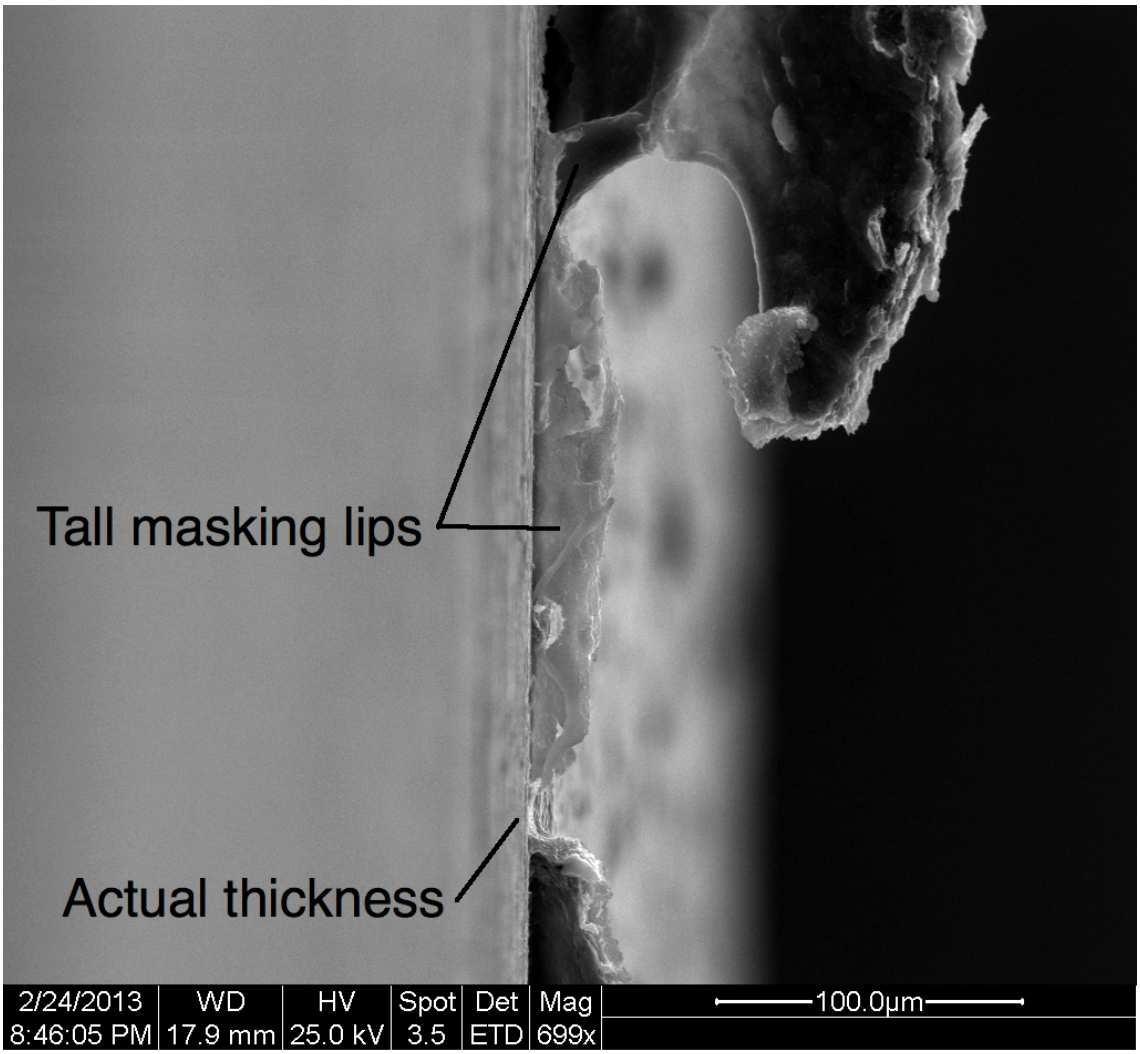

Figure 19: The border of graphite on copper. This is looked dead on at 700x zoom. The masking lip gives wrong and high measurements of thickness. A brief area without the masking lip shows the real thickness. The border is overshadowed by a large graphite feature, "The Behemoth," caused by using a thick masking tape. The copper surface is seen out of focus on the left.

By looking at the part of the border without tall lips it was estimated that that coating of ten applications was less than 10μm. For more SEM photos of the coating see Appendix A. Profilometry discussed in the next section would provide much more accurate results of the thickness which confirmed that ten coatings of graphite was thinner than 10μm.

1.3.2 Profilometry of Graphite Coating

A profilometer evaluates the roughness of a surface by dragging a very small stylus with a very small force, on the order of milligrams, over a surface and measures its displacement in the y-axis. The profilometer used was an Ambios XP1. Its specifications can be found in Appendix C

The same samples examined in the SEM were looked at with the profilometer. Three passes with the profilometer were done to each sample in different places along the length. The stylus would start on the graphite side and slowly move a distance of several millimeters until it crossed over to the copper. The data was then offset such that the flat copper was at zero displacement. The data as seen in Figure 20, was smoothed with a moving average in order to get rid of high frequency spikes. The profilometer took data every 430nm and this resolution was simply not needed.

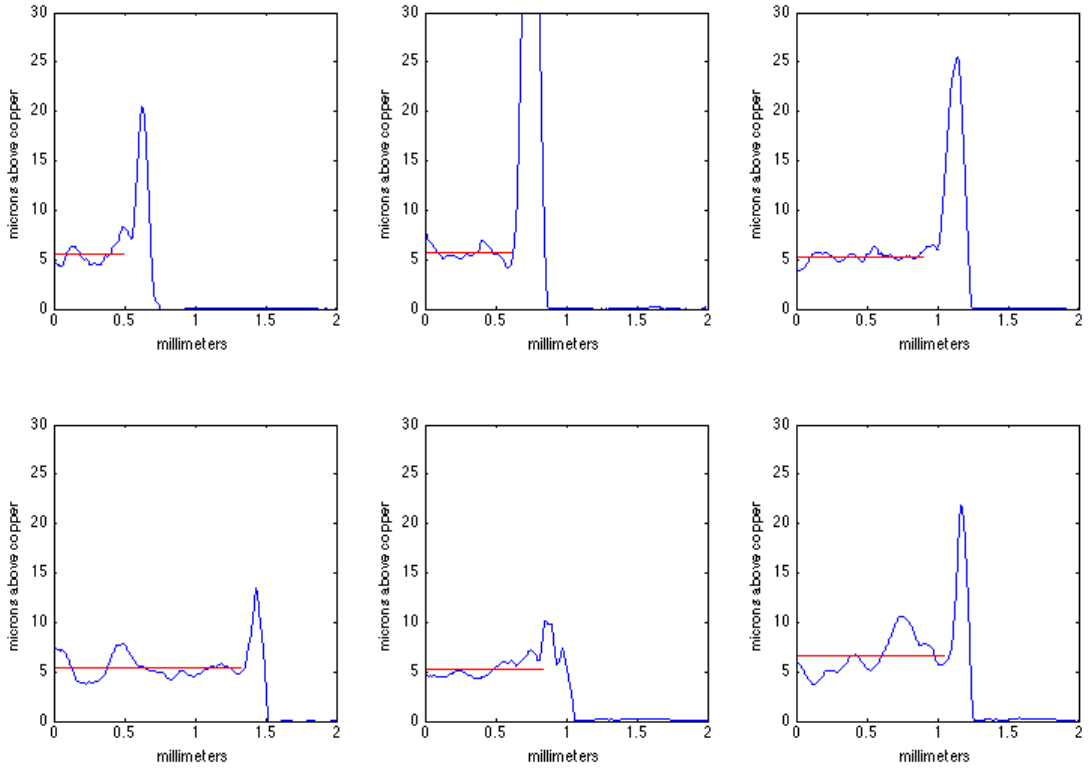

Figure 20: The thickness, in microns, of ten graphite coatings on copper. The first row is three different profilometer passes on the first sample. The second row is three passes on a second sample. The copper surface is set to be zero displacement. The mean thickness of each graphite coating up to the masking spike is plotted in red. The tall masking spikes are seen between the graphite and copper regions.

The huge spikes at the interface of the copper and graphite are the tall waves and lips resultant from the masking process described earlier. Examining the data shows that the copper is flat and has variations less than a half of a micron and the graphite coating is relatively rough, however there is clear minimum thickness where no troughs go below in each sample. To get a value for the thickness the mean of the displacement along with the standard deviation in the graphite region before the spikes was taken.

Since this measurement was of ten coatings the thickness of one coating was calculated by taking the mean and its errors and dividing by 10±1 since the uniformity of each application in the ten is not guaranteed. In the end, the thickness of one coating was determined to be 0.56±.10 μm. It is reassuring how repeatable the results are across different parts of a sample and between the two different samples.

In an attempt to make sure that ten coatings was about ten times as thick as one coating, a sample was prepared with one coating of graphite. There was almost no masking spikes this time but the data was harder to analyze because the variations were on the order of the thickness. Also, when given what seems like a globally flat sample, like the copper piece here, a profilometer will sometimes display curvature over longer scans. With the 2mm long scans being done on all the samples this curvature was clearly visible in scans of one coating. Instead of being flat, sections of the data had a slope. To adjust for this the data was detrended in the regions necessary. The data was again smoothed with a moving average to eliminate the high frequency spikes and a mean of the graphite area was taken. At this scale even the copper surface was not smooth but was offset such that the mean of the copper region gave zero height. The data was analyzed the same way as the ten coating samples were except this time value was divided by 1.5±.5 coatings to include the error of not controlling the exact amount that gets deposited in each application. Figure 21 shows three passes on the same sample with one coating of graphite.

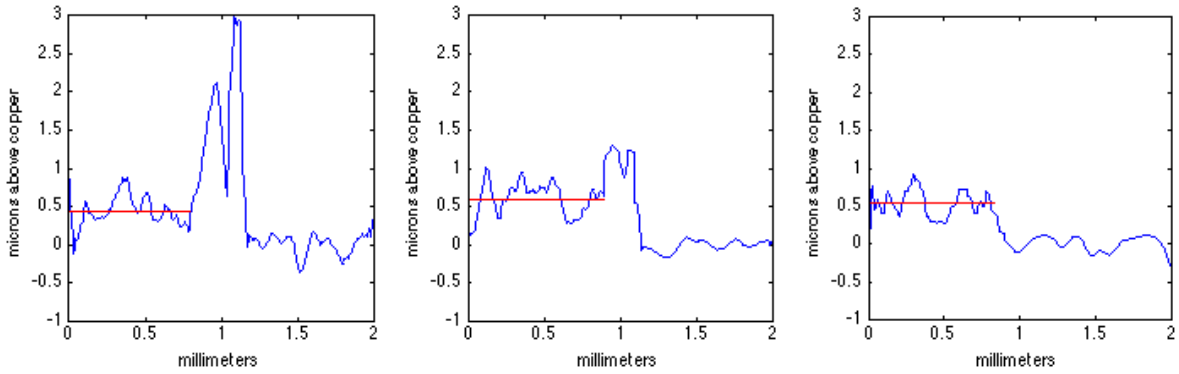

Figure 21: The thickness, in microns, of one application of graphite on copper. The three different plots are three different profilometer passes on different locations on the same sample. The copper surface is set to be zero displacement and the mean thickness is plotted in red. The variations in the copper surface are seen on this smaller scale.

The thickness from these measurements was calculated to be 0.35±.19 μm. The error is twice as high in this case since the variations are on the order of the thickness, but this value and its error is within agreement with the ten coatings measurement.

2 Liquid Metal Interface Coating

Another possible interface coating is liquid metal interface (LMI). A LMI is an application of some metal that is liquid at room temperature (or a little above room temperature) on the rails of the gun such that the projectile rides atop the liquid metal. A LMI can greatly reduce the coefficients of friction between the rails and projectiles making it possible to achieve higher velocities. Also, the use of a slightly viscous liquid metal allows the required tolerance of bore and projectile to be more lax since the liquid metal can fill small gaps between

the rails and projectile if needed. The Navy also conjectured that using a liquid metal in grooved rails would help stabilize the projectile as the slight expansion from heating would put a pressure on the projectile [1].

The Navy tried using silver paste as an LMI. The silver paste they used, produced by Cool-Amp and titled Conducto-Lube, is a fine pure silver powder suspended in about 30% mineral oil. Even though they saw increases in contact and performance they discovered that the application was ultimately not useful as the silver paste broke down at current densities above 28 kA/cm^2 [17], a value which is very easily exceeded in regular railgun operation. Since silver is the most conductive element the breakdown was most likely due to the oil part of the silver paste failing at conducting the high currents.

Students at the Navy also attempted to use indium which melts not much above room temperature in grooved rails. They were unable to wet the indium in the rails; it would not fill the grooves but would rather bead up like water on waterproof jacket. Their take away was that a liquid metal and rail material needed to be found which would allow easy wetting between the two and which would not break down under current densities typical for railguns. They also suggested the use of a liquid metal containing indium on steel rails as that combination has a very low coefficient of friction. The liquid metal chosen for this study is one the Navy did not look into extensively as an LMI, a eutectic alloy of gallium and indium (eGaIn).

2.1 eGaIn

eGaIn is a eutectic alloy meaning that its melting temperature, which is at 15.5°C, is lower than the melting temperatures of its separate elements [9]. See

Table 7 for basic properties of eGaIn [6, 9].

Table 7: Properties of eGaIn

Property	Value
% Ga (by weight)	75
% In (by weight)	25
Melting Point (C)	∼15.5
Boiling Point (C)	>1300
Resistivity ($\mu\Omega$·cm)	29.4
Surface Tension (N/m)	0.5 -0.62

Unlike graphite, eGaIn has a very specific electrical conductivity which was confirmed for this work with a four wire measurement. Therefore, major testing and measurements of resistance was not required like it was with the graphite. Also, since eGaIn is a liquid its contact resistance is so low that its volumetric resistivity and resistance is what needs to be monitored.

eGaIn has current applications in the micro-fabrication industry. It makes for a good low resistance conductor between thin films and is used as a flowing electrical and thermal conductor in micro-channels [9, 6]. A very similar alloy, Galinstan, which has 1.5% tin is often used as a less toxic Mercury substitute in things like thermometers and thermostats. In nearly all of eGaIn's and Galinstan's applications very little is used and the liquid metals are very expensive, approximately 19 dollars/ml, compared to water which is $\sim 10^{-7}$ dollars/ml and crude oil at $\sim 10^{-4}$ dollars/ml.

2.2 Wetting and Application

It was required to be able to wet, or apply and spread even and thin, the liquid metal to the rails before testing could be done. eGaIn has a high surface tension, approximately seven times higher than water, partly due to its gallium

oxide skin. This means that when deposited on most surfaces eGaIn forms up into little beads like water on a rainproof jacket. It turns out that eGaIn wets exceptionally easy to glass; it essentially paints on. The goal was to be able to apply it in the same way to the railgun rails, which in this case were made of copper and stainless steel.

A strong acidic flux meant for cleaning the surfaces of strong corrosion resistive metals like stainless steel was used to try to clean the rail surfaces to allow wetting. This flux gave off hazardous acidic fumes and needed to be worked with under a fume hood. It turned out that even though it did remove the oxide skins with ease off copper and steel, it did not help with wetting.

The best method found was using an abrasive pad. Scotchbrite was consistently used throughout this work to clean the copper rails. The scotchbrite removes very little amounts of material off the surface including any oxide skin. It also roughs up the surface of the copper. The lines from the abrasive pad can be seen in Figure 18b in the previous section. A very small drop of liquid metal was placed on the rails. In order to break through the oxide skin of the eGaIn the drop was then pressed on with a bit of the abrasive pad. Since the steel rails that were manufactured for this project were made out of strong corrosion resistive 316 stainless steel, the scotchbrite was less effective at removing the strong oxide skin and at roughing up the surface. Due to this is was harder and much more time consuming to wet the liquid metal to the steel rails. An approximate area of 1in by 0.5in of liquid metal on a segment of a 316SS rail can be seen in Figure 22 along with 0.25in wide segments of liquid metal on two copper rails.

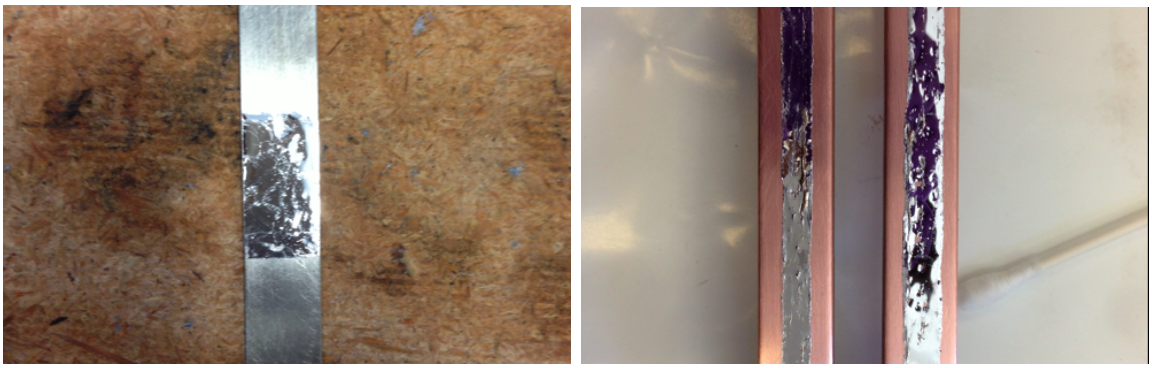

Figure 22: A small amount of liquid metal. It is wet on a .5in wide stainless steel rail and on two .5in wide copper rails. The right copper rails has an excess applied on it which is visible in the inconsistency of the surface.

The thickness of the coating was a lot easier to measure than it was of graphite. Since eGaIn is so dense, rail segments were measured on a milligram scale before and after wetting. Knowing the mass of applied liquid metal and the area it was applied over along with its density allowed easy calculations of thickness. After several applications the average thickness was between 0.003in and 0.010in, the lower end being right about the amount of variation in the bore of 31.25in Mk 1.1 barrel.

Grooved steel rails were also manufactured. The rails had three grooves cut down their length, 1/32in deep and wide. The idea was to wet the liquid metal into the grooves and flush with the surface of the rails so the projectile would ride along on top of them. It turned out that wetting the liquid metal into grooves so small was very difficult to do. It was done by pressing the liquid metal into the grooves with a paper towel but it was not really wetting inside the grooves but rather beading up inside them. In the end the grooved rails were not used because they were not machined accurately enough to be used in the Mk 1.1; they would have made the bore far too wide to use. It would be possible to shim the rails with layers of kapton tape which is about 0.003in thick for future use.

Also the difficulty of applying into the grooves and flush on top of the surface further reduced the usability of the rails. A small section of liquid metal in the grooves can be seen in Figure 23.

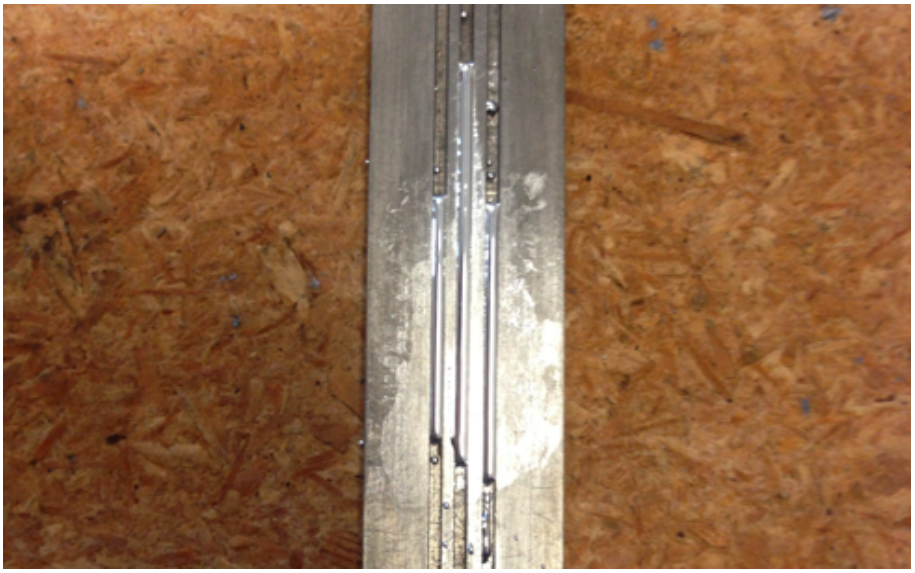

Figure 23: The attempt to wet the liquid metal into the grooved rails. The liquid metal beaded up rather than truly wetting and proved much harder to control.

To remove the liquid metal it was wiped away with a paper towel. This removed most of the liquid metal but there was clearly some left as visible by an ultra-thin layer of it. To get through this layer and to the bare metal scotchbrite and sandpaper were used. Since the steel was more resilient to the scotchbrite it took more effort and more time with the sandpaper to rid of all the liquid metal.

2.3 Projectile Corrosion

Gallium and eGaIn are corrosive to many metals, including aluminum[1]. Gallium, like mercury, easily eats through the protective oxide skin of aluminum and

[1]Fortunately it does not corrode copper, leaving the railguns rails unharmed after application.

continues to tear it apart, grain by grain. This presents a problem of coating the rails or aluminum projectile with eGaIn, however, it can still be done. The gallium in eGaIn exposed to even the slightest amount of oxygen will oxidize to gallium oxide and form a very thin skin on its surface. As seen in Figure 24, when eGaIn was placed on an aluminum projectile and not disturbed or had pressure applied on it, there was no damage since the aluminum was protected by its oxide skin and the gallium oxide layer of the eGaIn.

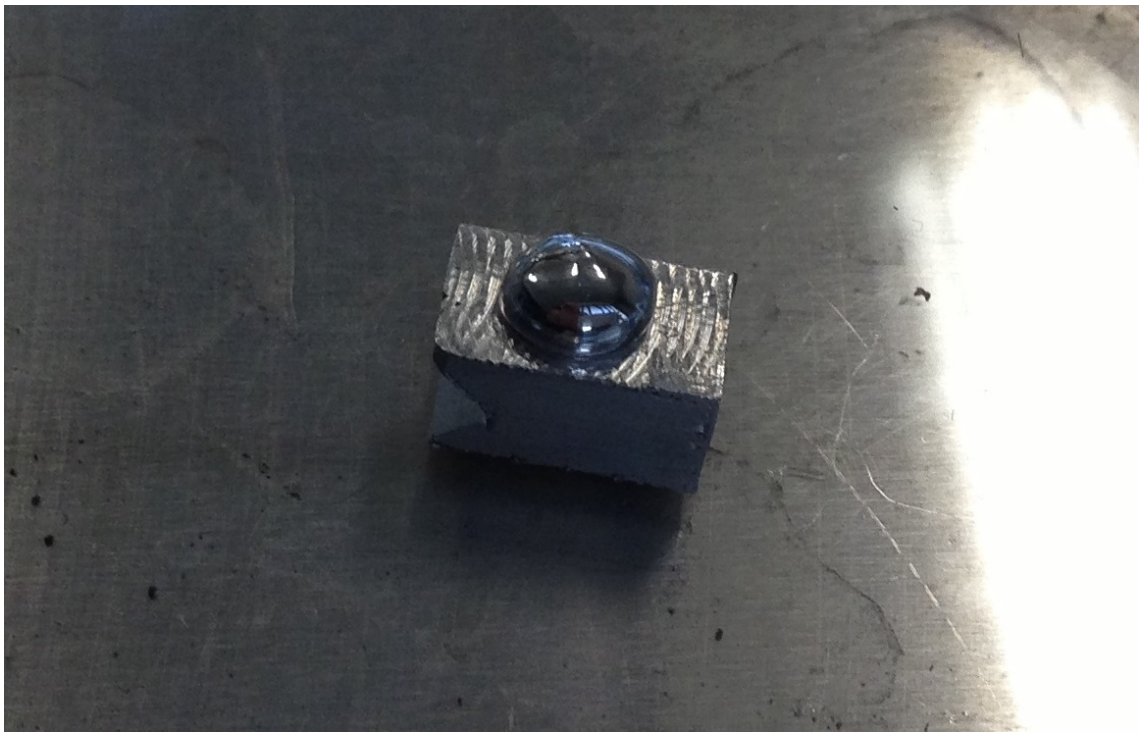

Figure 24: A drop of eGaIn on a 3/8th inch long Al projectile. Since the oxide skins are not broken the eGaIn does not corrode the Al, even after extended amounts of time.

When the same amount of eGaIn was placed on an projectile and pushed down upon by a q-tip to spread it onto the surface, the gallium in the eGaIn began to slowly eat away at the aluminum. A slight discoloration on the border of the eGaIn on the aluminum was seen after a few hours. After a day the damage was more serious as the eGaIn had fully started penetrating and displacing the

aluminum. After several days, as seen in Figure 25, the entire top surface of the projectile was destroyed and the corrosion was slowly making its way down the side of the projectile. The black resultant of the corrosion varied from a very fine powder to brittle millimeter scale flakes (after about a week of exposure).

Figure 25: Two views of an Al projectile corroded by eGaIn. The eGaIn can be seen on top, and the black particulate is the corroded aluminum. The corrosion can be seen making its way down the side faces of the projectile. This is the amount of damage after several days.

The eGaIn showed its ability to completely destroy an aluminum projectile but the process was slow. As long as a projectile was loaded, for example, in to a press fit railgun and fired quickly, within minutes the projectile would be able to maintain its integrity. As shown later in static test firings, projectiles that were firing on liquid metal rails suffered minimum corrosion from the brief exposure to the liquid metal.

2.3.1 X-Ray Diffraction of Corrosion

The black particulate left over from the corrosion of the projectile was looked at with X-Ray diffraction. The goal was to gain any insight into the makeup of the corrosion. It was suspected that a large part of the particulate would be aluminum oxide with maybe some remnants of eGaIn. The particulate was powdered to a very fine level and analyzed by a Siemens Diffraktometer D5000

XRD. Very clear peaks were seen in the spectrum along with an area of interest in the area between Bragg angles of 30° and 45°. It turns out that the peaks in the spectrum as seen in Figure 26 are the exact spectrum of pure aluminum. This means that the particulate is mostly aluminum with a very thin skin of aluminum oxide, so thin that the x-rays from the XRD penetrate it and then interact with the aluminum. After comparing the area of interest with many other spectral peaks of gallium, indium, and many phases of aluminum oxide it was deduced that the area of interest is a combination of many different phases of aluminum oxide. The fact that aluminum oxide is actually a very complicated molecule than can exist in many of its phases at once allows for this [22]. Since the reaction between the eGaIn and aluminum was by no means a carefully controlled reaction it is assumed that the outer part of the particulate was a very thin skin of possible several phases of aluminum oxide. If the skin had been thicker than its spectral participation would have been higher then maybe a specific phase of aluminum oxide could have been identified. For scanning electron microscope photos of the corrosion particulate see Appendix A.

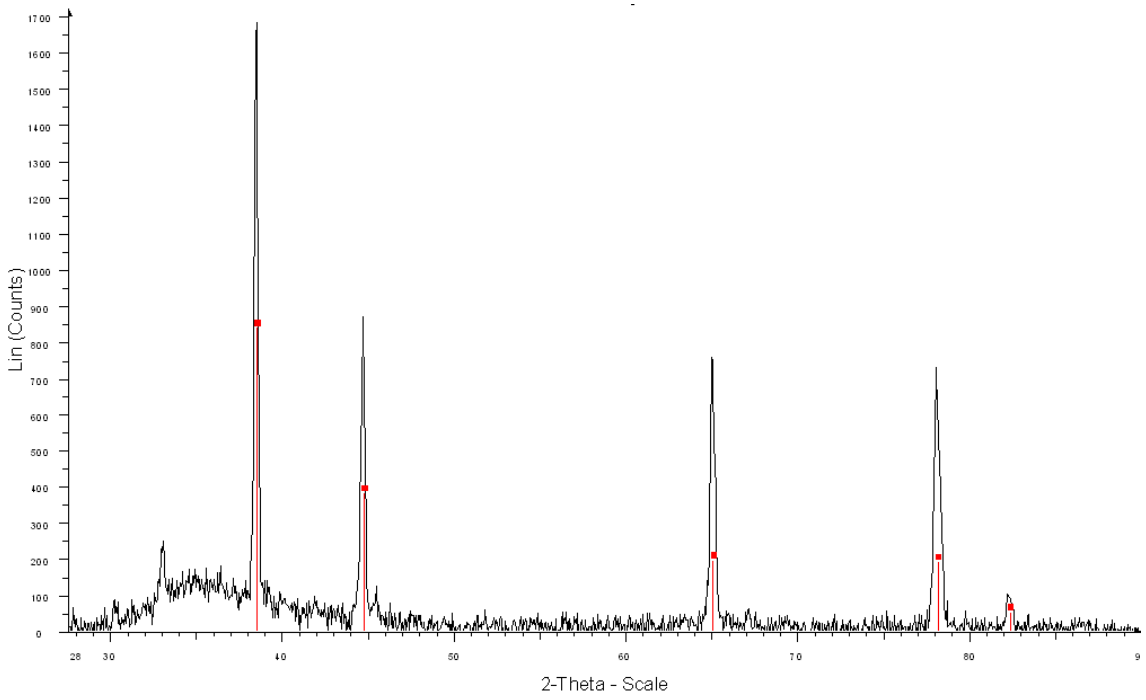

Figure 26: An XRD spectrum of corrosion particle. The spectrum peaks of pure Al are overlaid. The hump by the main peak is presumed to be the spectrum of the incredulously thin oxide skin. The x-axis is twice the scattering angle and the y-axis is the amount of counts at that angle.

3 Static Tests

Static tests, which did not use current to fire the railgun, were used to see effects of applying graphite and eGaIn. They are static tests in the sense that the there is no current flow; they are electrostatic. The projectile was still propelled down the bore using compressed nitrogen. Since there is no dangerous high voltage equipment involved static tests can be repeated quickly and with practically no damage to rails and projectiles. However, static tests have their drawbacks. Since there are no strong current and electromagnetic fields interacting with the railgun the conditions in the bore are not what they would be if a real firing was conducted. Since there is no heating and melting the damage that would be done

to the rails is not seen. Hence, the full possibly aiding and beneficial effects of the coatings are also not seen. These static tests were still useful as they showed the reduction in friction and the ability to help maintain contact with the use of these coatings.

3.1 Static Test Setup

3.1.1 Firing Mechanism

Since current was not propelling the projectile compressed nitrogen was used. The first Mk 1 system did not have switch mechanism so the projectiles were accelerated into the rails by compressed nitrogen. The same system was used with minor modifications.

A 2000psi nitrogen tank with a solenoid valve was connected to the back of the railgun. A metal fixture was added to the back of the breech with the same bolts that hold the railgun together. The tank would shoot compressed nitrogen into the bore for short specific amounts of time, specifically enough time to get the projectile out of the barrel.

The valve was controlled with the same equipment used on the Mk 1.1. Pressing the fire button would trigger an oscilloscope for data acquisition and would send a 5V trigger signal to the equipment in the room. A basic circuit was designed so that the 5V trigger would turn on a relay sending 120VAC to the solenoid valve, opening it. A photo of the static test firing can be seen in Figure 27.

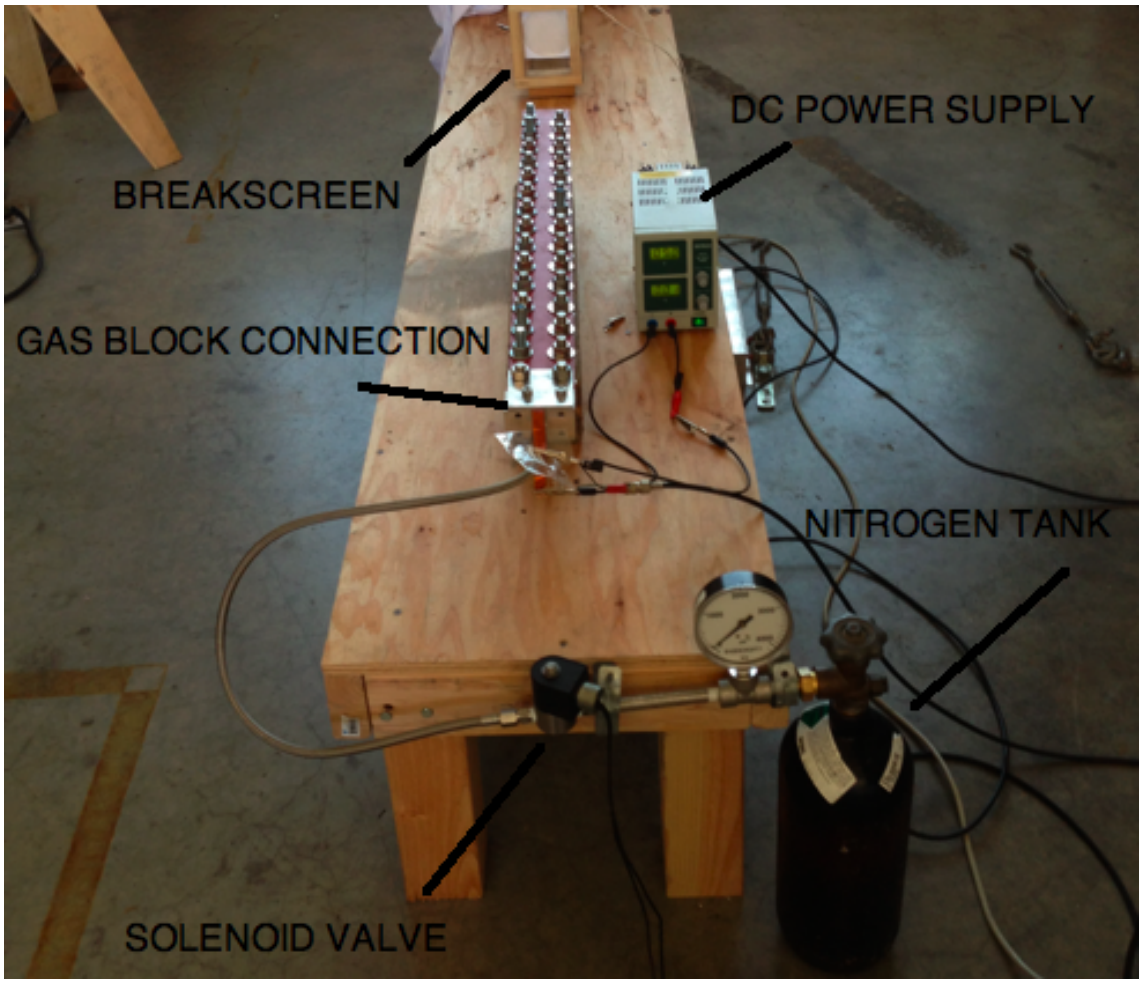

Figure 27: The static test setup. The nitrogen bottle is connected to the back of the railgun with a solenoid valve in between. The DC power supply powers the contact measurement as described in the following section. The electrical circuit for the contact measurement can be seen in Figure 28. The first breakscreen is seen at the top of the image. This was the setup for static test firings of bare rails and graphite coated rails. Firings with liquid metal included a plastic bag sealed around the muzzle of the railgun and connected to a HEPA filter, neither pictured here.

The Arduino microprocessor was setup to stop the 5V signal as soon as the break screens, which measured velocity, were broken. This meant that the valve was be closed after the projectile left the barrel, traveled for a few feet and punctured the break screens which were 8.5in apart. For the liquid metal firings where no breakscreens were used the Arduino code was set to open the valve for

a fixed amount of time, usually 75ms.

3.1.2 Contact Measurement

To measure contact during the firing a method based on the way some NPS students did it [7] was used. The idea was that given contact and an applied voltage on the rails current would flow through the projectile. When there was no contact there would be no current flow and the voltage would remain high. A DC power supply was attached to the breech end of the rails. Since the back of the rails were covered by the aluminum gas fixture thin copper tape strips covered in kapton tape were used. The aluminum gas fixture block was coated with a thin layer of spray-on rubber insulation such that it did not short the connection between the two rails. The copper tape was stuck on to the very back of the rails and the other end of the tape was connected to the power supply. In series with one of the connections a 1kΩ resistor was used to draw power. When current flowed through the rails and projectile in the case of contact all the voltage drop was across the resistor so the voltage drop across the rails would be near zero. When there was no contact the voltage across the rails rose to its highest value. A circuit diagram of this setup can be seen in Figure 28. The voltage measurement leads were connected at the same connection between the power supply and copper tape. Since the voltage from the power supply were on the order of a few volts there was no need for high voltage probes which we would have to use in a real firing. The voltage connection ran directly to the oscilloscope to monitor the voltage across the rails.

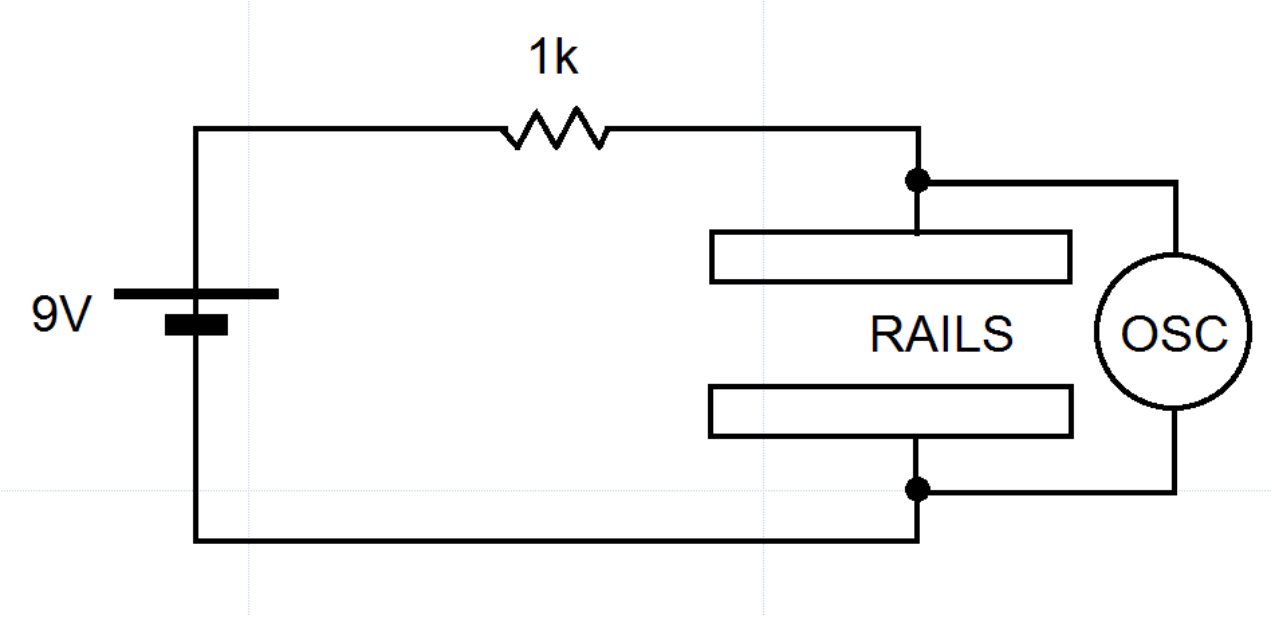

Figure 28: The circuit diagram of contact measurement used. The voltage was provided by a DC power supply and could have been set anywhere between 0 and 20 volts. The voltage measurement across the rails was sent to a digital oscilloscope.

3.1.3 Safety

These static tests were relativity safe since large voltages and currents were not involved. However, since the liquid metal used is hazardous, extra precautions had to be taken for the liquid metal firings. Heavy 6mil plastic was laid down around the entire test area in case of any spills of the liquid metal. The front of the railgun was sealed off in a heady duty plastic bag. This bag was connected to a hose that ran to a HEPA vacuum. After the firings the vacuum was turned on to suck out any loose or aerosolized liquid metal. Inside the bag a cardboard backstop was placed so the projectiles did not pierce and exit the bag. After the firings all the plastic and the backstop was discarded as hazardous waste. Since the muzzle was sealed off, breakscreens were not able to be used for velocity measurements.

3.2 Static Test Results

Static test firing were done with nothing on the rails followed by graphite coated and eGaIn coated rails. Several shots were done in each setup. Contact measurements were done for all tests and velocity measurements were done for the plain and the graphite firings. No velocity measurements were taken with the eGaIn firing since the muzzle of the railgun was sealed in a thick plastic bag for safety and the breakscreens could not be placed inside of it. For a procedure of the static test firings see Appendix B.

3.2.1 Uncoated Static Tests

Figure 29 shows the contact voltage for four shots with bare rails. Once again, a voltage of zero volts meant perfect contact and a voltage of nine volts meant no contact. The flat-lining at the high voltage meant that the projectile had left the barrel. The spiky data here indicated that the projectile never made good contact with the rails and bounced around in the barrel, occasionally touching both rails. This was partly expected since the projectiles chosen had to be the size of the tightest pinch point in the barrel. In general the bore was a thousandths of an inch bigger than the size of the projectiles. These firings were done at about 2000psi and the pressure went down by about 25psi each shot.

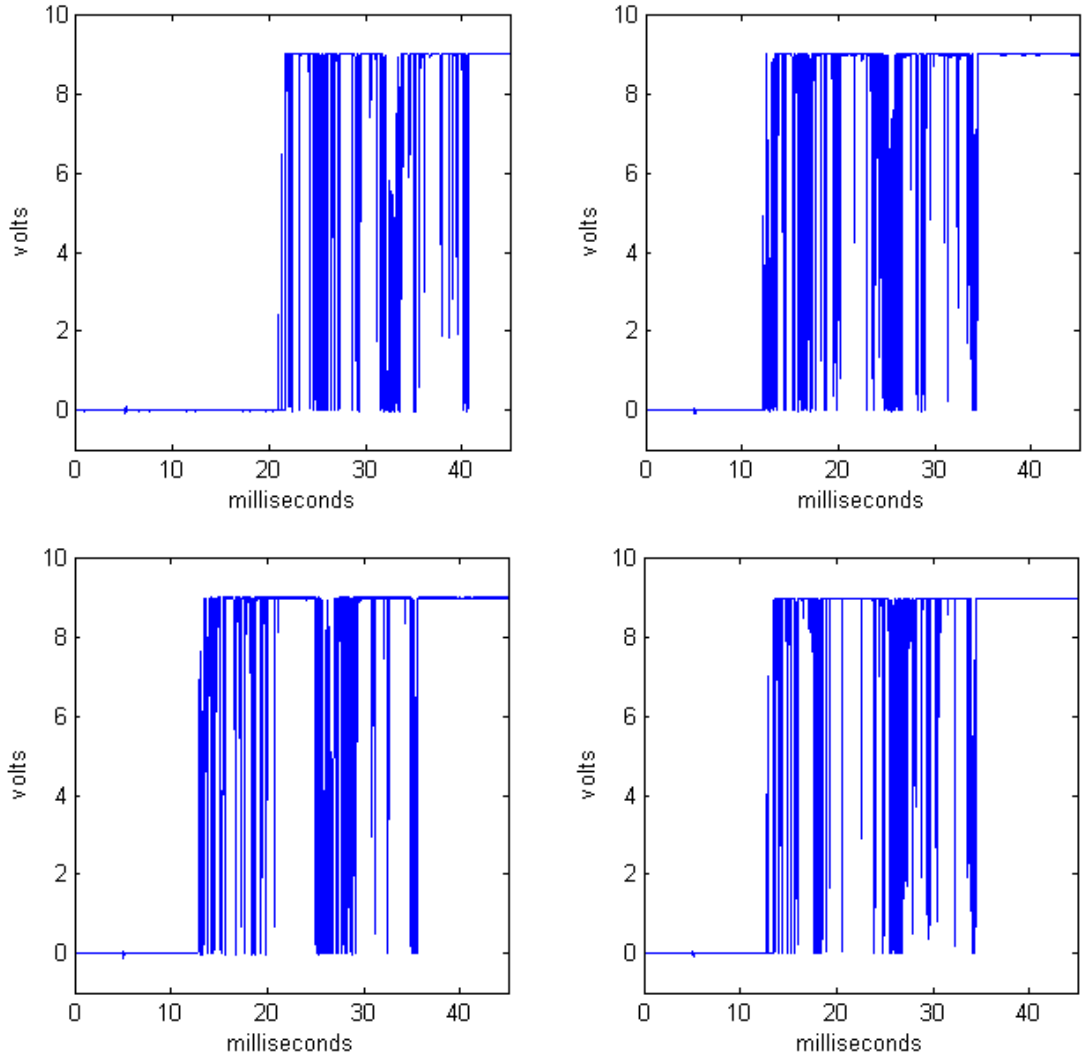

Figure 29: Contact voltage measurements of four static test firings with plain rails. The data indicates the projectile never makes good prolonged contact with the rails because it is a few thousands of an inch smaller than the bore. With the exception of the first firing the projectile starts moving after about 12ms after the pushing of the fire button and leaves the barrel at the 35ms mark. There are similarities of contact between the different firings due to the bore having pinch points in certain places and the projectile having more contact in those areas.

For these firings the same projectile was used for each shot. It was loaded into the gun such that is had contact to begin with. This is why all the data starts at zero volts. After the first firing light lines were seen on the contact faces of

the projectile indicating that on its first pass the projectile smoothed out areas of the bore by passing through it. This explains why all the following firings took less time as the projectile fit the bore better. It can be seen that the projectile starts moving at around the 12ms mark and leaves the barrel at about the 35ms mark. The average velocity for these firings was 70±2m/s.

3.2.2 Graphite Coated Static Tests

The following four static tests, as seen in Figure 30, were done with graphite coated on the rails. Once again, the same projectile was used. Since the graphite added a good amount of contact resistance there was a measurable voltage drop across the rails. This is why sometimes the data starts between zero and two volts. In the second firing the projectile is not making contact to begin with and the data starts at nine volts. These tests were done at pressures of about 1800psi. A lot of the data showed that the voltage went all the way down to zero. This was caused by the projectile scraping off the thin layer of graphite as it bounced around and made direct contact with the copper rails. In the beginning of the third firing it is seen that the projectile started with good low voltage contact and then slid a top of the graphite causing the voltage to rise until it completely broke contact and jumped to nine volts.

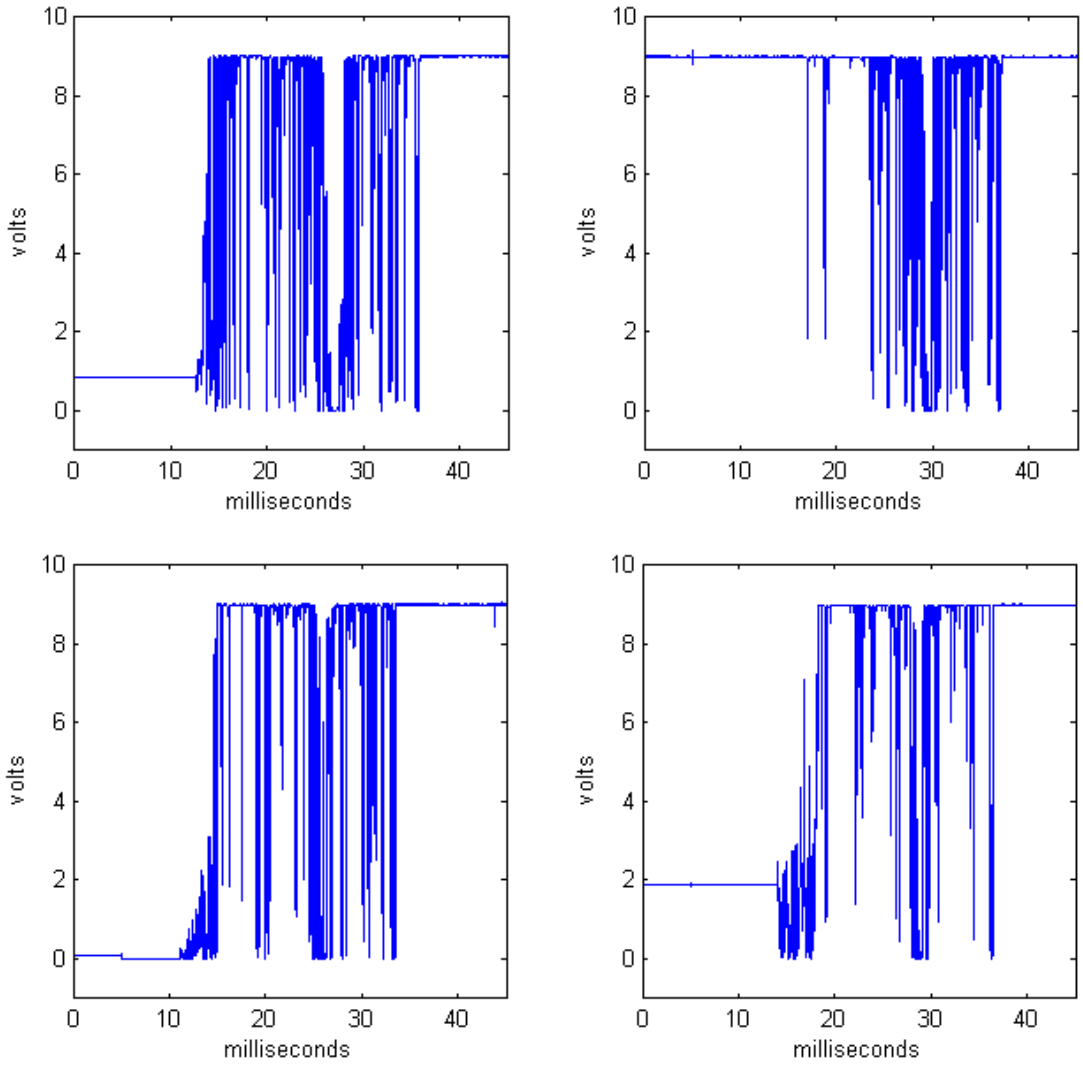

Figure 30: Contact voltage measurements of static test firings with graphite on the rails. The non-zero contact voltage indicated a measurable voltage drop across the projectile due to the added resistance of the graphite. The drop to zero volts meant that the projectile had dug through the graphite and was making contact with the bare copper. In the second firing the data starts at nine volts because the projectile was not making contact with the rails to begin with.

In the fourth firing it is seen that right after beginning to move the projectile dug through the graphite and made good contact with the copper for a few milliseconds. After the tests the railgun was disassembled and the rail examined;

it is clearly visible in Figure 31 where the projectile removed the graphite and made contact with the copper.

Figure 31: The graphite coated rails after all the static test firings. The places where the projectile dug through the graphite and made contact with the bare copper are seen.

Even though the contact is not improved with the graphite as seen with just as spiky data as with the bare rails, the average velocity of these firings was higher. Compared to the 70±2 m/s with bare rails the average velocity for the graphite firing was 81±2 m/s. The fact that these firing were faster even though the compressed nitrogen pressure was lower is attributed to the fact that the graphite acted as a lubricant. Whenever the projectile made contact with the rails as it was bouncing around less kinetic energy was lost.

3.2.3 eGaIn Coated Static Tests

eGaIn was coated on the rails in two segments. The first length of eGaIn started 4.5in past the breech end of the rails. A 9in length was applied followed by 3in of bare rails which can be seen in Figure 32. After that, another 7in of liquid metal was applied. The reason for the 3in break in eGaIn was to see if the projectile maintained contact in that region or if good contact occurred in regions of liquid metal only. In total about one milliliter of liquid metal was used

for both rails resulting in a thickness of approximately ten thousands of an inch. This turned out to be too much but most of it was removed in the first shot by the projectile leaving just the necessary amount on the rails.

Figure 32: eGaIn applied on the copper rails. The first nine inch segment of eGaIn on the copper rails followed by the plain copper and then finally the beginning of the second seven inch segment.

Figure 33 show the contact voltage for the four static tests shows with liquid metal. These shots were done at a pressure of about 1500psi and in all of them the projectile started moving at around the 18ms mark. The first shot took a lot of time because the projectile had to move a lot of liquid metal in its way. The shots following were a lot quicker as the first shot had caused a lot of excess eGaIn to come out of the bore. Compared to the graphite firings, when the projectile has perfect contact the voltage is zero indicating that the liquid metal's conductivity is not causing a voltage drop comparable to the resistor, across the rails. This is a sign that there is no increase in contact resistance when using the liquid metal. No velocity measurements were taken for the liquid metal firings since the muzzle of the railgun was sealed in the plastic bag. Also, it would be difficult to compare the speed of these shots to the plain or graphite shots since the tank pressure had made a significant drop to 1500psi by the time these firings were done.

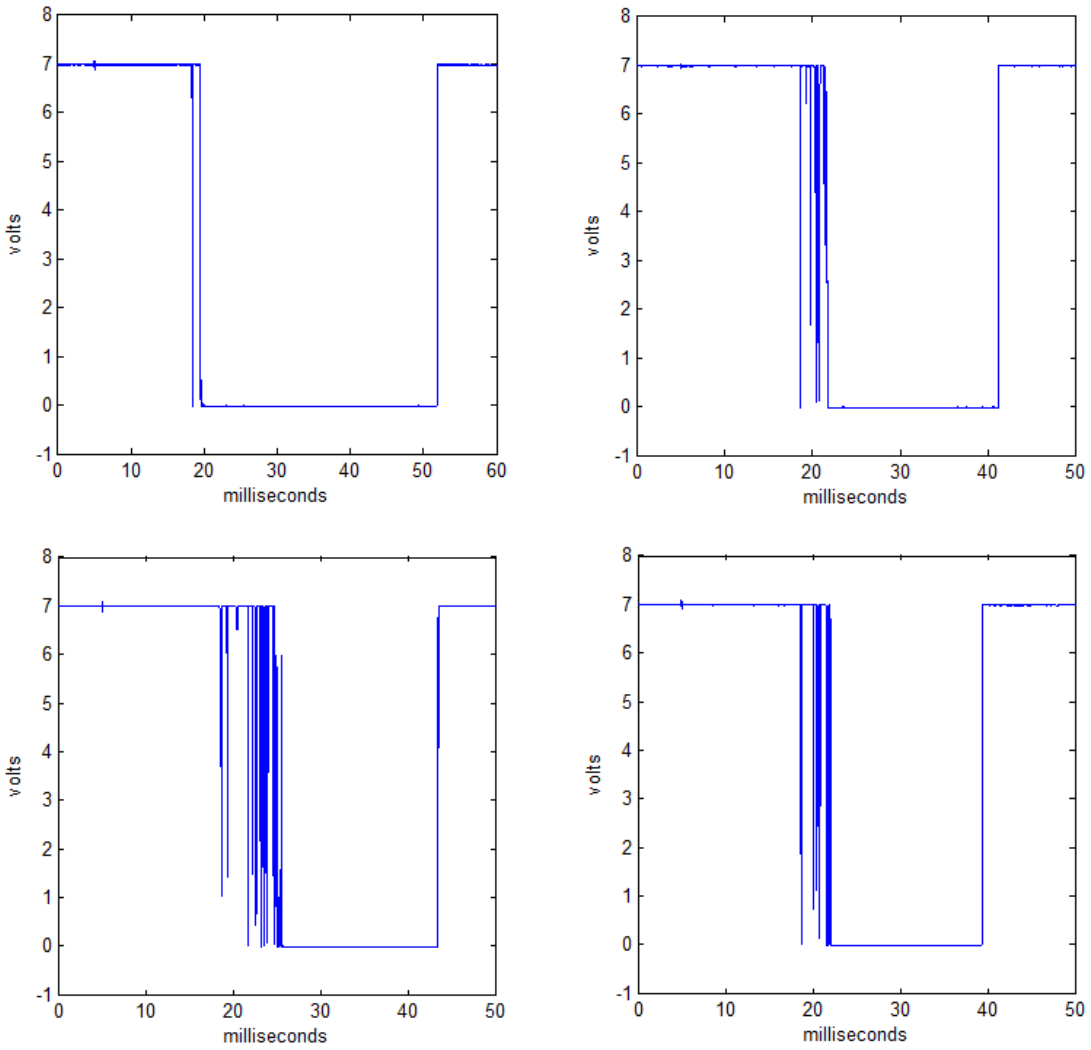

Figure 33: Contact voltage measurement for four static test firings with liquid metal on the rails. The continuous zero volts readings meant perfect contact occured. The first shot took a lot longer because there was so much liquid metal in the way of the projectile. The following shots all showed great contact but each time the contact in the very beginning was spiky indicating that the liquid metal the projectile encountered first was thinning out. In all the shots the projectile starts moving at the 18ms mark.

All four shots maintained perfect contact thanks to the liquid metal. Perfect contact was also maintained even in the regions of no liquid metal indicating that the projectile grabbed a little bit of it and rode it out of the bore. All these shots

were done with the same application of eGaIn; the gun was not taken apart to apply more after each shot. After the shots the railgun was taken apart and the rails were examined. The liquid metal stayed on the each rail in the exact same spot it was applied but it was a lot more smooth and thin as seen in Figure 34. The excess liquid metal that came out on the first shot was found on the target backstop inside the plastic bag wrapped around the muzzle of the gun.

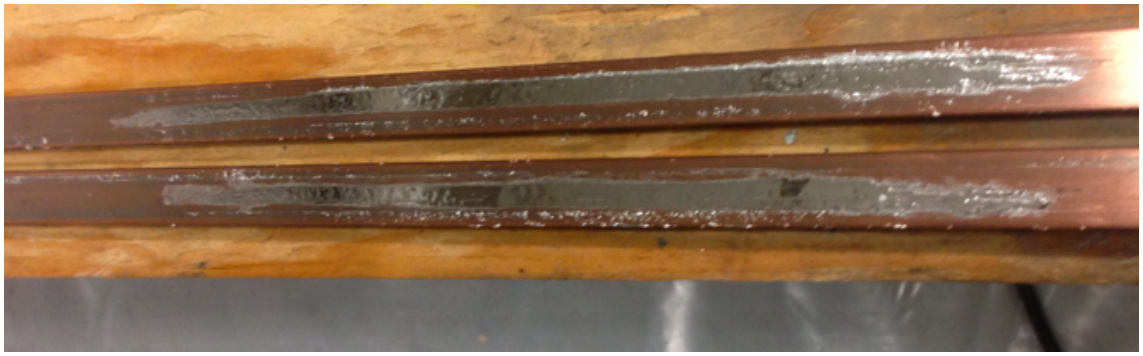

Figure 34: The thinned out liquid metal on the copper rails. This is after the static test firings. The liquid metal is in the exact spot it was applied, and the part between the two segments is still bare.

Even though the projectile maintained perfect contact with the rails in the bare segment between the two applications of liquid metal none of it spread onto the region even after four shots. Figure 35 shows the projectiles used in the liquid metal firings after one day. One projectile, the first one fired, showed heavy corrosion within 24 hours after the firing, but the rest which encountered less liquid metal were still in usable shape.

Figure 35: The projectiles a day after being fired on liquid metal coated rails. The heavily corroded projectile was the first one fired and had to push a lot of liquid metal out of the way. The other projectiles show minimal corrosion as dark lines on their contact faces.

In order to preserve the projectiles they can be simply cleaned with scotchbrite or some abrasive pad after being fired. That way any liquid metal that could corrode them is quickly removed.

3.2.4 Take-away and Limitations of Static Tests

As mentioned at the beginning of this section these tests were useful but not ideal. Since current is not being used to propel the projectiles and no heating or melting is caused, it is hard to make concrete conclusions from these static tests about how they would behave in real firings. However, some information can be deduced from these tests.

The liquid metal having a thickness on the scale of the bore variations allowed the projectile to have perfect contact through out. But the thickness of the coating and the gap it is filling between the projectile and bore cannot be too big. If the gap is too large then the current that passes through the liquid metal would have a substantial Lorentz force on it. Since the liquid metal is in

fact liquid and separate from the projectile nothing would stop the liquid metal from getting quickly accelerated forward, faster than then projectile, and hence breaking contact between it, the projectile and rails. This is especially true in a press fit firing where the projectile starts off stationary. This effect was seen in an attempted Mk 1.1 firing where the projectile was in the bore too tight, the aluminum at the interface quickly melted and shot forward due to the current running through it and it all of a sudden being free from the projectile. In an injection type firing where the projectile is already moving would be better at preventing this.

Since the velocity was not measured for the static tests it is not possible to conclusively say that the reason contact was perfect was because the liquid metal filled in the bore gaps. There is the chance that either the slowing (due to viscous effects) or speeding up (due to lubricating effects) of the projectile due to the liquid metal could have changed its dynamics, and for example, made it tumble less. The most likely conclusion is a combination of both effects, the viscous effects stabilized the projectile making it tumble less and the lubricating effects made it stay in the bore for similar amount of time as the graphite tests.

If the railgun were to be fired with currents and the amount of liquid metal which was present for the first static test, the results would not be good. In a real firing the current could conduct through the excess liquid metal being pushed by the front of the projectile. It would then possibly just pass through the liquid metal rather than the projectile causing the liquid metal to exit the bore at substantial velocities. The fact that the liquid metal used in this work is corrosive and hazardous this is not ideal. After the first shot liquid metal did not come out of the bore so in real firings either the amount applied in the beginning would have to be very even and thin or a projectile would need to be pushed

through to remove any excess liquid metal.

Since eGaIn has good electrical and thermal conductivity and its boiling point is higher than the melting point of copper it should maintain its integrity as thousands of amps are passed through it. However how it really reacts to that much current needs to be evaluated to make sure it does not deteriorate and become useless in a real firing.

As far as the graphite goes, after these tests it seemed it would only be useful in railgun applications with much better tolerances and railguns with bigger bores. A graphite coating is desired due to it not being hazardous and expensive compared to the liquid metal but for it to really be beneficial it needs to be used in a railgun with very flat rails and projectiles. Since the bore variations were so much higher than the thickness of the projectile it did not help in maintaining contact. Having larger contact faces would lower the contact resistance and make it have less influence on the efficiency of the system. However the resistance of the graphite does aid in diffusing the current a slightly lowering the build-up of current in the back of the projectile. Furthermore, because the graphite is so thin and its "operating temperature" as provided by the manufacturer is lower than the melting point of aluminum it is expected to deteriorate. But since the graphite is applied down the entire length of the rails the projectile is constantly encountering new graphite for the current to pass through it should still perform well. Unlike the liquid metal the graphite can be applied to both the projectile and the rails lowering the forces of friction since the coefficient of friction between graphite and graphite is lower than graphite and aluminum or copper. Graphite was actually used in a few of the Mk 2.0 firing tests. Even though the tests did not achieve the desired velocities due to projectile failure, the armature used moved further down the bore when graphite was applied to the rails. This is a

testament to the benefit in lowering the forces of friction. The measured current in those tests was also lower indicating that the graphite coating did add extra resistance to the system, but not enough to cripple it like in the case of the Mk 1.1. The Mk 2.0 firings removed the graphite from the rails. This was either caused by the armature scrapping it off or, more likely, the graphite deteriorating in the presence of the high current and undesired plasma arcs.

In addition to these static tests the contact resistance measurements of flat and non-flat projectiles really conveyed the importance of having good initial contact. Since contact resistance is higher when only a portion of the projectile is making contact with the rails and it is even more higher when that contact is not solid and is loose, it is critical to have a good tight fit in the beginning of a firing, press fit or injected. If initial contact is poor and melting occurs quicker due to more resistance and heating then the projectile will not have good contact in the rest of bore. This of course leads to efficiency loses, substantial projectile mass loss, more deposition on the rails and large amounts of arcing plasma.

Chapter 5

Resistivity Augmented Projectiles

As shown in section 2 current does not flow evenly through a projectile but rather bunches up in the back. This causes local heating and quick melting of the projectile. Enough melting causes the loss of contact and projectile integrity. Since deposition damage is the most harmful to the rails it is worth trying to mitigate this. This chapter proposes and simulates a new type of projectile, one in which the fundamental property of the projectile material, its ability to conduct electricity, is manipulated in such a way to condition the current to flow more preferably. The way the resistivity or conductivity of the projectile changes will be called conductivity gradients. Different gradients using analytical math functions were devised and the current flow through them was simulated. The idea was to have less current flowing through the very back of the projectile and to spread it out evenly throughout the entire cross section of the projectile.

It is important to note that at this time it is not possible to produce a piece of

aluminum, for example, in which its alloy composition varies such that the electric conductivity varies. However with the advent of 3D printing already being able to print metals it might not be long until 3D printers could manipulate alloys as they are printing them. Since this means that continuous conductivity/resistivity gradients are not yet feasible, the closest analog is making a projectile out of several different alloy layers. This creates discrete levels of conductivity. This idea has been explored but with the projectile being made of different metals, rather than alloys, such as aluminum, copper, titanium or molybdenum [18]. However, the increased mass of some of those metals causes slower velocities and there are discontinuities in current density at the interfaces between the different layers. Hence, the following simulations look into what kind of conductivity gradients could be used to improve current flow if it were possible to produce projectiles with continuous gradients.

1 Simulation Setup

The following simulations were ran in COMSOL Multiphysics, an FEA software which allows the coupling of different physical phenomena. For this work the AC-Module in COMSOL was used to simulate current flow, current densities, and voltages. A simple railgun model was built consisting of two parallel copper rails, 8in long, 1in wide and 0.125in thick. The projectile was a simple rectangular piece of aluminum, 1in long and 0.75in wide and thick. COMSOL allows the manipulation of any property of the model and therefore allows for intricate control of the projectile's conductivity. The dimensions chosen for the rails and projectile are roughly that of several of the railguns built at the Naval Postgraduate School in Monterey, CA [4]. The model can be seen in Figure 36.

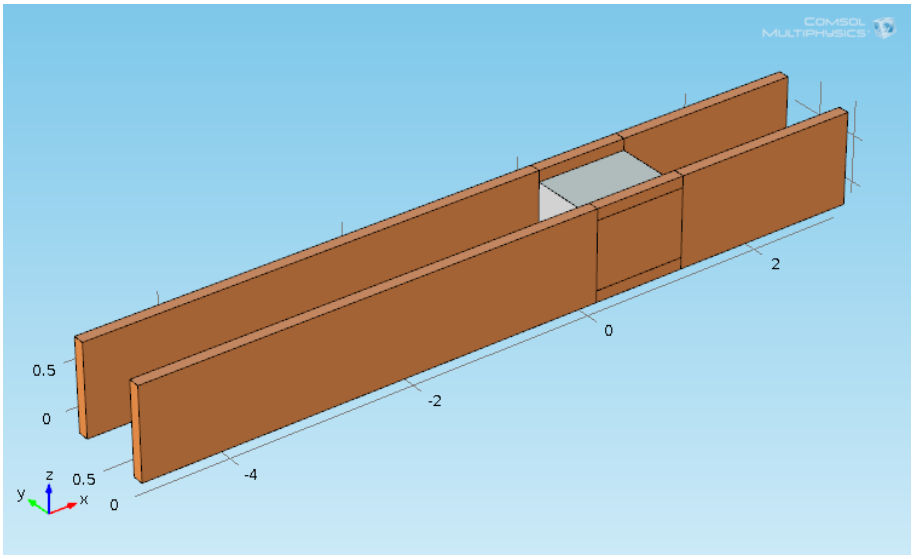

Figure 36: The simple railgun model in COMSOL. The rails have the material properties of copper while the projectile is aluminum. The rails have divisions where the projectile is in order to mesh different regions more precisely.

In this model the x direction was down the bore, the y direction was through the rails and projectile, and the z direction was through the side of the model. The gradients used in these simulations were functions of these directions.

To power the simulation a current density on the ends of the rails was chosen such that exactly 100000A was flowing into one rail and out the other. The number is arbitrary but is about the amount that was run at the NPS. Since the initial current is an exact number, post simulation measurements of the current in different areas were able to give a scale of the simulations accuracy. As shown later, the total measured current flowing through regions of interest, like the interface between the projectile and a rail did not add up to exactly 100000A, a sign of numerical error in the simulation.

This model is static; the projectile does not move even though there is current running though it. Hence, this is not a perfect model since the amount of velocity

skin effect current build up cannot be controlled. The model still shows a large amount of current build-up in the back of the projectile and therefore is still useful in simulating conductivity gradients to try and condition the current. Building a dynamic railgun model requires the coupling of many COMSOL modules and is beyond the scope of this work.

The simulation was meshed with most detail on the interface of the projectile and rails since measuring accurate current densities at the interfaces was most important. A coarse tetrahedral mesh was chosen for the rails and interfaces and a quad mesh was chosen for the projectile body. The mesh and a zoomed in region at the corner of one of the projectile rail interface is shown in Figure 37.

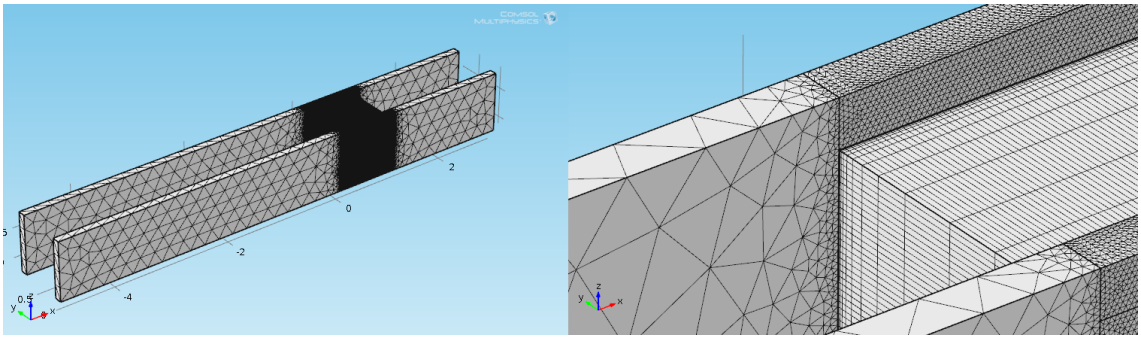

Figure 37: The mesh of the entire system. Most of the detail is near the projectile interface. A zoomed in view shows the quad mesh on the projectile and a fine tetrahedral on the rails.

A finer mesh could have been used in order to minimize the total current errors previously measured. But since the simulation run time significantly increased it was deamed not worth it since the errors using this size of mesh were acceptable.

2 Gradients

A handful of gradients are proposed in this section. After discussing them individually their simulation results and performances are presented.

2.1 Linear

The simplest gradient that was simulated was a linear one where the conductivity increases closer to the front end of the projectile. Since projectiles are commonly aluminum the range of conductivity was chosen to range from Al 221 (most resistive) to pure Al (least resistive, most conductive). For a comprehensive list of the conductivity of aluminum alloys see reference [2]. The linear conductivity gradient is

$$\sigma(x) = \sigma_m + \nabla_\sigma x \tag{4}$$

where $\sigma(x)$ is the conductivity of the projectile as a function of x, σ_m is the lower end of the conductivity and in this case is 12.2 MS/m (mega-Siemens per meter), ∇_σ is the gradient and is 23.2 MS/(m·in) since the geometry of the projectile is in inches. x ranges on [0 1] since the projectile is 1in long. Figure 38 shows the simple conductivity gradient.

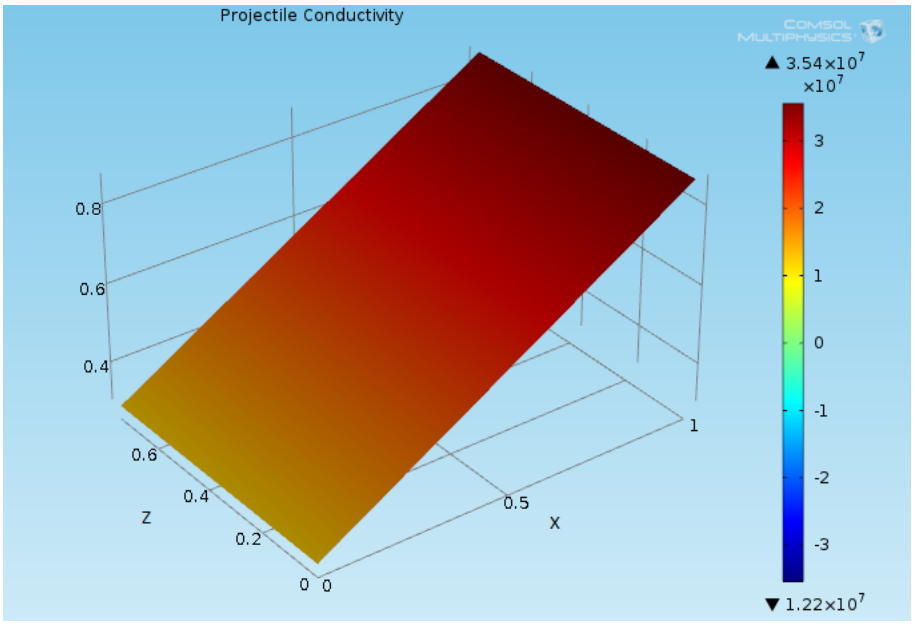

Figure 38: The linear conductivity gradient. The values on top and bottom of the color bar indicate the min and max conductivity values. The 12.2 MS/m corresponds to the back of the projectile and and the 35.4 MS/m to the front. The numbering on the y-axis is not be to confused with the conductivity (explained below).

Note that while the x-axis label is correct as it goes from 0 to 1, the y-axis does not correspond to the y position in the projectile; COMSOL by default just puts that label there. The height and color of the plot corresponds to the conductivity; while the numbers on the y axis are still spacial they are not to be confused with the magnitude of the conductivity. This also goes for all of the following plots in this chapter: the vertical numbering is to be ignored.

2.2 Parabolic

This gradient is very similar to the linear one but the x term is now squared so the gradient has the form

$$\sigma(x) = \sigma_m + \nabla_\sigma x^2 \tag{5}$$

where ∇_σ now has units of MS/(m·in^2). The range of conductivity is still the same as in the linear case. Figure 39 plots the the shape of the parabolic gradient.

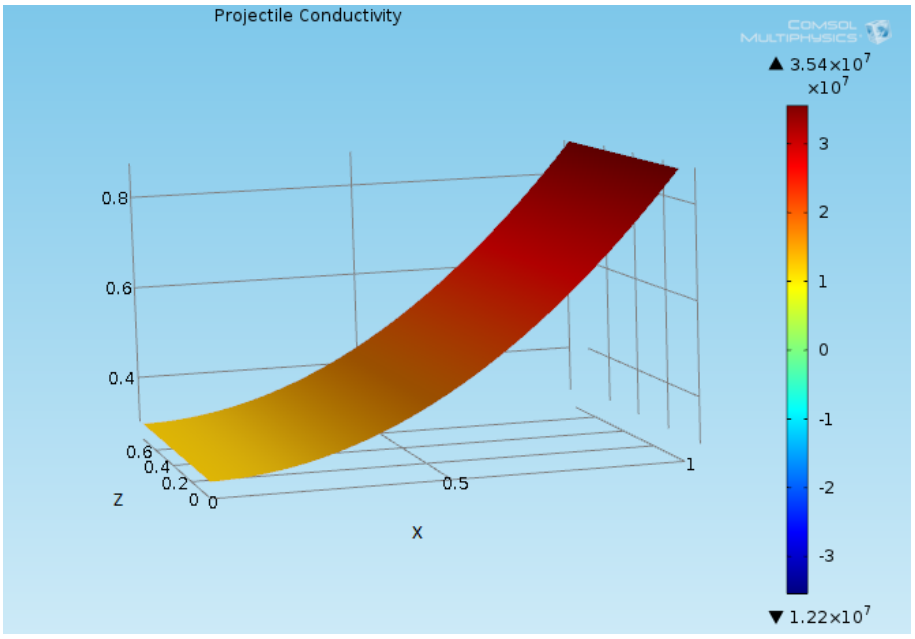

Figure 39: The parabolic conductivity Gradient. It only varies in the x direction. The max and min values at the edges are the same as in the linear case.

2.3 Multivariate

This gradient is like the linear case but with a sine term in the z direction. The sine term diminishes to zero at the front of the projectile. The gradient has

the form

$$\sigma(x,z) = \sigma_m + \frac{(1-x)\nabla_\sigma \sin(z\frac{4\pi}{3})}{2} + \nabla_\sigma x \tag{6}$$

The idea with this gradient was to pull the current away from the side edges of the projectile by making it more conductive in the middle of the z direction. The $1/2$ scaling on the second term ensures that the maximum conductivity at the back of the projectile is not equal to the maximum at the front. See Figure 40 for this gradient.

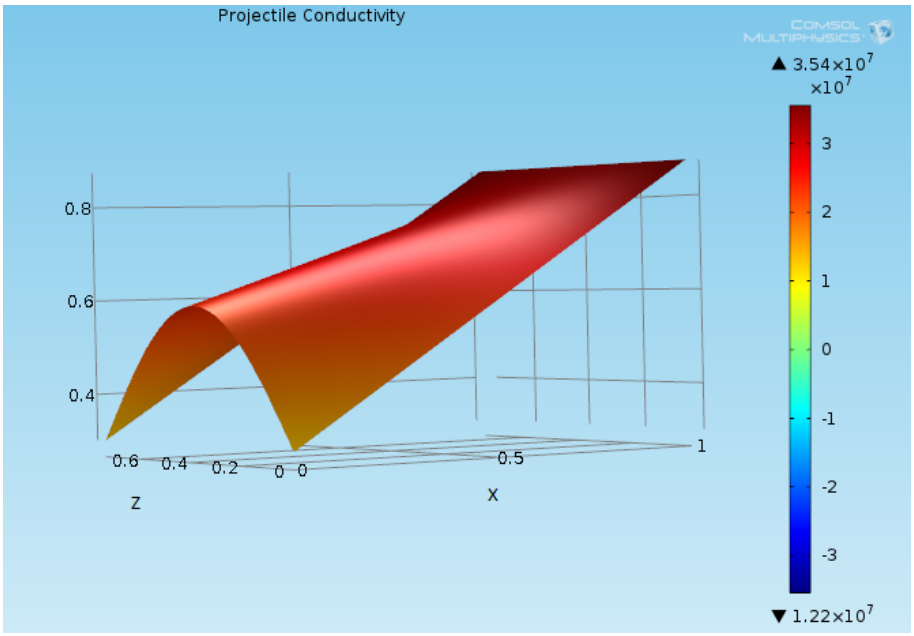

Figure 40: The multivariate gradient. Notice the sine term in the z direction which gets smaller as x increases. The gradient is linear in the x direction.

2.4 Multivariate 2

This gradient has a parabolic term along with the sine to try to pull the current to the middle of the projectile. It has the form

$$\sigma(x,z) = \sigma_m + (x^2 - x)\nabla_\sigma \sin(z\frac{4\pi}{3}) + \nabla_\sigma x \tag{7}$$

The conductivity is at a minimum all around the back edge of the projectile and then increases in the middle of the projectile and closer to the front, as seen in Figure 41.

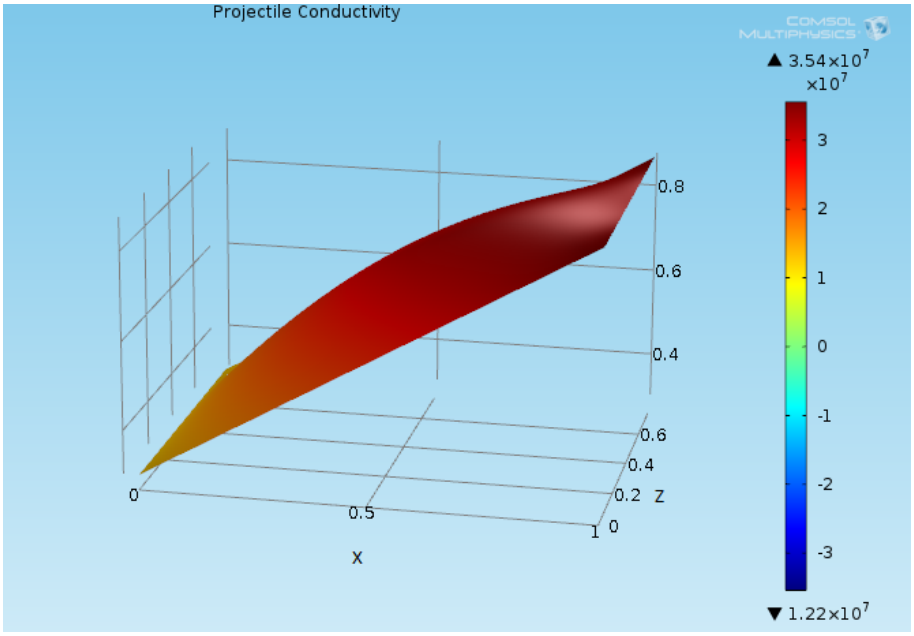

Figure 41: The second multivariate gradient. The parabolic term makes it so the sine hump in the z direction does not start at the very back of the projectile and is pushed forward.

2.5 Multivariate Parabolic

This gradient rid of the linear term and is solely parabolic in x and a sine in z. It focuses most of the conductivity to the front of the projectile. The gradient has the form

$$\sigma(x, z) = \sigma_m + x^2 \nabla_\sigma \sin(z\frac{4\pi}{3}) \tag{8}$$

The sine term further focuses the high conductivity away from the edges of the projectile. See Figure 42 for the plot of the gradient.

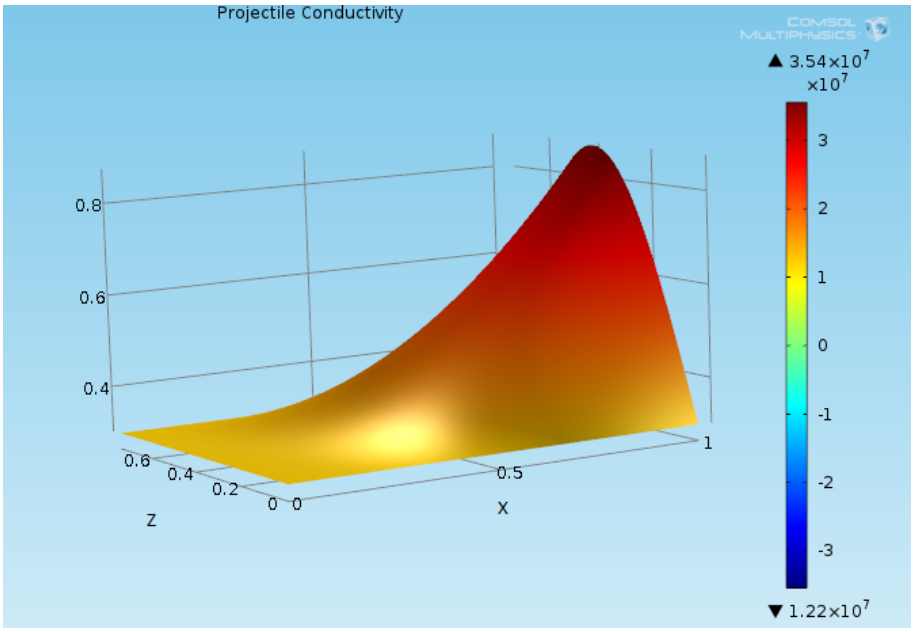

Figure 42: The multivariate parabolic gradient. It has most of the high conductivity in the very front and center of he projectile.

2.6 Corner Radial

This gradient made the back edges of the projectile the least conductive. The conductivity then increased radially away from those two back edges. The gradient needed to be piecewise in order to create both resistive edges. Unlike all the other gradients this one was a function of x and y. The gradient has the form

$$\sigma(x,y) = \begin{cases} \sigma_m + \nabla_\sigma \sqrt{(x^2 + \frac{8y}{3}^2)/2} & \text{if } y \in [0...0.375] \\ \sigma_m + \nabla_\sigma \sqrt{(x^2 + \frac{8(.75-y)}{3}^2)/2} & \text{if } y \in [0.375...0.75] \end{cases} \tag{9}$$

The 8/3 scaling on the y term was used to make the two piecewise functions continuous in the middle of the projectile, and weigh the square root since the projectile is not a perfect square and there is symmetry of the function in the

y direction. Figure 43 shows the corner radial gradient where the minimum is the conductivity of titanium, 2.5 MS/m, and the upper end is the same one used previously, the conductivity of pure aluminum.

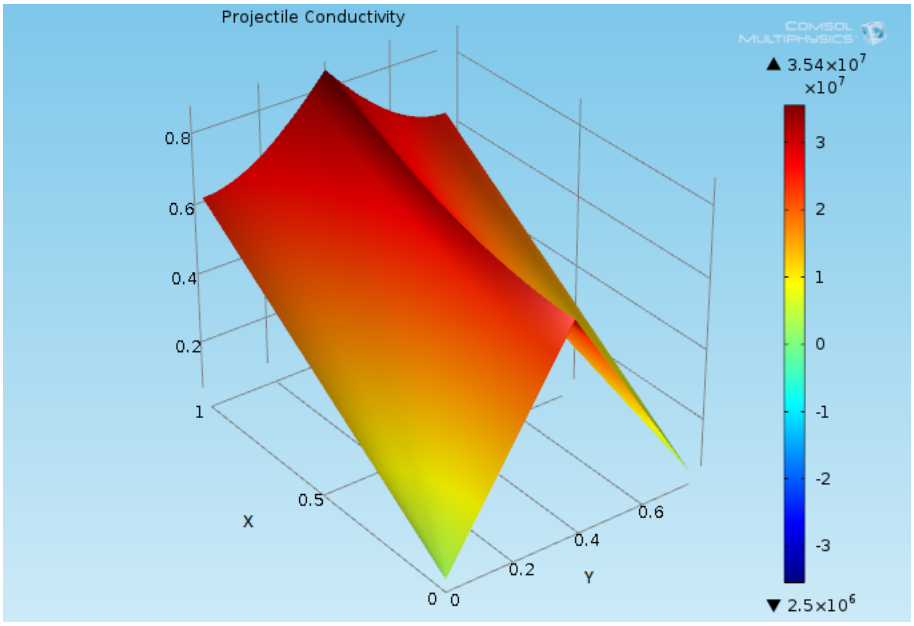

Figure 43: The corner radial gradient. The long axis is the x direction and the shorter one is the y direction. The gradient has the lowest conductivity at the very back at $x = 0$ and $y = 0$ and 0.75 and then increases radially from there. Since it is two mirrored functions the gradient is not differentiable in the middle at $y = 0.375$. Also, in this case the gradient varies from the conductivity of titanium to pure aluminum.

Even though this gradient is continuous it is not differentiable at $y = 0.375$ where the two piecewise functions meet. This will cause some error when calculating the total current through the middle of the projectile. The simulation was run twice with the minimum conductivity being that of titanium and then of Al 221. In both cases the maximum conductivity was that of pure Al as used in all the other gradients.

2.7 Resistive Layer

Unlike all the previous gradients this one varies only in y and causes the projectile to have resistive contact surfaces and full conductivity everywhere else through the projectile. The gradient is composed of hyperbolic tangents because they can be made in to essentially differentiable step functions. The gradient has the form

$$\sigma(y) = \sigma_r + \left(1 - \frac{4y}{3}\right) \nabla_\sigma \tanh(50y) + \frac{4y}{3} \nabla_\sigma \tanh(50(.75 - y)) \qquad (10)$$

where σ_r is the constant low conductivity at the interfaces and ∇_σ is now the difference of the maximum conductivity and the resistive layer conductivity. The conductivity of titanium, 2.5 MS/m, was chosen for σ_r since titanium is a common material for resistive layer when discussing railguns. Each of the tanh terms describes one of the projectile contact interfaces. The coefficient inside the tanh dictates how steep the rise is of the function and was chosen so that it was a steep jump but not so steep that COMSOL would have issues calculating derivatives there with the size mesh that was chosen. The 4/3 scaling on the y terms is added because y ranges from 0 to .75, and that needed to be normalized to be from 0 to 1. See Figure 44 for a visual representation of the gradient.

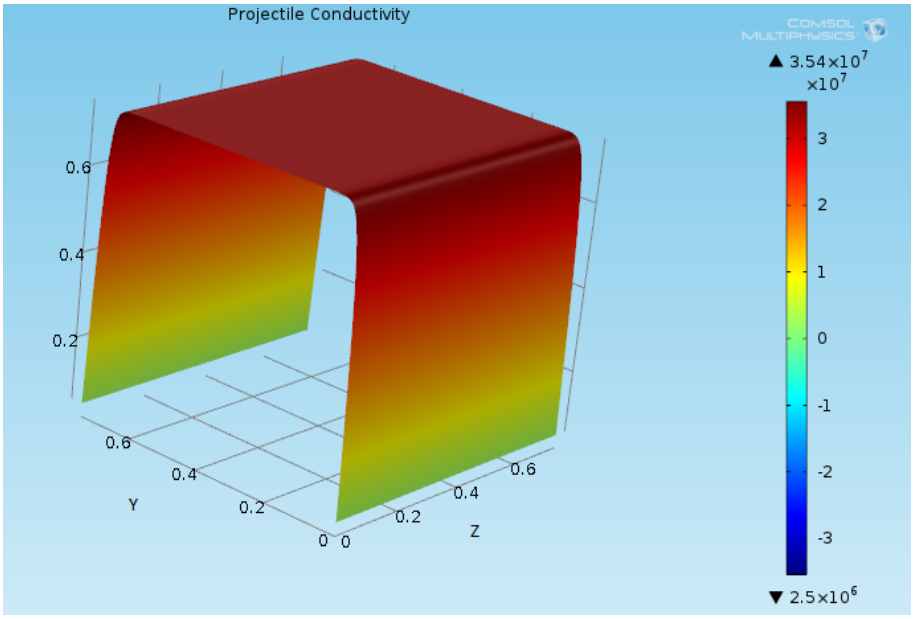

Figure 44: The resistive layer gradient. The conductivity is low on the interface faces and quickly jumps to the maximum value inside the projectile. This gradient only varies in the y direction but is plotted here as it appears in the z and y directions.

2.8 Gradients in x and z with a Resistive Layer

In order to have a gradient which has the resistive layer on the interfaces and any of the x or z gradients elsewhere from this section the following form was derived,

$$\sigma(x, y, z) = \sigma_r(1 - \sigma_n(y)) + \sigma(x, z)\sigma_n(y) \tag{11}$$

where $\sigma(x, y, z)$ is now an up to three dimensional gradient which describes the entire projectile, $\sigma(x, z)$ is any of the gradients from this section save the corner radial gradients, σ_r is the conductivity of the interface layer and is a constant, and $\sigma_n(y)$ is the function that creates the resistive layer but now is normalized to

1 such that $\sigma(x, z)$ controls the region inside the projectile. $\sigma_n(y)$ has the form

$$\sigma_n(y) = \left(1 - \frac{4y}{3}\right) \tanh(50y) + \frac{4y}{3} \tanh(50(.75 - y)) \tag{12}$$

where $\sigma_n(y)$ is the unit-less function that is 0 at $y = 0$ and $y = 0.75$ and quickly rises to 1 inside of those boundaries. The first tanh is for the $y = 0$ edge and the second one is for the edge at $y = 0.75$. Since y ranges from 0 to 0.75 the 4/3 scaling is required to make the function range from 0 to 1.

3 Simulation Results

To evaluate the performance of each of the gradients the current flow through a regular projectile was simulated first. Figure 45 shows the current density at the interface and at the center of the projectile. The interface current density is on the left and the middle current density is on the right. This will hold for all of the following results. Once again, the numbering in the vertical axis is to be ignored just like it was for all of the conductivity plots in the previous section.

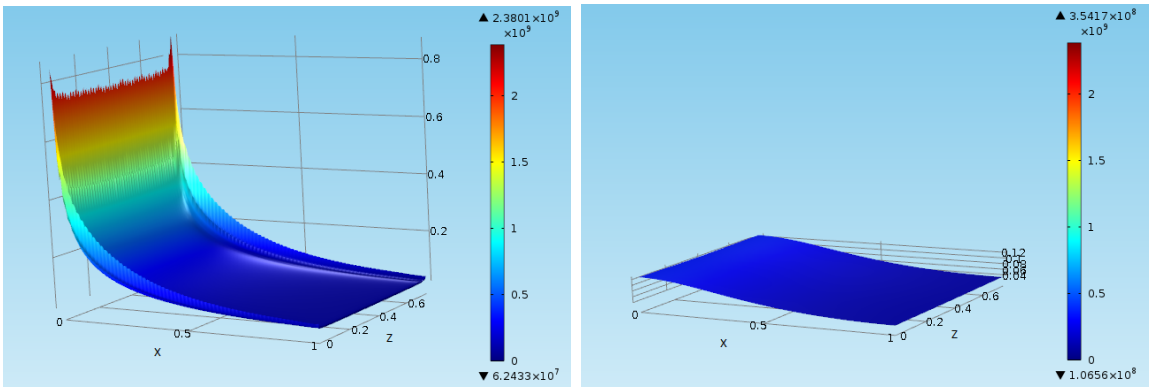

Figure 45: The current flow through a regular projectile. The current density at the interface (left) and in the middle of a regular projectile (right). Notice the huge spike in the back of the projectile of the interface current density. This is representative of the current build up at the edge. The maximum current density at the interface and the center is 2.38 GA/m^2 and 0.354 GA/m^2, respectively. The minimum is 62.4 MA/m^2 and 0.107 GA/m^2, respectively. These are the max and min values on top and bottom of the color scales in the images

The difference between the two current densities shows that the current diffuses by the time it gets to the middle of the projectile, however it is not completely even in the center of the projectile; there is still more flowing through the back than the front. The spiky sides on the interface current density show that there is slight current build up on the side edges of the projectile. The rough nature of the slope at the back of the interface is due to the derivatives becoming too high for COMSOL to evaluate smoothly with chosen mesh size.

Next, the simplest gradient, the linear gradient was simulated. The resultant current densities are plotted in Figure 46.

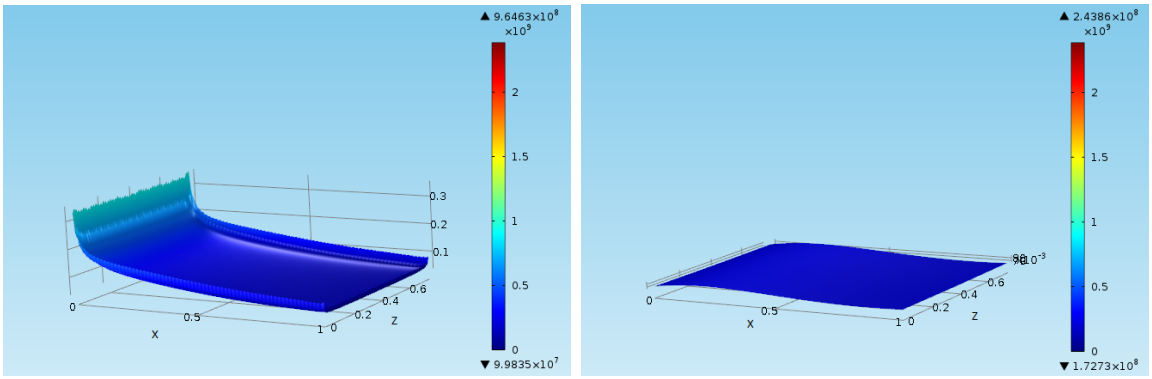

Figure 46: The current densities through the linear gradient. The large current density spike at the interface is greatly reduced and now the current flow through the center is pushed forward a little bit. The maximum current density at the interface and the center is 0.964 GA/m^2 and 0.244 GA/m^2, respectively. The minimum is 99.8 MA/m^2 and 0.172 GA/m^2, respectively.

The linear gradient brings down the current build up in the back of the projectile to 0.964 GA/m^2 compared to the 2.38 GA/m^2 of the regular projectile. The current spiking at the side edges is not mitigated. The current in the middle of the projectile is still not flat and is pushed a little bit forward from the very back. Note that the color range was kept constant for all of the interface and center plots in order to compare the magnitude of the current densities between different gradients.

The parabolic gradient, the results for which are shown in Figure 47, also brought down the current spike but not as much as the linear gradient.

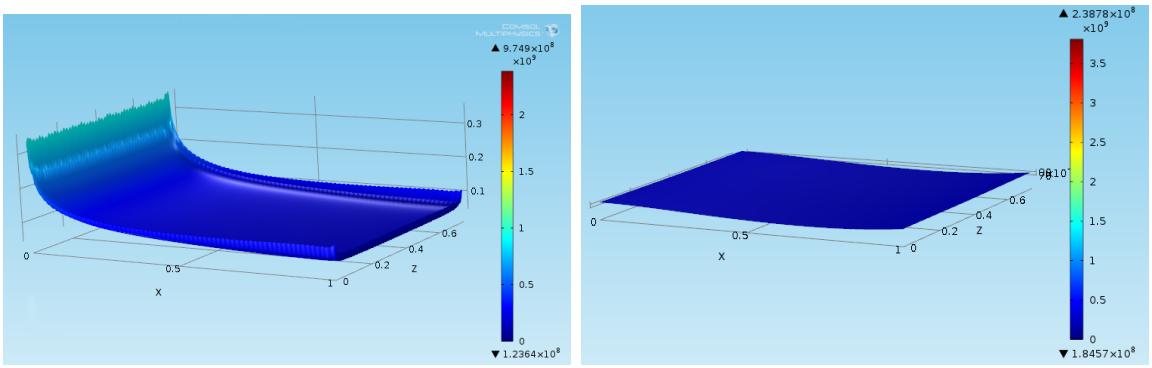

Figure 47: The current densities through the parabolic gradient. The current spike in the back is reduced but not as much as in the linear case. Flow through the center is pushed forward a little bit. The maximum current density at the interface and the center is 0.975 GA/m^2 and 0.239 GA/m^2, respectively. The minimum is 123.6 MA/m^2 and 0.185 GA/m^2, respectively.

The current in the middle of the projectile is a little concentrated in the very back and also in the very front of the projectile, something that is not seen in the linear case.

The current flow through the multivariate gradient which tried to pull current away from the side edges is showed in Figure 48. The sinusoidal variance in the z direction forced the current to pull more towards the middle of the contact face in the back.

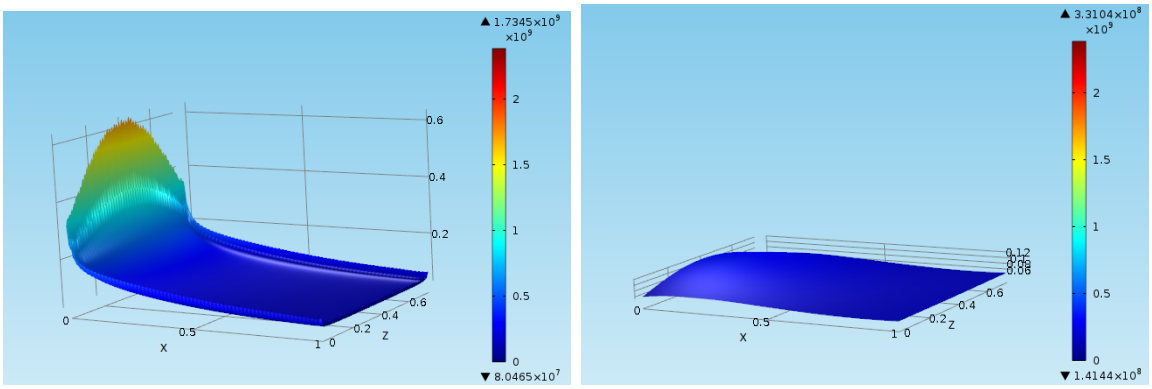

Figure 48: The current densities through the multivariate gradient. The current is pulled from the edges but is focused in the middle of the back edge, which is not ideal. The maximum current density at the interface and the center is 1.73 GA/m^2 and 0.331 GA/m^2, respectively. The minimum is 80.4 MA/m^2 and 0.141 GA/m^2, respectively.

Even though the current density at the edges is less, there is still some spiking on the side edges and there is a large spike in the middle of the back edge, making this gradient not very effective. The current through the center of the projectile has a slight increase in the middle of the back of the projectile.

Figure 49 shows the resultant current densities for the second multivariate gradient. The current no longer builds up in the middle of the back edge like in the first multivariate gradient. The results are very similar to that of the plain linear gradient.

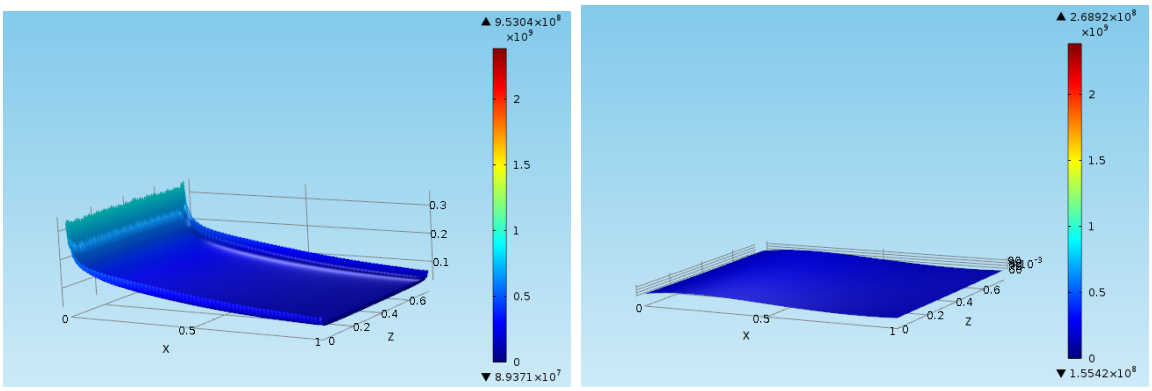

Figure 49: The current densities through the second multivariate gradient. The maximum current density at the interface and the center is 0.953 GA/m^2 and 0.269 GA/m^2, respectively. The minimum is 89.4 MA/m^2 and 0.155 GA/m^2, respectively.

The results for the multivariate parabolic gradient are shown in Figure 50. There is an interesting rise in current density at the front of the projectile. However, it is a lot smaller than the density spike at the back of the projectile. This rise in density is caused by practically all of the conductivity of this gradient being in the very front and middle of the projectile.

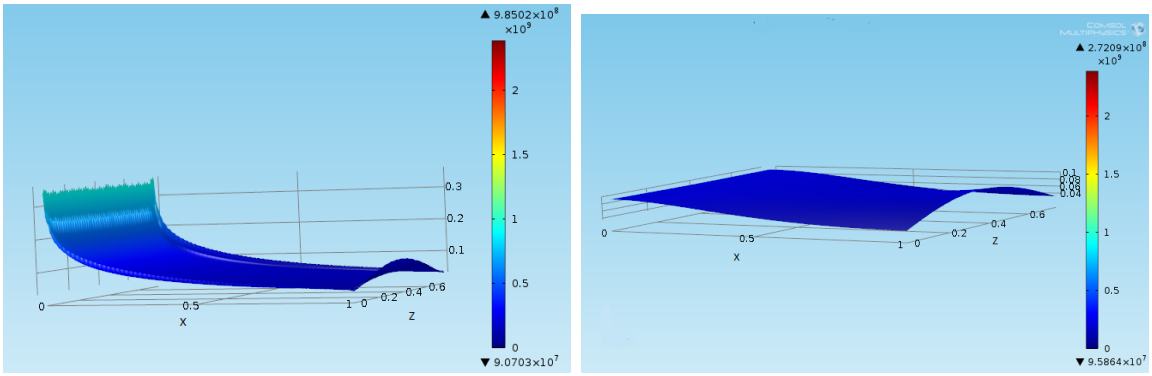

Figure 50: The current densities through the multivariate parabolic gradient. The concentration of conductivity at the front middle of the projectile results in increase of current densities at the front. The maximum current density at the interface and the center is 0.985 GA/m^2 and 0.272 GA/m^2, respectively. The minimum is 90.7 MA/m^2 and 95.9 MA/m^2, respectively.

The current density through the center of the projectile also has this feature

and effectively lowers the current density at the front side edges of the projectile by a slight amount. The current densities of the corner radial gradient in which the range of conductivity was that of aluminum alloys is shown in Figure 51.

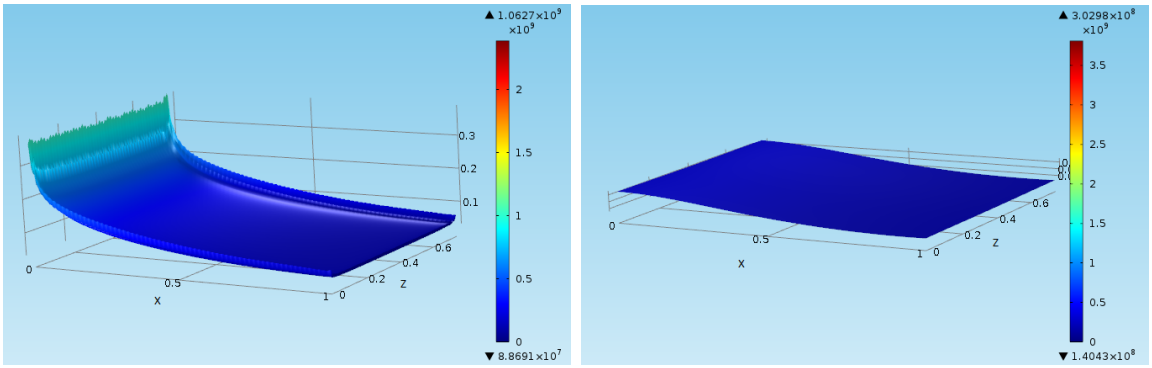

Figure 51: The current densities through the corner radial Al gradient. Using the range of conductivity of aluminum gives similar performance to other gradients. The maximum current density at the interface and the center is 1.06 GA/m^2 and 0.303 GA/m^2, respectively. The minimum is 88.7 MA/m^2 and 0.140 GA/m^2, respectively.

The range of conductivities of aluminum are not low enough to completely squash the current build-up in the back. However, when the lower end of the conductivity was set to that of the titanium using the corner radial gradient, as seen in Figure 52, the current build-up in the back was almost completely mitigated.

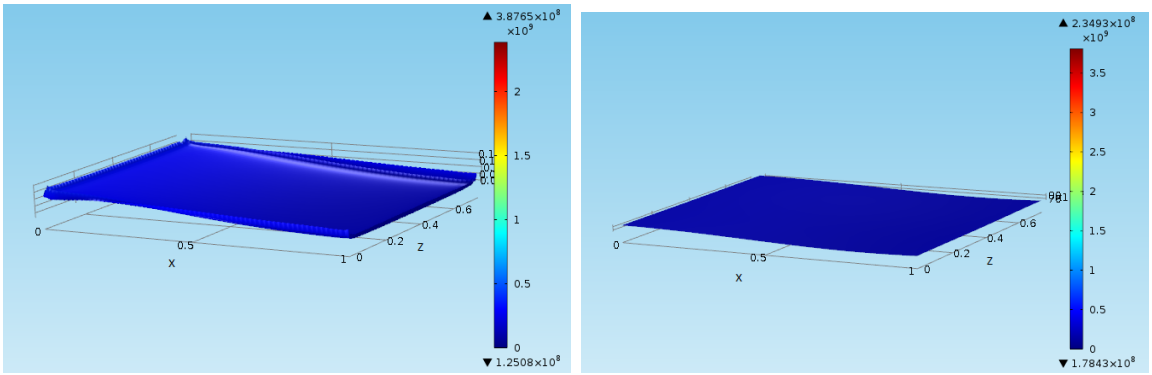

Figure 52: The current densities through the corner radial Ti gradient. The current density at the interface is almost completely flat due to the use of the lower titanium conductivity. The maximum current density at the interface and the center is 0.388 GA/m^2 and 0.235 GA/m^2, respectively. The minimum is 0.125 GA/m^2 and 0.178 GA/m^2, respectively.

The current through the center of the projectile with this gradient was the flattest of all the gradients meaning it defused all the way through the entire projectile. Finally, the results for the resistive layer gradient are shown in Figure 53.

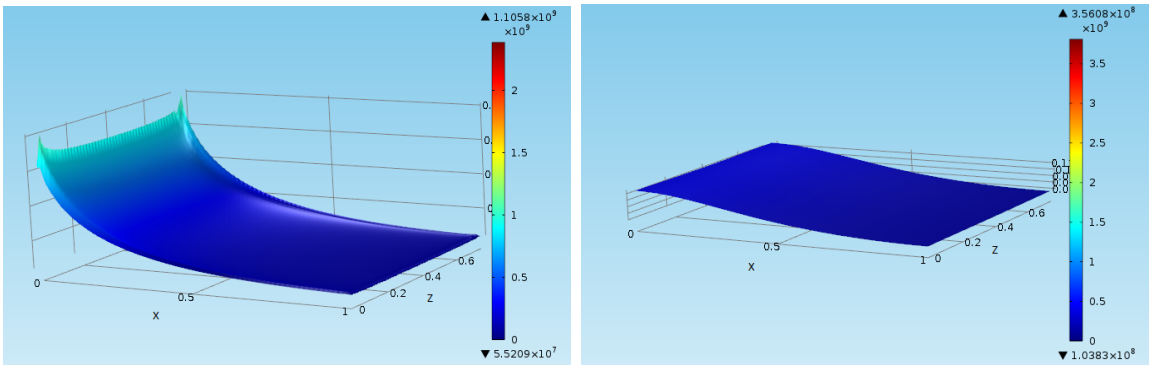

Figure 53: The current densities through the resistive layer gradient. By itself this gradient does not perform as well as the x and z gradients. The maximum current density at the interface and the center is 1.11 GA/m^2 and 0.356 GA/m^2, respectively. The minimum is 55.2 MA/m^2 and 0.104 GA/m^2, respectively.

The current spike is the highest of all the gradients. However, if the resistive layer was thicker then the spike in the back would have been smaller. After the

resistive layer was simulated by itself it was also simulated with all of the x and z gradients using the form in section 2.8. The results for those simulations and all of the other gradients are shown in Table 8. The multivariate gradients are abbreviated with MV, and all the gradients which included the resistive layer are abbreviated with RL. The maximum and minimum current densities at the interface are listed for each gradient. The maximum error of the total system current of each gradient is also listed. Finally voltages in percent of the regular projectile needed to achieve 100000A of current flow are listed. The more resistive the projectile the more voltage is required.

Table 8: Gradient Simulation Summary

Gradient	J_{max} (GA/m^2)	J_{min} (GA/m^2)	Max Error (%)	Voltage (%)
Regular	2.38	0.06	2.3	100
Linear	0.96	0.10	0.9	102
Parabolic	0.99	0.13	0.8	103
MV	1.73	0.08	1.3	101
MV2	0.95	0.09	0.8	102
MV Parabolic	0.99	0.09	0.6	104
Corner Radial Al	1.06	0.09	1.7	103
Corner Radial Ti	0.39	0.13	1.8	104
RL	1.10	0.06	4.3	100
RL-L	0.61	0.10	2.0	103
RL-P	0.63	0.13	1.7	104
RL-MV	0.81	0.08	2.6	101
RL-MV2	0.60	0.09	2.3	102
RL-MVP	0.63	0.08	1.3	104

The lower the J_{max} value and the higher the J_{min} value, the better since it implies that the current distribution was more even at the interface. The corner radial gradient with the titanium minimum conductivity outperformed all of the other gradients. The current density at the interface was essentially flat. The fact that the conductivity needed to be lowered at the corners to that of titanium indicated that within the range of conductivities of aluminum it is not possible

to rid of the current build-up in the back of the projectile, at least within the scope of this simulation. The corner radial gradient performed better than all the resistive layer gradients, even though they also included the conductivity of titanium because the resistive part of the gradient was focused at the very back edge of projectile. The corner radial performed the best but it also required the most voltage to achieve the constant 100000A of current in the model. It is also interesting to note that the maximum error in calculating the total current with the corner radial gradients occurred at the center of the projectile. All the other gradients showed their maximum error at the interface and essentially no error in the center. The reason the corner radial gradients had the most error in the center of the projectile is because there, at $y = 0.75$, the conductivity gradient was continuous but not differentiable since that is where the two piecewise functions met.

The worst gradient was the first multivariate as it reduced the current build-up by the least amount. When all the x and z gradients were coupled with the resistive layer gradient the J_{max} went down for all of them, however the J_{min} was not always increased. It was also surprising to see that the regular parabolic performed slightly better than the multivariate parabolic. This suggests that having the sine term in the z direction to pull the current away from the edges may not be that helpful. Its presence in the multivariate parabolic gradient caused an unnecessary rise in current density at the very front of the projectile. Since the goal was to make the most even current distribution, the sine term took away from the performance of the parabolic term in the x direction.

Chapter 6

Conclusions

1 Graphite Coating

The graphite coating investigated in this work proved to have its benefits. The graphite was of very little cost and reduced the frictional forces in the bore. The coating was too thin however, at least for railgun used in this work. The Cal Poly Mk 1.1 railgun had a bore tolerance of several thousandths of an inch while the graphite coatings were on the order of microns. Due to this difference in scales the coating did not improve contact in static test firings. In a railgun with much tighter tolerance this coating should be applicable. The graphite was very easy work with and also very safe. It was also very easy to remove without damaging or having to replace rails. The main setback of this graphite is its contribution to resistance in the system. However, in press-fit applications where the projectile has a tight fit to the rails and the graphite is applied to both the rails and the projectile, the roughness of the graphite which causes higher contact resistance could be smoothed out by the pressure. The graphite being used in different railgun applications is definitely easier to imagine than the liquid metal,

but the quality of the railgun build needs to be high to use the graphite to its maximum potential.

2 Liquid Metal Coating

The liquid metal was a direct contrast to the graphite. While it helped maintain near perfect contact in static tests, it is very expensive and presents safety risks due to its corrosive nature. The liquid metal corroded away aluminum projectiles with ease but on time scales which still allow for firings as long as the projectile is not in contact with the liquid metal for extended periods of time. Since the liquid metal remains on the rails after multiple shots it bests the graphite since the graphite needs to be applied for each firing as the projectile removes it with ease. In all, when thinking about the orbital space debris impact testing application, the liquid metal interface seems like a poorer choice compared to the graphite since the graphite does not come out of the bore and is essentially free (as compared to the tremendous cost of eGaIn or Galinstan.). In a weaponized application where the barrel is meters long this liquid metal is even more unlikely to be used due to its cost and difficulty in handling.

3 Resistivity Augmented Projectiles

The resistivity augmented projectiles simulated in this work showed that they can even out the current density at the interface which helps mitigate melting of the projectile. Within the range of conductivity and resistivity of aluminum it was not possible to completely smooth out the current density at the interface. However when the range was increased to include titanium the current build-

up due to the velocity skin effect was mitigated. The best gradient was the corner radial gradient which concentrated the resistivity on the back edges of the projectile and then decreased it radially. Manufacturing pieces of aluminum with such varying material properties is not currently possible. But, it very well may be in the near future with constant advancement in 3D printing and manufacturing. Projectiles with varying conductivity as described in this work could greatly improve the lifespan and performance of railguns.

Chapter 7

Future Work

In the future it could be attempted to apply the graphite coating very heavily, until its thickness is on the order of a certain bore tolerances. The possibly serious rise in resistance of the thicker coating needs to be considered and measured. The ability of the coating to maintain its integrity in the presence of melted aluminum needs to be tested. Without doing actual firings liquid aluminum could be poured onto copper covered in graphite to see how the graphite responds and if it shields the copper from amalgamating with the aluminum.

The ability of the liquid metal to withstand the high current and current densities needs to be measured to find out if it has an upper current density limit, like the silver paste, after which is breaks down. Also it is important to find out whether the liquid metal stays in its same position in the rails in the presence of the strong magnetic fields during a firing. If the liquid metal maintains in location like in the static tests and does not break down it could be used to fire multiple times with only one coating. An easy way to test this would be to start by firing current through the railgun while it has liquid metal on the rails and a shunt at the end with no projectile in the bore.

Liquid metal could only be applied for a short distance near the breach. Since contact was maintained in between the two sections of liquid metal during the static tests, a small amount of it near the breach might let the projectile grab some and ride out the length of the bore. This would be a more cost effective way of using the liquid metal. Furthermore, the projectiles could be looked at with microscopy after after liquid metal firings to see if the aluminum retains or grabs small amounts of liquid metal as it rides along on top.

Another thing that could be tried is using the liquid metal and the graphite at the same time. This would only be worthwhile with actual firings rather than static tests because it seems the static tests already showed the best ways the graphite and liquid metal help.

The spiky data from the plain and graphite coated static tests could be further analyzed with a moving average smooth or frequency analysis to see where contact occurs more in the bore. This would allow for characterizing the smoothness and variation of the bore.

A more in depth simulation of the resistivity augmented projectiles, one where the model is dynamic, needs to be done since the velocity skin effect is more pronounced at high velocities. A dynamic model requires the coupling of several modules in COMSOL and is much more complicated than the model used here. The heat-transfer module could be used to measure the heating of the projectile with different gradients over a span of time that the projectile would spend in the bore. Since materials which are more resistive often heat up, more work needs to be done to look into whether it would take less current flow through a more resistive area of the projectile to make it start melting. However, this needs to be tread carefully as the ability to vary the resistivity in a metal is theoretical in this work, and how it would affect other material properties is unknown.

Bibliography

[1] M. T. Adamy. An investigation of sliding electrical contact in rail guns and the development of the grooved-rail liquid-metal interfaces. Master's thesis, Naval Post Graduate School, December 2001.

[2] Conductivity and resistivity values for aluminum and alloys. `http://www.ndt-ed.org/GeneralResources/MaterialProperties/ET/Conductivity_Al.pdf`, 2002. Accessed: 2013-03.

[3] S. Barros. Powerlabs rail gun research. `http://www.powerlabs.org/railgun2.htm`. Accessed: 2013-02.

[4] B. C. Black. Design, fabrication and testing of a scalable series augmented railgun research platform. Master's thesis, Naval Post Graduate School, March 2006.

[5] Em pulse power systems. `http://www.ga.com/railgun-programs/em-pulse-power-systems`. Accessed: 2013-04.

[6] R. Chiechi, E. Weiss, M. Dickey, and G. Whitesides. Eutectic gallium-mindium (egain): A moldable liquid metal for electrical characterization of self-assembled monolayers. *Angewandte Chemie International Edition*, 47(1):142–144, 2008.

[7] W. Cilpeper. Rail erosion and projectile diagnostics for an electromagnetic gun. Master's thesis, Naval Post Graduate School, June 2002.

[8] K. Cooper, H. Jones, and R. A. Meger. Analysis of railgun barrel material. *Magnetics, IEEE Transactions on*, 43(1):120–125, 2007.

[9] M. D. Dickey, R. C. Chiechi, R. J. Larsen, E. A. Weiss, D. A. Weitz, and G. M. Whitesides. Eutectic gallium-indium (egain): A liquid metal alloy for the formation of stable structures in microchannels at room temperature. *Advanced Functional Materials*, 18(7):1097–1104, 2008.

[10] I. Dutta, L. Delaney, B. Cleveland, C. Persad, and F. Tang. Electric current induced liquid al deposition, reaction and flow on cu rails at rail-armature contacts in railguns. In *Electromagnetic Launch Technology, 2008 14th Symposium on*, pages 1–6, 2008.

[11] Emals. `http://www.ga.com/emals`, 2011. Accessed: 2013-02.

[12] T. G. Engel, J. M. Neri, and M. J. Veracka. Characterization of the velocity skin effect in the surface layer of a railgun sliding contact. *Magnetics, IEEE Transactions on*, 44(7):1837–1844, 2008.

[13] General atomics team powers navy rail gun to new world record. `http://www.ga.com/press-releases/older/212-general-atomics-team-powers-navy-rail-gun-to-new-world-record`, 2008. Accessed: 2013-04.

[14] Conductors and conductivity. `http://www.engineeringtoolbox.com/conductors-d_1381.html`. Accessed: 2013-03.

[15] A. Handbook. Friction, lubrication and wear technology. *American Society for Metals*, 18:942, 1992.

[16] W. Harris. How rail guns work. http://science.howstuffworks.com/rail-gun1.htm. Accessed: 2013-02.

[17] M. W. S. Jr. Barrel wear reduction in rail guns: An investigation of silver paste liquid-metal interface. Master's thesis, Naval Post Graduate School, December 2002.

[18] G. C. Long and W. F. Weldon. Limits to the velocity of solid armatures in railguns. *Magnetics, IEEE Transactions on*, 25(1):347–352, 1989.

[19] B. Maier. Selected topics in railgun technology. Course Notes.

[20] J. Maniglia, J. Smiroldo, A. Westfall, and G. Zohar. Design, fabrication, and testing of an electromagnetic rail gun for the repeated testing and simulation of orbital debris impacts. http://digitalcommons.calpoly.edu/aerosp/58/, 2011. Accessed: 2013-04.

[21] Orbital debris frequently asked questions. http://orbitaldebris.jsc.nasa.gov/faqs.html, 2012. Accessed: 2013-05.

[22] G. Paglia. Determination of the structure of y-alumina using empirical and first principle calculations combined with supporting experiments. 2004.

[23] Resistivity of carbon, graphite. http://hypertextbook.com/facts/2004/AfricaBelgrave.shtml, 2004. Accessed: 2013-05.

[24] Resistivity of steel. http://hypertextbook.com/facts/2006/UmranUgur.shtml, 2006. Accessed: 2013-04.

[25] J. C. Schaaf Jr and N. Audeh. Electromagnetic coaxial railgun. *Magnetics, IEEE Transactions on*, 25(5):3263–3265, 1989.

[26] G. Shvetsov and S. Stankevich. Problem of materials for railguns. In *Pulsed Power Conference, 2005 IEEE*, pages 104–107, 2005.

[27] F. D. Witherspoon, A. Case, S. J. Messer, R. Bomgardner, M. W. Phillips, S. Brockington, and R. Elton. A contoured gap coaxial plasma gun with injected plasma armature. *Review of Scientific Instruments*, 80(8):083506–083506, 2009.

Appendix A

SEM Photos

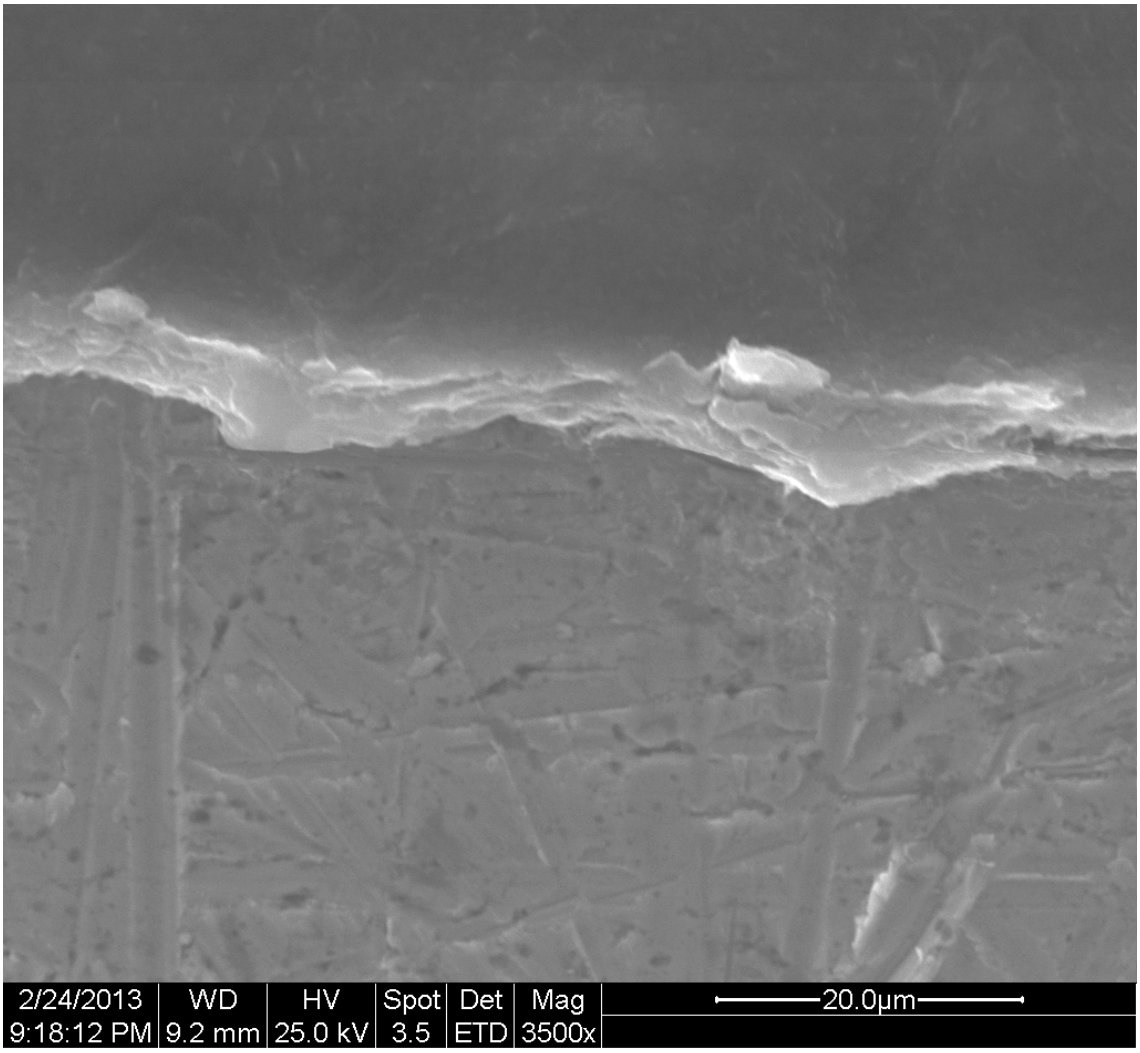

Figure 54: The graphite coating border at 3500x magnification. The features of the copper can be seen.

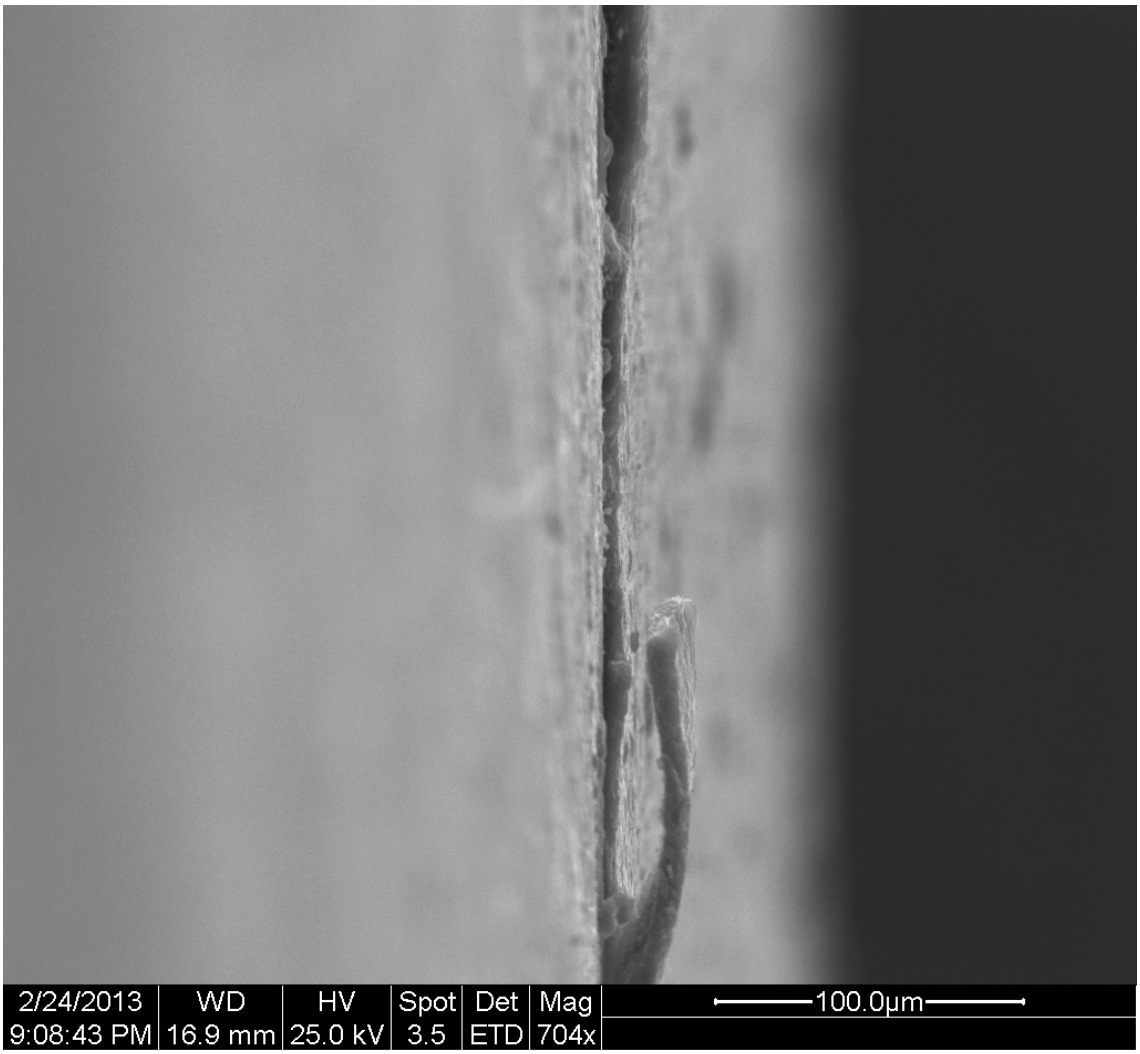

Figure 55: The graphite coating border profile at 700x magnification. The application is ten coatings thick. A tall vertical feature of the graphite caused by masking is seen.

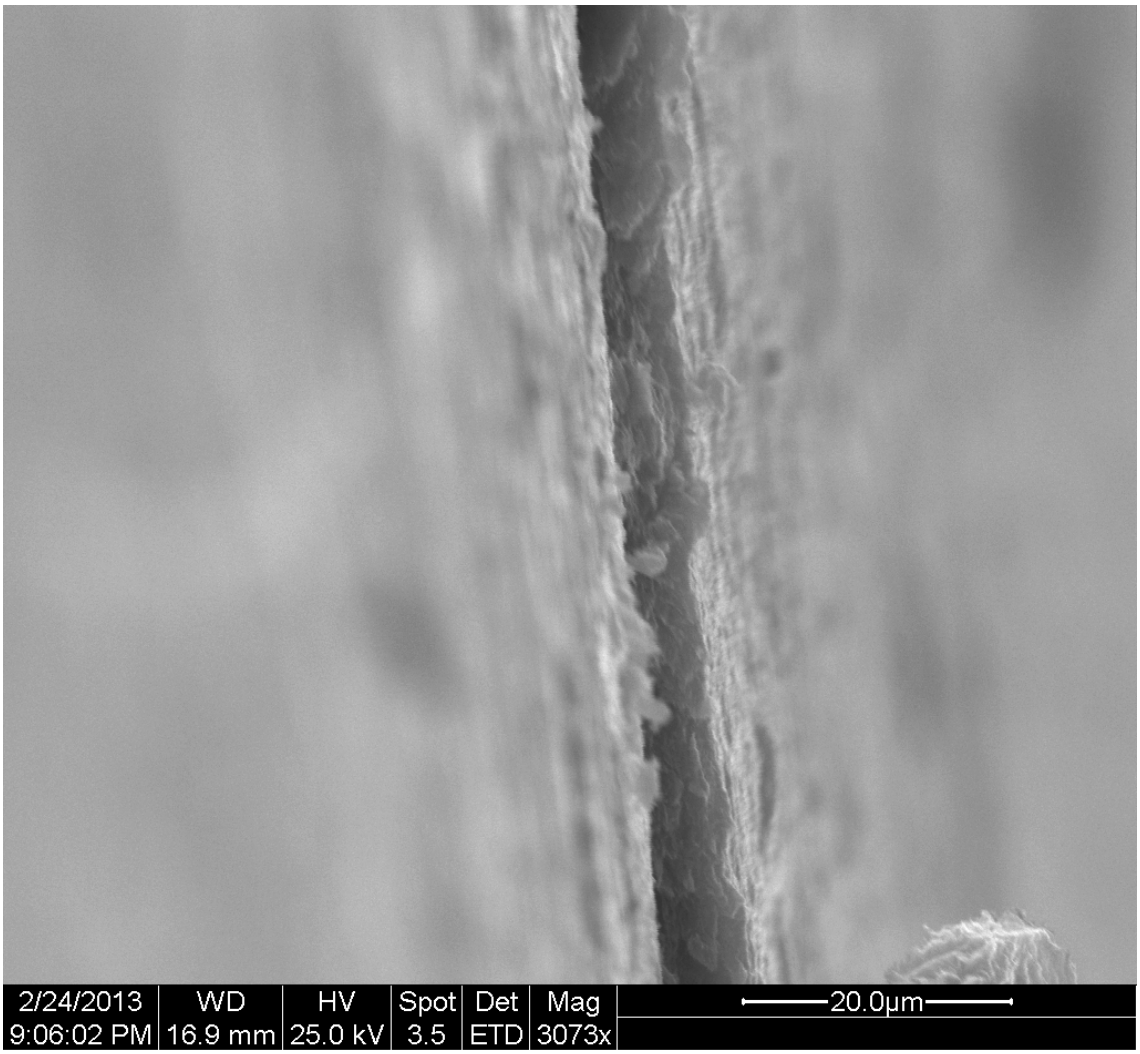

Figure 56: The graphite coating border profile at 3000x magnification. The application is ten coatings thick. An even heighten masking lip is seen. The end of a taller feature is seen protruding from the bottom.

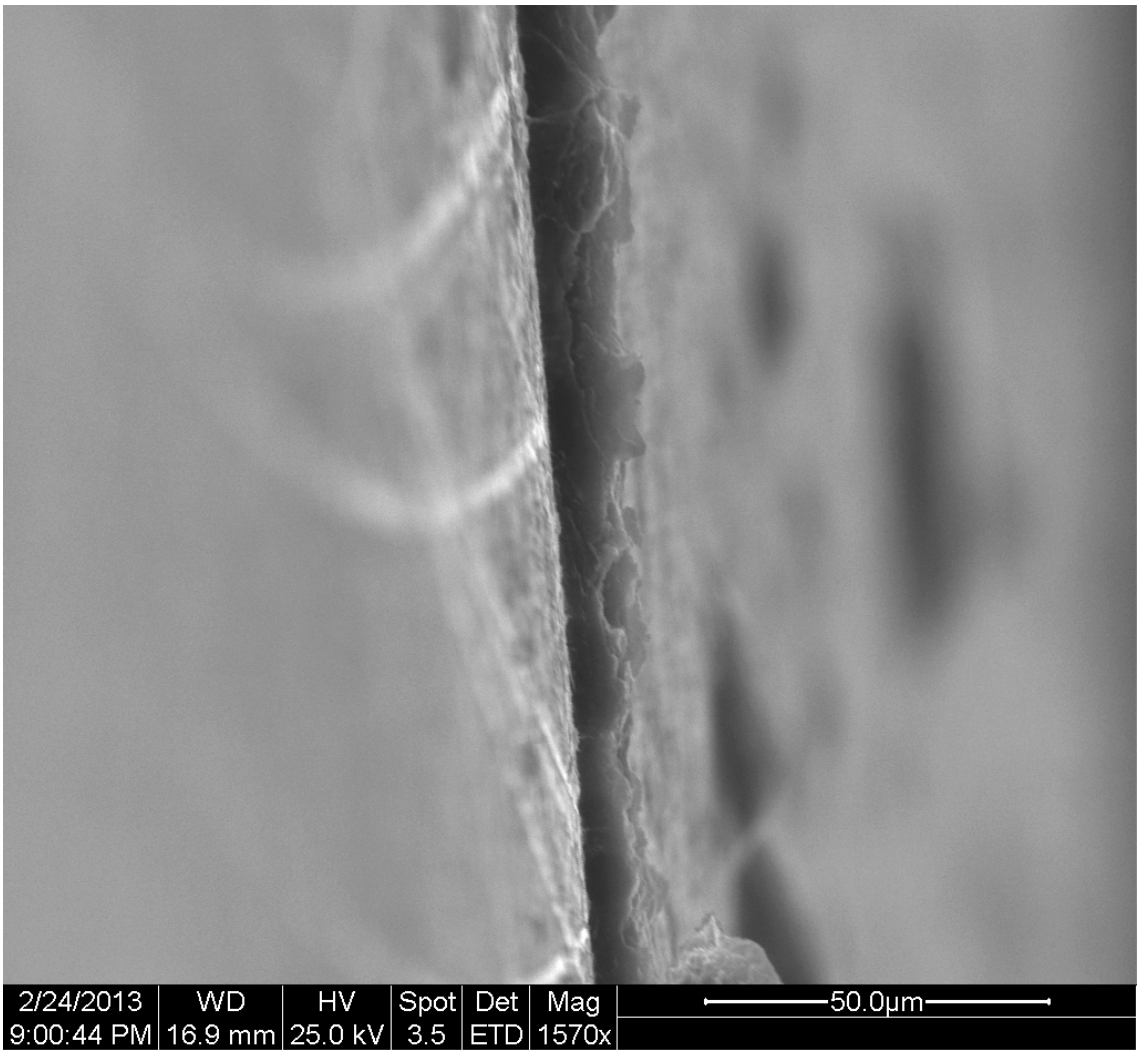

Figure 57: The graphite coating border profile at 1550x magnification. The application is ten coatings thick. The curling of the masking lip due to peeling off the masking tape is seen. The white lines in the copper are surface features from sanding the copper with very fine sandpaper.

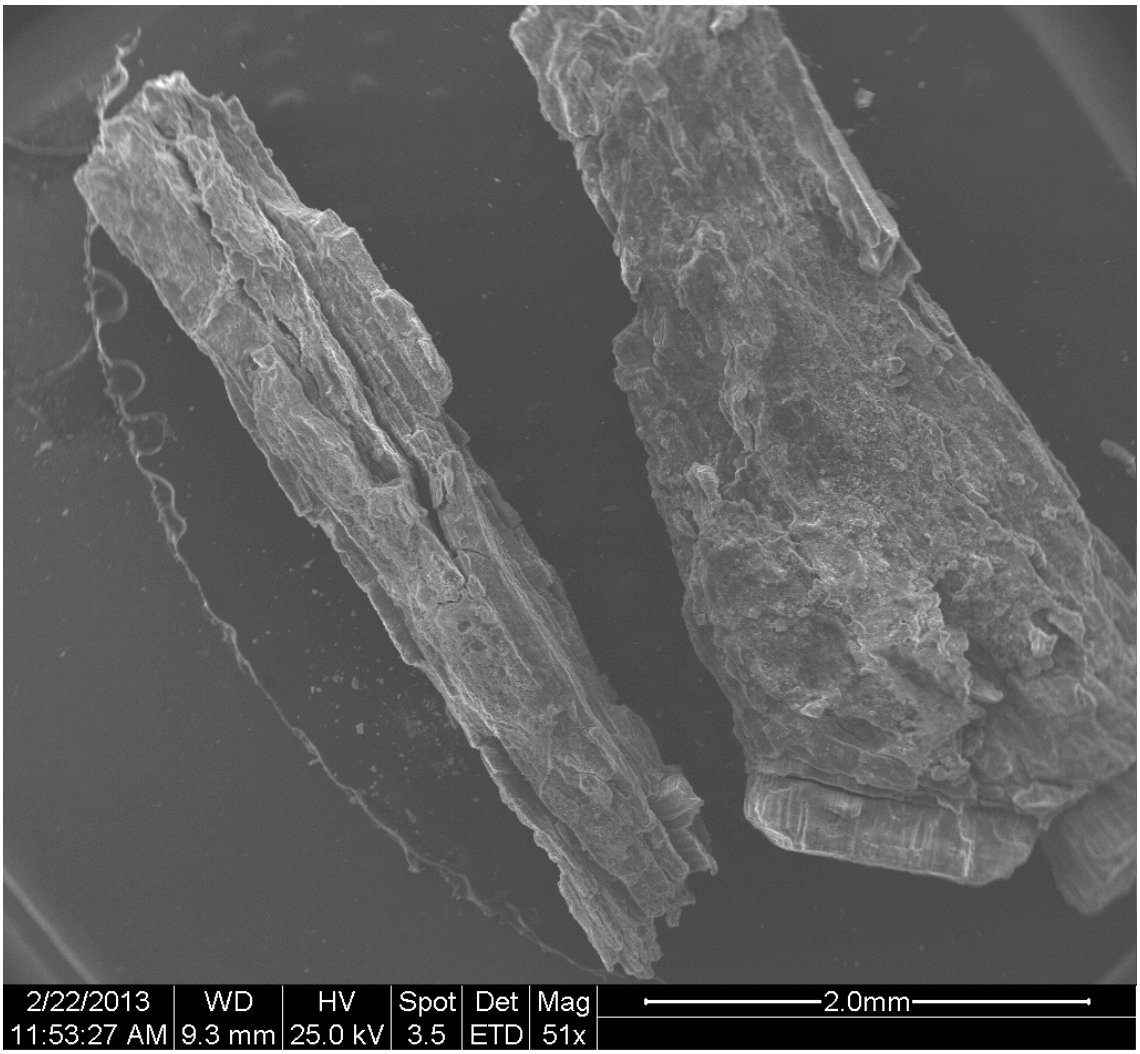

Figure 58: Corrosion flakes at 53x magnification. Several larger flakes of the result of corroding an aluminum projectile with liquid metal are seen. The very rough topography is clear. These flakes were taken after the projectile had been exposed to the liquid metal for several days and large pieces of the brittle and destroyed aluminum broke off.

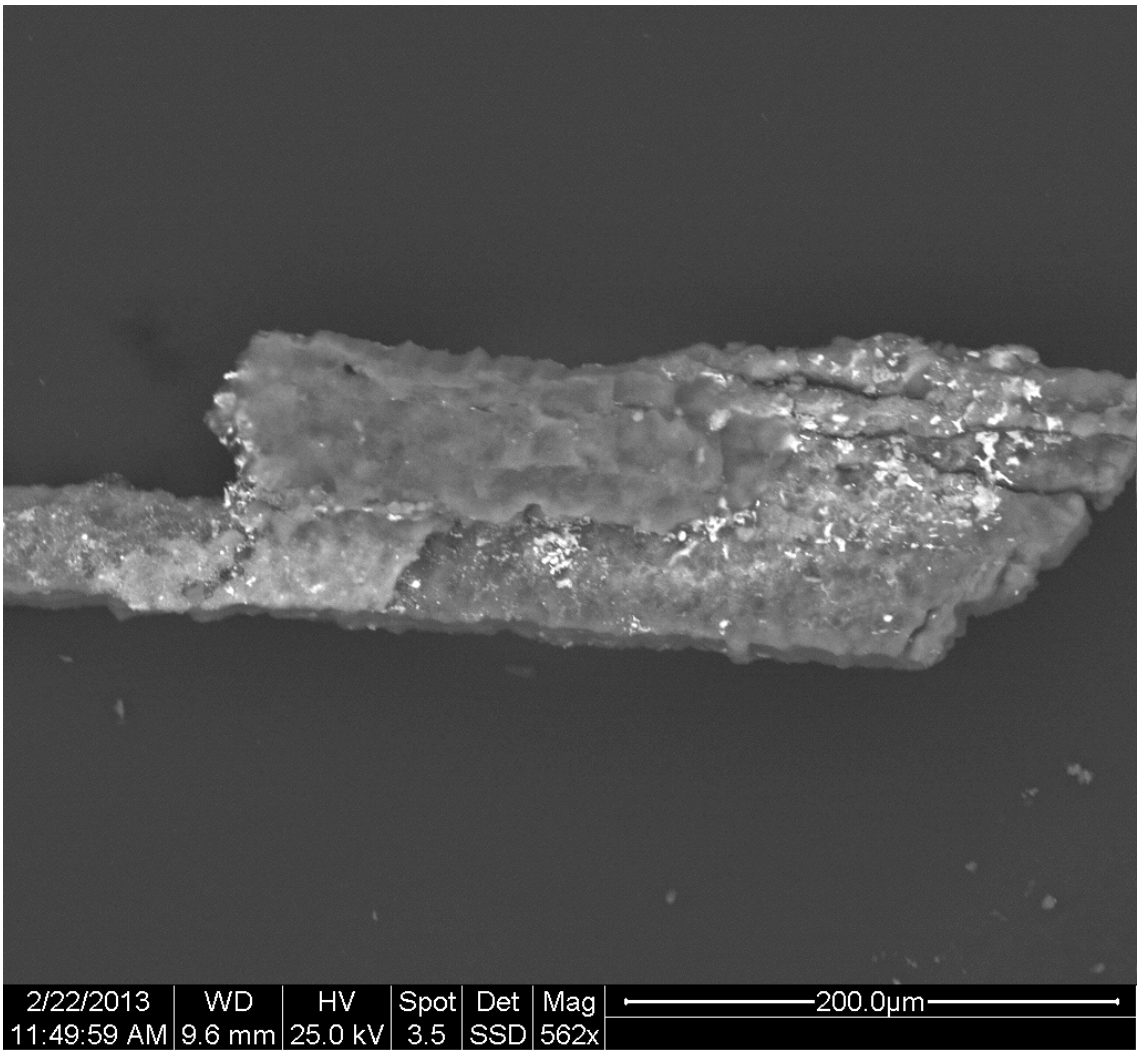

Figure 59: A corrosion flake at 562x magnification. This is seen under backscatter mode. The bright sputtering indicates a change in elemental make up, specifically possible left over indium or gallium.

Appendix B

Static Firing Procedure

Static Railgun Firing Procedure

Aleksey Pavlov

05/20/2013

This document outlines the procedure for doing a static railgun firing in the case of a regular fire and one with liquid metal.

1 Setup

1. Assemble the railgun and ensure the bolts are torqued down an appropriate amount (at least 5ft-lb). Run a projectile down the bore with the push rod to make sure there are no pinch points that completely stop the projectile. If liquid metal is applied on the rails, this may or may not be done and is at the tester's discretion.

2. Place the railgun on the test stand. If this is firing with liquid metal, then lay down protective plastic covering where required. Place the compressed air tank where it will stand and make sure it is tied down to something. Hook up the solenoid valve box to the ITC power out and the BCN connector to the 5V trigger out on the boxes in the test room. If breakscreans are being used hook up the 5V cable to the power supply in the test room.

3. If this is a liquid metal test, wrap the front of the railgun with the thick protective plastic bag. Use duct tape to close the bag and make a good seal. Inside the bag should be a target stop of appropriate size for the test. A thick cardboard box should suffice. The bag should have a slit cut into it and the hose that goes from the HEPA filter should be inserted and duct taped to make a seal. Test the HEPA filter to make sure it turns on. It might take some time to turn on. When it does

it sucks out the air inside the bag rather fast and should be quickly turned off.

4. Hook up the control equipment in the control room. This includes the fire box which contains the Arduino and the box with the ITC power switch.

5. Make the sure tank is closed. Using a proper arduino code make sure that pressing the fire button opens and closes the solenoid valve. An audible click should be heard for the opening and closing, however the closing of the valve may be quieter.

6. Load the projectile. If this is a liquid metal test it has to be breech loaded, if its a graphite or other test then it can be loaded either way.

7. Attach the gas block to the back of the railgun and hand tighten the two bolts that go through it. Make sure the o-ring that makes contact with the rails is there.

8. If it is non liquid metal test hook up the breakscreens.

9. Set up the DC power supply and connect the two leads to the copper tape/wires sticking out of the back of the railgun. Connect one of the BNC cables from the wall to the BNC on the lead cables. Connect that cable to the digital oscilloscope inside the control room. Set the voltage to whatever desired value and the current knob up. If the projectile is making contact at that moment then the current should show .01A on the power supply. In the control room check in the picoscope software that the reading is either the high voltage value (if no contact) or some low, or 0V (if there is contact).

10. Prepare any data taking devises. Set picoscope to take data for however long and make sure arduino code is set to close the valve once the breakscreens break or after a certain amount of time (if no breakscreens are used).

2 Firing

1. Make sure ITC power switch is down.

2. Enter the test room and open the tank all the way.

3. Enter the control room, make sure picoscope is ready to take data. Flip the ITC power switch up.

4. Press the fire button.

5. If the projectile does not break the breakscreens or the valve does not close for whatever reason, flip the ITC power switch down.

6. Save any data on the picoscope and note any output from breakscreens.

7. Enter the room and close the tank all the way. Note that there is still pressure between the tank and the valve. This pressure will leak out within minutes. The valve can also be opened by pressing fire several times in the control room after the tank has been closed to relieve the pressure.

8. Switch off the DC power supply and disconnect the leads from the copper tape from the back of the railgun.

9. If this is a liquid metal fire or was the last test remove the gas block from the railgun.

10. If this is a liquid metal fire, breech load another projectile. Reattach the gasblock and turn on the power supply. Repeat the firing procedure.

11. If this is a regular test, replace the breakscreens and load another projectile. Repeat the firing procedure.

12. If this was the last test and was a liquid metal test, turn on the HEPA filter to suck out the air in the bag. The bag can now be carefully removed from the railgun and thrown away in a hazardous waste container. Any target stop inside needs to be discarded as well. Use gloves when removing and discarding any materials that may have had contact with liquid metal.

13. Remove the railgun from the test stand, unplug all cables, and return the tank to a safe position.

Appendix C

Data Sheets

PRODUCT DATA SHEET

Graphite Plus Aerosol

Description:	***Graphite Plus Aerosol*** is a multi-purpose graphite aerosol coating.	
Physical Properties: (as supplied)	Drying time Lubricating Solid Particle Size Weight Shelf Life Electrically conductive	: Air dries quickly – requires no baking : Synthetic graphite : Less than one micron : 11 oz. : One year
Method of Use:	***Graphite Plus*** can be sprayed on most any clean, dry surface. ***Shake well before using***.	
Precautions:	The customary safeguards employed in storing, handling and applying flammable aerosol coatings should be employed. Please refer to Material Safety Data Sheet for safe handling and first aid procedures. ****** Flammable *** Keep away from open flames and sparks*** ******Pressurized Container*** Do not puncture or incinerate Do not store above 120°F***	
Container Size:	11 oz. can	

ASBURY CARBONS

ASBURY GRAPHITE MILLS, INC.
405 Old Main Street • PO Box 144 • Asbury, New Jersey 08802
Phone: 908.537.2155 • Fax: 908.537.2908
www.asbury.com

Product Data Sheet

Indalloy® Alloys Liquid at Room Temperature

Introduction

Several low melting point **Indalloy®** alloys are liquid at room temperature. These gallium-based alloys are non-toxic replacements for mercury. The gallium-based alloys have far lower vapor pressure than mercury, reducing both the amount and toxicity of metal vapor exposure.

Excellent Thermal and Electrical Conductivity

Metals conduct heat and electricity with their valence electrons. This very effective conduction mechanism is a property of liquid as well as solid metals and alloys. Accordingly, liquid metals have thermal conductivity far superior to non-metallic liquids. Liquid metals are used in applications for dissipating concentrated heat loads such as thermal interfaces for microprocessors, reactors, and heat exchangers. Liquid gallium alloys are inherently high density and low viscosity (similar to that of water, <8 cP at room temperature[1]). As an electrically conductive metal, gallium alloys are used for mercury replacements in switches and contacts.

Wetting to Metallic and Non-Metallic Surfaces

These alloys will wet to most metallic and non-metallic surfaces. This wetting behavior and lubricity enable gallium alloys to serve as high temperature lubricants in journal bearings. However, gallium will attack (it alloys with) some metals, even at room temperature. At higher temperatures, gallium dissolves most metals although the refractory metals, particularly tungsten and tantalum, are resistant to this dissolution. Columbium, titanium, and molybdenum also have this resistance, but less than tungsten and tantalum.[2,3]

Structural materials such as steel, stainless steel, and nickel alloys can generally tolerate gallium service up to the 300–500°C range. However, even at ambient temperatures, gallium is particularly aggressive in dissolving aluminum; care should be taken to avoid contact with aluminum components.

Like indium, gallium and gallium alloys have the ability to wet to many non-metallic surfaces such as glass and quartz. Gently rubbing the gallium alloy onto the surface may help induce wetting.

Note: These alloys form a thin, dull-looking oxide skin that is easily dispersed with mild agitation. The oxide-free surfaces are bright and lustrous.

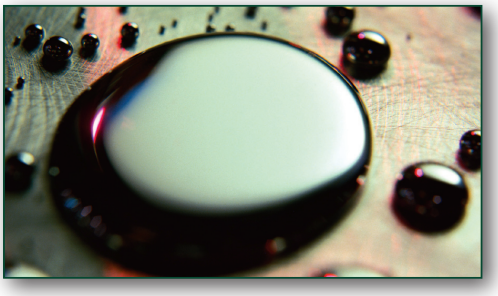

Applications

Typical applications for these materials include thermostats, switches, barometers, heat transfer systems, thermal cooling and heating designs, and TIM2 interfaces.

Packaging

Alloys are packaged in polyethylene bottles and 3cc, 5cc, and 6 oz. syringes and are shipped in accordance with applicable federal regulations.

Note: Gallium alloys expand when they solidify. Accordingly, these alloys should not be stored in glassware below the melting temperature.

Storage and Shelf Life

Unopened bottles and syringes have a guaranteed shelf life of one year. Syringes should be stored in an upright position with the tips down. If stored in polyethylene bottles, it is recommended that as the material is removed from the bottle, the volume should be replaced with dry argon. This minimizes the possibility of oxidation on the surface of the alloy. If the alloy has been stored below its melting point and has solidified, it should be remelted and thoroughly shaken or mixed before use. When reheating the alloy in its original packaging, do not exceed 65°C.

1. Smithells, Colin J, ed. *Metals Reference Book*, 5th edition, London, UK 1976.
2. *Pergamon Texts in Inorganic Chemistry Volume 12, The Chemistry of Aluminum, Gallium, Indium and Thallium* by K. Wade & A.J. Banister, University of Durham, Pergamon Press, 1975
3. Lyon, Richard N, ed. *Liquid Metals Handbook*, 2nd edition, Washington DC, 1952

OVER→

Form No. 97826 R5

www.indium.com askus@indium.com

ASIA: Singapore, Cheongju: +65 6268 8678
CHINA: Suzhou, Shenzhen, Liuzhou: +86 (0)512 628 34900
EUROPE: Milton Keynes, Torino: +44 (0) 1908 580400
USA: Utica, Clinton, Chicago: +1 315 853 4900

INDIUM CORPORATION®

ISO 9001 REGISTERED

Indalloy® Alloys Liquid at Room Temperature

Indalloy® Number	Liquidus	Solidus	Composition	Density (lb/in^3)	Specific Gravity	Thermal Conductivity (W/mK)	Electrical Resistivity (10^{-8} Ω-m)
46L	7.6°C	6.5°C	61.0Ga/25.0In/13.0Sn/1.0Zn	0.2348	6.50	15*	33*
51E	10.7°C	10.7°C	66.5Ga/25.5In/13.0Sn	0.2348	6.50	16.5 (1)	28.9 (1)
51	16.3°C	10.7°C	62.5Ga/21.5In/16.0Sn	0.2348	6.50	16.5 (1)	28.9 (1)
60	15.7°C	15.7°C	75.5Ga/24.5In	0.2294	6.35	20*	29.4 (2)
77	25.0°C	15.7°C	95Ga/5In	0.2220	6.15	25*	20*
14	29.78°C	29.78°C	100Ga	0.2131	5.904	28.1 (3)	14.85 (4)

* Estimated

References:
1. Geratherm Medical AG, Material Safety Data Sheet, 93/112/EC, 2004
2. Michael D. Dickey, et al., Eutectic Gallium-Indium (EGaIn): A Liquid Metal Alloy for the Formation of Stable Structures in Microchannels at Room Temperature, *Advanced Functional Materials*, 2008, 18, 1097–1104
3. C.Y.Ho, et al., Thermal Conductivity of the Elements, *Journal of Physical Chemical Reference Data*, Vol. 1. No 2, 1972.
4. Charles Kittle, *Introduction to Solid State Physics*, 7th Ed., Wiley and Sons, 1996.

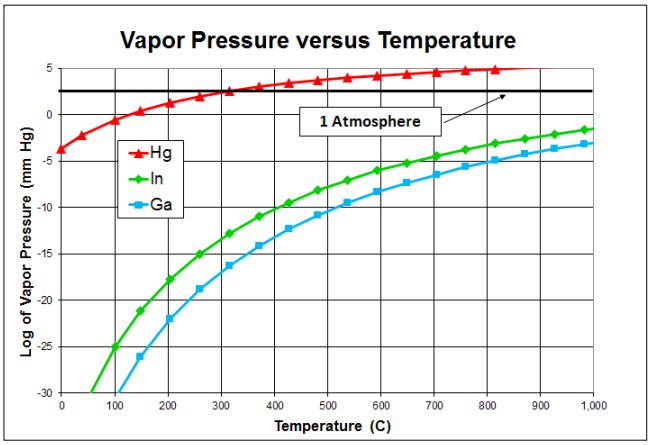

www.indium.com askus@indium.com

ASIA: Singapore, Cheongju: +65 6268 8678
CHINA: Suzhou, Shenzhen, Liuzhou: +86 (0)512 628 34900
EUROPE: Milton Keynes, Torino: +44 (0) 1908 580400
USA: Utica, Clinton, Chicago: +1 315 853 4900

The Ambios Technology Guarantee

We are so sure you will be completely satisfied with our instruments that we offer a 30-day evaluation period prior to payment. If for any reason you decide within 30 days of installation that the instrument does not meet your expectations, we will take it back, no-questions-asked! This gives you enough time to test the instrument under your working conditions and on your samples before you make a final decision.

Go ahead and compare — you won't find a better deal! Many of our standard features are not available or cost thousands of dollars more on competitive models.

XP-1 General Specifications and Options

Specifications

Sample Stage Diameter	140mm
Scan Length Range	30mm maximum
Sample Thickness	20mm maximum
Vertical Resolution	1Å at 10µm, 15Å at 100µm, 62Å at 400µm
Vertical Range	400µm maximum
Max. Data Points per Scan	60,000
Sample Viewing	Color Camera
Magnification	100X fixed
Stylus Tip Radius	2.0 microns
Stylus Force Range	.05-10mg (programmable)
Software Leveling	Yes, cursor-controlled
Scan Filtering	Low-pass, high-pass, band-pass, and adjustable filter
Translation Stage	Allows sample movement of 20 x 80mm and rotation
Step Height Repeatability	10Å, or 0.1% of nominal step height; whichever is greater

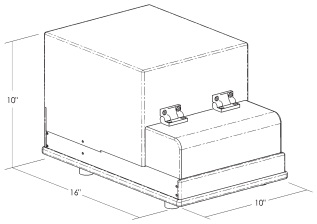

Standard Analytical Software

Roughness Parameters	Ra, Rq, Rp, Rv, Rt, Rz
Waviness Parameters	Wa, Wq, Wp, Wv, Wt, Wz
Step Height Parameters	Avg. Step Ht., Avg. Ht., Max. Peak, Max. Valley, Peak to Valley
Geometry Parameters	Area, Slope Radius, Perimeter
Other Parameters	Stress analysis, height histogram, skewness, profile subtraction, step detection, auto level, auto measure

- *Filtering algorithms allow measurements on round or unusual surfaces and permits removal of surface waviness and/or roughness*

Options

- ***Stylus radius:*** *.2 micron (+/- .1 micron) .5 micron, (+/- .4 micron), 2.5 micron radius, 5.0 micron radius*
- ***Vibration Isolation System***
- ***Ambios Technology Reference Standard:*** *1 micron nominal step height*
- ***Step Height Standards:*** *20nm, 50nm, 100nm, 200nm, 0.5µm, 1.0µm, 5µm, 10µm*
- ***HP DeskJet Color Inkjet Printer***
- ***1-day installation and training*** *(U.S. Only)*
- ***12-month extended warranty*** *(includes parts and labor)*

	XP-1 Profiler	XP-2 Profiler
Linear Scans	Yes	Yes
Data Points	60,000	60,000
Operating System	Windows XP	Windows XP
Software Leveling	Yes	Yes
Camera	Color	Color
Standard Magnification	100X Fixed	40-160X (Motorized Zoom)
Acoustic Isolation Hood	Yes	Yes
Analytical Functions	30+	30+
Stress Option	Yes	Yes
Stage Translation	X=80mm, Y=20mm (manual)	X=150mm, Y=178mm (motorized)
Stage Diameter	140mm	200mm
Stylus Force	.05-10mg (programmable)	.05-10mg (programmable)
Stage Positioning	Manual	Motorized and Programmable
Vacuum Chuck	No	Yes
Optional 3D	No	Yes

AMBiOS TECHNOLOGY
Tel 877.429.4200
100 Pioneer Street, Suite A
Santa Cruz, CA 95060
Fax 831.427.1160
www.ambiostech.com

Product Data

Quanta™ 250

Discover what a truly versatile SEM can do

Addressing the need to investigate a wide variety of materials and characterize structure and composition, the FEI Quanta™ provides flexibility and versatility to handle the challenges of today's wide ranging research needs. View any sample and get all the data: surface and compositional images can be combined with accessories for determining material properties and elemental composition.

Today's research extends beyond simple metals and coated samples and the Quanta series can handle challenges to produce top quality images and analysis. The Quanta 50 series from FEI is the advanced, flexible solution for current and future research applications. Featuring three imaging modes — high vacuum, low vacuum and ESEM™, it accommodates the widest range of samples of any SEM system. Characterization of both traditional samples from metals, fractures and polished sections, to non-conductive soft materials.

The Quanta series has an easy-to-use and flexible user interface with functions to maximize productivity and allow all the data to be collected. Designed by microscopists for microscopists, this instrument series is truly above and beyond 'easy to use'. Navigation features include auto navigation montage, double-click stage-movements, drag-to-zoom and other useful features incorporated as standard. SmartSCAN™ technology is smart scanning strategy to reduce noise and provide better data. Additional new options such as beam deceleration to improve low kV performance, Nav-Cam™ color image navigation, and new retractable detectors provide even greater flexibility to the Quanta series.

Better data. More flexibility. Higher efficiency. The Quanta series delivers more value for your investment.

Key benefits

- Characterize conductive and non-conductive samples with SE and BSE imaging possible in every mode of operation
- Minimize the amount of sample preparation, low vacuum and ESEM capability enables charge-free imaging and analysis of non-conductive and/or hydrated specimens
- Increase analytical capabilities by enabling EDS and EBSD analysis on conductive and non-conductive samples in high and low vacuum thanks to Quanta's patented through-the- lens pumping. Stable high beam currents (up to 2 µA) enable fast, accurate analysis
- Perform dynamic *in situ* analysis of diverse samples in their natural state above or below ambient temperatures from - 165 °C to 1500 °C with specialized *in situ* stages
- Enable surface imaging with optional beam deceleration mode to get surface and compositional information from conductive samples
- Easy to use, intuitive makes highly effective operation possible for novice users

Typical applications include:

NanoCharacterization
- Metals & alloys, oxidation/corrosion, fractures, welds, polished sections, magnetic and superconducting materials
- Ceramics, composites, plastics
- Films/coatings
- Geological sections, minerals
- Soft materials: polymers, pharmaceuticals, filters, gels, tissues, plant material
- Particles, porous materials, fibers

***in situ* NanoProcesses**
- Hydration/dehydration
- Wetting behaviour/contact angle analysis
- Oxidation/corrosion
- Tensile (with heat or cooling)
- Crystallization/phase transformation

NanoPrototyping
- Lithography
- EBID

Essential specifications

Electron optics
- High performance thermal emission SEM column with dual-anode source emission geometry
- Fixed objective aperture for ease of operation
- 45° objective lens geometry with through-the-lens differential pumping
- Maximum horizontal field width: 6.5 mm at analytical working distance (10 mm); 11.3 mm at 25 mm WD
- Accelerating voltage: 200 V to 30 kV
- Probe current: up to 2 µA, continuously adjustable
- Magnification: 13 to 1000000 x

Electron beam resolution
- High vacuum
  - 3.0 nm at 30 kV (SE)
  - 4.0 nm at 30 kV (BSE)*
  - 8.0 nm at 3 kV (SE)
- High vacuum with beam deceleration option
  - 7.0 nm at 3 kV (BD mode* + vCD*)
- Low vacuum
  - 3.0 nm at 30 kV (SE)
  - 4.0 nm at 30 kV (BSE)*
  - 10 nm at 3 kV (SE)
- Extended vacuum mode (ESEM)
  - 3.0 nm at 30 kV (SE)

Detectors
- Everhart Thornley SED (secondary electron detector)
- Large Field Low vacuum SED (LFD)
- Gaseous SED (GSED) (used in ESEM mode)
- High sensitivity low kV SS-BSED*
- IR camera for viewing sample in chamber
- Gaseous BSED (BSE detector for high pressures, used in ESEM mode)*
- 4 quadrant solid-State BSED*
- Scintillator BSED/CLD*
- vCD (low voltage high contrast detector)*
- Electron beam current measurement*
- Gaseous analytical BSED (GAD)*
- STEM detector*
- Nav-Cam™ - color optical camera for sample navigation*
- Cathodoluminescence*
- EDS*
- WDS*
- EBSD*

Vacuum system
- 1 x 250 l/s TMP (turbomolecular pump), 1 x PVP
- Patented through-the-lens differential pumping
- Beam gas path length: 10 mm or 2 mm
- Optional upgrade to oil free scroll/dry PVP
- Chamber vacuum (high) < $6e^{-4}$ Pa
- Chamber vacuum (low) < 10 to 130 Pa
- ESEM vacuum < 10 to 2600 Pa
- Evacuation time: ≤ 150 s to high vacuum and ≤ 270 s to ESEM (FEI standard test procedures)

Chamber
- 284 mm size left to right
- 10 mm analytical WD
- 8 ports
- EDS take-off angle: 35°

* optional

Stage
- X-Y = 50 mm
- Z = 50 mm (25 motorized)
- T = - 15° to + 75° (manual)
- R = 360° continuous
- Repeatability: 2 µm (x and y)
- Tilt-eucentric at analytical height (10 mm)
- x and y movements are in the tilt plane
- Beam deceleration (cathode lens/sample bias)*

Sample holders
- Multi-stub holder
- Single stub mount, mounts directly onto stage
- Various wafer and custom holder(s) available by request
- Universal sample holder kit*
- Specimen holder kit

System control
- 32-bit graphical user interface with *Windows® XP*, keyboard, optical mouse
- One/Two* 19-inch LCD displays, SVGA 1280 x 1024
- MagicSwitch™ (software-controlled switchbox)*
- Joystick*
- Manual user interface*

Image processor
- Up to 4096 x 3536 pixels (~14 MP)
- File type: TIFF (8 or 16-bit), BMP or JPEG
- Single frame or 4-quadrant image display
- 4 quadrants live
- Live or static signal mixing in color or grayscale
- 256 frame average or integration
- Digital video recording (.avi)
- Image histogram and measurement software

Supporting software features
- SmartSCAN™ scan strategy
- Navigation Montage automated routine
- SW temperature control
- Interval image acquisition in 1 to 4 quads
- Multiple image saving function
- FEI Movie Creator Utility (custom .avi file creation from automatically acquired TIFF image series)
- Large Image Window Functionality (displays image on a separate monitor allows dual full screen imaging from different detectors)

System options
- Beam deceleration
- Manual user interface
- Support PC (including 2nd 19-inch monitor)
- SW controlled Peltier cooled specimen stage
- SW controlled WetSTEM™ system
- SW controlled 1000 °C heating stage
- SW controlled 1500 °C heating stage
- Cryocleaner
- Cryocleaner spare vessel
- Joystick
- Specimen current meter
- Remote control SW
- Video printer
- Specimen holder kit
- Acoustic enclosure for vacuum pump
- 7 or 52 pin electrical feedthrough
- Electrostatic beam blanker
- WDS completion kit
- Scroll pre-vacuum pump kit
- Auxilliary gas kit (for gases instead of water)

Common 3rd party accessories
- EDS
- WDS
- EBSD
- Cryo stage
- Cathodoluminescence
- Sample current detector
- Nanomanipulators
- Lithography system
- CAD navigation
- Electrical probing

Documentation and support
- On-line help
- 'Quanta Getting Started' training CD
- RAPID™ enabled (remote diagnostic support)
- Free access to FEI for owners on-line resources
- Free membership in the FEI ESEM User Club

Software options
- Remote control/viewing software
- Image analysis software
- Web-enabled data archive software
- Height mapping/roughness measurement software

* optional